

FEASIBILITY OF PHYSICAL PROPERTIES AND  
SOFT X-RAY ATTENUATION PROPERTIES FOR  
NON-DESTRUCTIVE DETERMINATION  
OF QUALITY OF NUTMEAT IN  
IN-SHELL PECANS

By

NACHIKET KOTWALIWALE

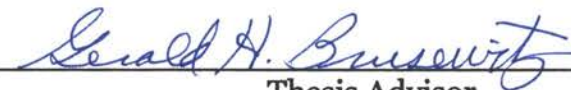
Bachelor of Technology  
Jawaharlal Nehru Krishi Vishwa Vidyalaya,  
Jabalpur, India  
1988

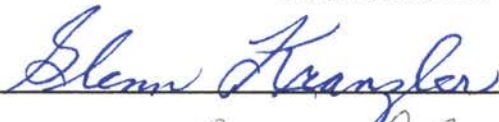
Master of Engineering  
Rajasthan Agricultural University,  
Bikaner, India  
1990

Submitted to the Faculty of the  
Graduate College of the  
Oklahoma State University  
In partial fulfillment of  
The requirement for  
the Degree of  
DOCTOR OF PHILOSOPHY  
August, 2003

FEASIBILITY OF PHYSICAL PROPERTIES AND  
SOFT X-RAY ATTENUATION PROPERTIES FOR  
NON-DESTRUCTIVE DETERMINATION  
OF QUALITY OF NUTMEAT IN  
IN-SHELL PECANS

Thesis Approved:

  
\_\_\_\_\_  
Thesis Advisor

  
\_\_\_\_\_

  
\_\_\_\_\_

  
\_\_\_\_\_

  
\_\_\_\_\_  
Dean of the Graduate College

## **ACKNOWLEDGEMENTS**

It gives me great pleasure to present my gratitude to Dr. Gerald H. Brusewitz, my 'Guru' for the Ph.D. program. He not only educated me, but also kept me focused on my goal. My thanks are also due to members of my advisory committee: Drs. Glenn A. Kranzler, Niels O. Maness, and Paul R. Weckler. Their encouragement, patience, and curiosity gave me the required impetus to complete my doctoral program.

I am also grateful to the Head, all faculty and staff members of the Department of Biosystems and Agricultural Engineering at OSU, Stillwater especially, Dr. Marvin Stone, Dr. Glenn Brown, Wayne Kiner, Mike Veldman, and Craig Tribble. I would like to acknowledge help from Dr. Carla L. Goad, Professor, Department of Statistics, OSU, Stillwater. My special appreciations to Jeyamkondan Subbiah for help during research.

My family members and relatives always showed that they were proud of me; I am thankful and proud of them for this. My parents Prof. Prabhakar S. Kotwaliwale and Dr.(Mrs.) Pratibha Kotwaliwale, my father-in-law Dr. Keshav L. Asanare and mother-in-law Mrs. Pratibha Asanare enthused me for this endeavor. While going through pains of study and research, life was made fantastic by my daughter Gouri and wife Shreya.

## TABLE OF CONTENTS

Chapter	Page
I. INTRODUCTION .....	1
Objectives .....	5
II. REVIEW OF LITERATURE .....	6
Composition and Physiology of Pecan .....	6
Physiology .....	7
Quality of Pecan .....	8
Losses in Pecans .....	9
Methods of Quality Evaluation .....	11
Physical Properties .....	12
Optical Properties .....	19
Acoustic Properties .....	21
Electrical Properties .....	23
Electro-magnetic Properties .....	26
Theory of X-rays .....	27
X-ray Production .....	28
X-ray Attenuation .....	28
Effects of Radiation .....	29
X-ray Shielding .....	30
X-ray Imaging .....	31

Chapter	Page
Applications.....	32
Image Processing Algorithms .....	34
Dual Energy X-ray Measurements.....	38
Comments.....	40
<b>III. MATERIALS AND METHODS.....</b>	<b>41</b>
Determination of Physical Properties .....	41
Sample Preparation .....	41
Size Characteristics.....	42
Specific Gravity.....	43
Moisture Content.....	44
X-ray Imaging Equipment Development.....	44
Components of the Equipment .....	44
Shield Design.....	48
Construction of Equipment.....	49
Controls on the Equipment.....	51
Operating Procedure .....	53
Testing of the Shielding.....	55
Theoretical Dose Rate Calculations .....	55
Actual Dose Measurement .....	56
Determination of Attenuation Coefficient .....	57
Fabrication of Pecans of Desired Quality.....	58
Imaging of Pecans .....	59
Fabricated Pecans.....	59

Chapter	Page
Imaging of Unknown Samples .....	59
Image Processing .....	60
Preprocessing .....	60
Determination of Attenuation Coefficient .....	63
Determination of Appropriate X-ray Energies for Pecan Imaging ...	64
Statistical Analysis .....	65
IV. RESULTS AND DISCUSSION.....	66
Physical Properties .....	66
Moisture Content.....	66
Nutmeat-to-Shell Ratio (NSR).....	68
Principal Dimensions .....	69
Geometric Mean Diameter (GMD) and Sphericity.....	72
Shell Thickness .....	73
Specific Gravity.....	75
Effectiveness of Shielding .....	76
Equipment Calibration.....	79
Attenuation Coefficient .....	79
Regression Equations for Attenuation Coefficient .....	85
Appropriate X-ray Energies for Good Contrast Imaging .....	87
Quality Detection from Images .....	94
Image Segmentation.....	95
Determination of Damaged, Missing, and Shriveled Kernel.....	95
Estimation of Nutmeat Quantity.....	101

Chapter	Page
Algorithm.....	101
Nutmeat Weight Estimates .....	104
Features Visible in Pecan X-ray Images .....	105
V. SUMMARY AND CONCLUSIONS .....	107
Challenges for Future .....	110
REFERENCES .....	112
APPENDICES .....	128
Appendix - A -- Development and Calibration of a Soft X-Ray Digital Imaging System for Agricultural products .....	129
Appendix - B -- X-ray Images of Pecans.....	149
Appendix - C -- Features from X-ray Images for Quality Detection .....	160
Appendix – D – Photographs of Equipment .....	174
Appendix - E -- Computer programs .....	175

## LIST OF TABLES

Table	Page
2.1	Nut characteristics of selected pecan varieties..... 8
2.2	Grade classification for pecans in the shell..... 9
2.3	Size classifications for pecans..... 9
3.1	X-ray tube features ..... 45
3.2	Thickness of pecan nutmeat and shell samples used to determine attenuation coefficient.....57
3.3	Characteristics of fabricated nuts..... 58
4.1	Size characteristics of whole pecan nuts for four cultivars equilibrated at 40% and 78% Rh..... 70
4.2	Geometric mean diameter and sphericity of whole pecan nuts of different cultivars equilibrated at 40% and 78% Rh..... 73
4.3	Shell thickness of four cultivars at two humidity levels..... 73
4.4	Specific gravity values for whole nut, shell, and nutmeat of four pecan cultivars equilibrated at 40% and 78% Rh.....75
4.5	Mean linear attenuation coefficients ( $\mu$ ) of pecan nutmeat at different X- ray energies for two cultivars and different sample thicknesses. ....81
4.6	Mean linear attenuation coefficients ( $\mu$ ) of pecan shell at different X-ray energies for two cultivars and different sample thicknesses. .... 82



Table	Page
4.7	Regression models of linear attenuation coefficient based on X-ray tube voltage and pecan nutmeat thickness..... 85
4.8	Means of percent image pixels with intensity falling within central 2/3rds part of the image dynamic range for 10 fabricated pecan samples. .... 88
4.9	Conditions for good contrast image. .... 89
4.10	Mean image variance for fabricated samples..... 89
4.11	Number of pecan images with more than 90% pixels having intensity in the central 2/3rds dynamic range. .... 92
4.12	Mean width of histogram base for images acquired at given X-ray energies. .... 93
4.13	Mean difference in first two modes of histogram. .... 93
4.14	Histogram-based features for 'unknown' samples..... 94
4.15	Threshold pixel intensity values at different X-ray energies to identify defects in pecan..... 97
C.1	Nutmeat features and percent area occupied by nutmeat inside shell for fabricated pecans. .... 160
C.2	Mean and standard deviation of pixel intensity of ROI-1 for fabricated pecan samples. .... 161
C.3	Percent area occupied by the nut inside shell of natural pecans and decision based on a threshold value of 75% for 'unknown' samples. ....162
C.4	Mean and standard deviation of pixel intensity inside the shell of pecan for 'unknown' pecan samples. ....164

Table	Page
C.5	Weights: actual and X-ray estimated, for nutmeat in fabricated pecan...167
C.6	Weights: actual and X-ray estimated, for nutmeat in 'unknown' pecan samples. .... 168
C.7	Correlation between actual and estimated weights and estimation error values for 'unknown' pecans having good quality.....170
C.8	Feature comparison for 'unknown' pecan samples..... 171

## LIST OF FIGURES

Figure	Page
3.1 Principal dimensions of a pecan nut in three Cartesian coordinates. ....	43
3.2 Schematic of the equipment setup. ....	45
3.3 Cut-away view of the X-ray tube. ....	46
3.4 Front, side, and isometric view of X-ray camera. ....	47
3.5 X-ray imaging system. ....	49
3.6 Joining aluminum sheet with lead sheet.....	50
3.7 Camera stand. ....	50
3.8 Circuit diagram for the X-ray tube controller. ....	51
3.9 Power supply system. ....	52
3.10 X-ray power controller.....	53
3.11 Flow chart for X-ray image preprocessing. ....	61
3.12 A blank image ( $I_0$ ) taken at 50 kVp, 0.22 mA, 460 ms demonstrating detector variation.....	63
4.1 Effect of air humidity on moisture content of shell for four pecan cultivars. .....	67
4.2 Effect of air humidity on moisture content of nutmeat for four pecan cultivars.....	68
4.3 Length of whole nuts for four cultivars at two air humidities. ....	71
4.4 Diameter of whole nuts for four cultivars at two air humidities. ....	71

Figure	Page
4.5	Frequency distribution of pecan length for four cultivars. .... 72
4.6	Shell thickness of cultivars as affected by humidity. .... 74
4.7	Specific gravity of pecan components as affected by humidity for four cultivars..... 78
4.8	Variation in dose rate with distance and effect of shielding..... 79
4.9	Sample thickness vs. variation in linear attenuation coefficient of pecan nutmeat and shell. ....80
4.10	Predicted vs. observed linear attenuation coefficients for improved cultivar 'Squirrels Delight'. .... 86
4.11	Predicted vs. observed linear attenuation coefficients for native cultivar 'Native - A'..... 86
4.12	Predicted vs. observed linear attenuation coefficients for combined model. .... 87
4.13	Histogram of image taken at low X-ray power (25 kVp, 0.25 mA). .... 90
4.14	Histogram of image taken at high X-ray power (50 kVp, 1 mA)..... 90
4.15	Histogram of image acquired at a 'good' X-ray power (35 kVp, 0.75 mA). 91
4.16	Mean intensity based thresholding to identify damaged pecans at 30 kVp and 1 mA. .... 99
4.17	Variation of each pixel from mean of its 5 x 5 neighborhood for image taken at 40 kVp - 0.5 mA. .... 100
4.18	Representation of a conical X-ray beam hitting the detector surface. .... 103
B.1	X-ray images of fabricated pecans at one orientation. .... 151
B.2	X-ray images of 'unknown' pecans at one orientation. ....159

Figure	Page
D.1 The X-ray imaging system showing shielded box, X-ray tube controller, computer, and monitor.....	174
D.2 View inside the shielded box showing X-ray tube above and camera mounted on adjustable platform.....	174

## NOMENCLATURE

A/D	-	analog to digital
B	-	radiation built-up factor from scattering
B/W	-	black and white
CV	-	coefficient of variation
db	-	dry basis
DEXA	-	dual-energy X-ray absorption
DLE	-	delayed light emission
Eq.	-	equation
Fig.	-	figure
GMD	-	geometric mean diameter
I	-	attenuated X-ray power
I <sub>o</sub>	-	incident X-ray power
keV	-	kilo electron volt
kVp	-	kilo volt peak
m.c.	-	moisture content
mA	-	milli ampere
Max	-	maximum
Min	-	minimum
NSR	-	nutmeat-to-shell ratio

p	-	statistical probability for the null hypothesis
R	-	roentgen
R <sup>2</sup>	-	square of the Pearson product moment correlation coefficient
Rh	-	relative humidity
ROI	-	region of interest
STD	-	standard deviation
USDA	-	United States Department of Agriculture
wb	-	wet basis
wt.	-	weight
z	-	material thickness through which the X-ray passes, cm
$\mu$	-	linear attenuation coefficient
$\mu_m$	-	mass attenuation coefficient
$\rho$	-	material density

# CHAPTER I

## INTRODUCTION

Pecan [*Carya illinoensis* (Wangenh.) K. Koch] is a tree nut crop with high consumer and commercial importance. Pecans have a smooth shell. The kernel makes up to 40-60% of the in-shell weight. The principle producing countries are the U.S., Mexico, Australia, and Israel. Pecans are consumed for their taste and for nutrition. They are used in the bakery, confectionery, and the dairy industry in chocolate and ice creams. Pecans are also added to cereals, breads, pastries, and cookies and are popular in salads, main dishes, as toppings on desserts, and as a snack. These nuts are excellent sources of protein and contain numerous energy-producing nutrients – carbohydrates (USDA, 2002 a). The fat found in pecans is mostly polyunsaturated and contains no cholesterol. Pecans add fiber to the diet and contain iron, calcium, vitamins A, B, and C, potassium, and phosphorous. Pecans also add flavor and a desirable crunchiness to a variety of foods. Pecans are recommended by the American Heart Association and U.S. Dietary Guidelines as a desirable source of heart-healthy unsaturated fat.

Tree nut consumption, at an average of 1.32 kg per person in 2001/02, reached its highest level and was 31 percent higher than the previous season and 15 percent above the second highest level in 1999/2000 (USDA, 2002 b).



Average production of tree nuts in the USA for the years 2000-2002 was 1.27 million tons. Of these, 110,000 tons were pecans with a value of about \$205 million. Average production and value of pecans in the state of Oklahoma during this period was 5,500 tons and \$ 7 million, respectively (USDA, 2003).

Pecan quality evaluation is important for establishing price at various stages in marketing. Size, weight, density, kernel color, appearance, and physical and pathological damage are the major factors influencing pecan quality. These factors mainly depend on variety, environmental conditions during growth, processing, packaging, and storage practices (Reid and Heaton, 1977; Heaton et al., 1977; Kays, 1979; Verma et al., 1985). Quality evaluation is mostly done using a combination of destructive and non-destructive methods (Mohsenin, 1986; Brennan et al., 1990; Thompson, 1996). The non-destructive part, generally carried out by the producer/ grower or the first buyer, includes separation of material based on size and specific gravity (Sims, 1994). Rotary or oscillatory sieves with or without aeration will separate larger and/or smaller material from the desired size. Aeration helps by blowing away the lighter impurities of the crop. Manual inspection of the crop is also practiced to separate nuts that are deformed, off color, or surface damaged. There are many varieties of pecans, but in general pecan cultivars are differentiated into 'Native' and 'Improved.' Physical properties of pecans (both shell and nutmeat) vary with varieties, and hence it is very difficult to grade them based on a common parameter. The presence of any insects is undesirable. Heavily insect-damaged nuts are easy to separate due to low nut specific gravity and also due to the presence of an oily

shine on the shell surface. However, nuts with any insects inside are difficult to identify on the basis of specific gravity or visual inspection.

These aforesaid separation practices provide few means to assess the quality of nutmeat. It is therefore a common practice to draw a small weighed sample from the crop lot, break each nut, inspect it manually, weigh the good nutmeat part, and determine the 'yield' of the sample. Typically, a sample of 0.1% of the saleable load is recommended (Anon., 1979). The method is time-consuming and labor-intensive; therefore it is common practice to draw samples even smaller than 0.1% of the lot (like one sample of 300 g from pecan lots of about 2000 kg and two to four samples of 300 g from larger lots). Such a small sample may not be a true representative of the lot. Typically, it takes about 20 minutes for four people to individually break and grade a sample of about 300 g. Taking a larger sample for destructive quality determination is undesirable from the seller's point of view, because this causes loss of saleable product. Sometimes this destructive method becomes more subjective, and the quality of the same crop can be assessed differently at different points of sale.

A number of techniques based on optical, acoustic, magnetic resonance, and X-ray imaging have been explored for non-destructive determination of internal quality of variety of agricultural products (Gunasekaran et al., 1985; Chen and Sun, 1991). These and other techniques are discussed in the chapter 'Review of Literature.' Each technique has certain advantages and limitations such as computer image resolution, imaging duration, safe handling, and sample-specific requirements, availability of details such as surface color, texture, and internal details, etc. Radiography of agricultural materials for quality

determination is an upcoming field showing promising results for some nuts, fruits, and grains (Keagy et al., 1996; Kim and Schatzki, 2000; Haff and Slaughter, 2002). X-rays, because of their high energy, can penetrate through many objects. However, there are differences in penetration through different materials due to differences in the material properties. Photons in an X-ray beam, when passing through a body, are transmitted, scattered, or absorbed. Radiography intends to capture the difference in transmitted X-ray beam, due to material difference, in the form of a visual contrast in the image. This contrast can be a measure of spatial and quantitative distribution of a certain material(s) within a composite of materials. In pecans, the radiography technique can determine the extent of internal damage, and also estimate volume of nutmeat.

One of the major problems associated with use of X-rays is that high-energy electromagnetic radiations, like X-rays, can ionize and kill biological cells. It is therefore mandatory to provide a shield between the radiation source and people working in the vicinity. Equipment designed for radiography, therefore, needs to fulfill functional as well as radiation safety requirements. Design procedure for radiation shielding is presented in Chapter III.

Manual extraction of information from radiographs is common practice in medical science. Similar subjective approaches have been attempted successfully on agricultural products to detect internal damage (Morita et al., 1997; Tollner, 2002).

## **Objectives**

It is perceived that this study would culminate in the development of a pecan grading and sorting method based on internal quality determined by some means. The short-term aim of this work was to combine knowledge of physical and X-ray attenuation properties of pecan and to determine if they could lead to internal quality determination of pecan. Following are specific objectives of this research are to:

1. Determine physical properties vis-à-vis, size & specific gravity of nut, shell, and kernel and shell-to-kernel ratio of native and improved pecans in relation to nut quality.
2. Design, construct and test a system for X-ray imaging of pecans.
3. Evaluate feasibility of soft X-ray digital imaging to determine quality and quantity of nutmeat while still in the shell.

## **CHAPTER II**

### **REVIEW OF LITERATURE**

Pecan [*Carya illinoensis* (Wangenh.) K. Koch] is one of the most important tree nut crops of USA. Pecan trees can be found in all the southern states of the USA and in Mexico, Israel and Australia (Wood et al., 1994). Pecans can be found in their original habitat, in a semi-domesticated form where wild trees have been cleared of competing trees and brush, and in orchards or dooryard plantings where they have been vegetatively propagated. These pecans are called wild, native, and improved, respectively (Harris et al., 1986). The nut characteristics of 'native' vary greatly due to different genetics for each tree. The 'natives' are generally small, have thicker shell, and are difficult to shell; however, preferred due to excellent flavor. There are more than 1000 named pecan varieties. Only a few of these have commercial importance (Worley, 1994 a).

#### **Composition and Physiology of Pecan**

Pecan kernels, also called 'nutmeat,' are made up of carbohydrates, proteins, and fat. The relative proportions vary with variety and environmental condition. High quality kernel contains 70-75 % oil, 12-15 % carbohydrates, 9-10 % protein, 3-4 % moisture, and about 1.5 % minerals (Stein, 1980). A pecan also contains vitamins A, B, C, & E. Pecan oil is highly unsaturated (of the total lipids

present 8.0% is saturated, 62.3% is monounsaturated, and 24.8% is polyunsaturated) (Santerre, 1994); good from a nutritional point of view, but prone to rancidity or staleness. Fatty acids are generally found in pecans in the form of triglycerides, diglycerids, monoglycerides, or as phospholipids. Major sugar found in the kernel, shell, and shuck are fructose, glucose, sucrose, and inositol. Small quantities of iron-containing pigments and tannins in the kernel and phenolics in the shell are also found. A pecan kernel also contains 0.9 to 1.5 µg of carotenoids per gram of lipid (Kays, 1979).

### ***Physiology***

The development period for pecan is: (1) time from blossoming until kernel filling (May to late August); and (2) the filling and ripening period. Most of the nut volume is formed during the first period of development. Growth is rapid during this period, and the kernel consists of liquid-filled seed coat. This liquid endosperm later congeals, and solid material is deposited on the interior of the seed coat and forms cotyledons. When cotyledons are filled, ethylene is released which induces the shucks to split along the suture. As the nut and shucks dry, the shuck opens fully, and the nut is held loosely by the dried remnants of the vascular system which nourished the nut. Most of the oil, protein, minerals, and acid hydrolyzable polysaccharide content of the kernel develop during the second period. During this second period, there is a rapid intake of nutrients by the tree (Worley, 1994 b). Most of the color development of the kernel takes place after the onset of dehiscence or shuck split period (Kays, 1979).

## Quality of Pecan

Pecan nuts are mainly characterized on the basis of physical characters, viz. size, weight, etc. Nut characteristics of a few pecan varieties are presented in Table 2.1.

**Table 2.1 Nut characteristics of selected pecan varieties.**

Variety	Nuts/kg	Percent Kernel	Shell Thickness	Maturity Date
Stuart	25	46	Medium	Midseason
Desirable	22	51	Medium	Midseason
Schley	31	56	Thin	Midseason
Western Schley	32	54	Thin	Early
Gloria Grande	21	46	Medium	Midseason
Cape Fear	25	53	Medium	Midseason
Sumner	24	52	Thin	Late
Elliott	35	51	Thick	Early
Wichita	26	58	Thin	Midseason
Curtis	41	54	Thin	Late
Maramek	22	55	Medium	Midseason
Woodard	27	55	Very Thin	Late
Moneymaker	31	44	Thick	Early
Frotscher	29	46	Thin	Mid-Late

Source : Worley, RE, 1994 a

Commercially pecans are graded as US No.1, US No. 2, etc. Some objective commercial quality considerations for grading are presented in Tables 2.2 & 2.3.

**Table 2.2 Grade classification for pecans in the shell.**

Characteristics	US No. 1	US No. 2
Loose extraneous or foreign material	< 0.5%	< 0.5%
Shells fairly uniform in color	Yes	No
Damage of shell by any cause	< 5%	< 10%
Serious damage to shells	< 2%	< 3%
Serious damage to kernels	< 7%	< 10%
Kernels – rancid, moldy, decayed, or injured by insect	< 6%	< 7%
Live insects inside shell	< 0.5%	< 0.5%

Source : Erickson, 1994

**Table 2.3 Size classifications for pecans.**

Nuts (pecans in the shell)		Kernel	
Label	Nuts/kg	Label	Number of Halves/kg
Oversize	< 121	Mammoth	440-550
Extra large	123 – 139	Jr. Mammoth	553-661
Large	141 – 169	Jumbo	664-772
Medium	172 – 209	Extra Large	774-992
Small	211 – 264	Large	994-1213
		Medium	1215-1433
		Topper	1435-1653
		Small Topper	1656-up

Source : Erickson (1994) - nuts & Wagner (1980) – kernel.

### ***Losses in Pecans***

The factors causing losses in pecans in general can be categorized as pre-harvest factors and post-harvest factors. The pre-harvest factors include environmental/climatic, physiological, entomological, and pathological factors.



Occurrence of early frost causes intensely dark pigment that is quite bitter to taste (Kays, 1979). Premature shuck opening, leading to early nut drop, deteriorates pecan quality, prevents proper filling of nuts, and reduces weight, shelling efficiency, and grade (Chin & Young, 1980). Harris et al. (1986) have concluded that 0 to 62.7 percent of initial cohorts borne by the tree remain good till the time of harvest. The losses can be attributed to disappearance, infestation by pecan nut casebearer, pecan weevil, scab, pops, and part fills, etc. The pecan weevil loss ranges from 0.5 to 38.3% and is observed at the time of harvest. Besides pecan weevil, stinkbug also feeds during pecan development (Maness & Brusewitz, 2000) resulting in round or irregular shaped black discoloration of the testa. Other physiological disorders include: opalescence, a condition characterized by opaque or oiled stained appearance of all or a portion of the nutmeat; 'sticktights' – nuts that fail to shed the shuck at harvest; vivipary (sprouting of nuts while still on the tree) and; 'wafering' – due to poor kernel fill during development. Adverse climatic conditions, like prolonged draught followed by early frost, mar the kernel development and may lead to a condition where the shuck does not open at all, as happened in the year 2000 (Nascenzi, 2000).

### Post Harvest Losses

The post harvest losses occur during harvesting, handling, and storage. Proper harvesting time is important, since oil content (Worley, 1994 a) and kernel color quality (Kays, 1979) depend on harvesting time as well. Improper harvesting and handling can lead to physical damage to the shell and kernel (Reid

and Heaton, 1977). In the absence of a canopy, the nuts falling on the ground that remain there for some time may become contaminated, infected with microorganisms, develop rot and molds, sprout (Heaton et al., 1977) or may lose color quality (Kays, 1979). If harvested early, pecans may be 'mature with a green shuck.' The shuck removal process may cause losses, since each wetting and drying event deteriorates the quality of the kernel by about 10%. Alternative mechanical deshucking may cause cracks in up to 22% of nuts (Verma et al., 1985). Forced air drying is commonly used, however excessive heat (temperature above 38°C) causes more visible and latent cracks in the nut (Reid & Heaton, 1977) and kernel darkening (Kays, 1979). The pecan kernel is prone to maximum physical damage during shelling. Other handling operations, like loading or unloading from trucks or containers, can also cause physical damage. Improper storage temperature, humidity, and oxygen concentration often deteriorate the kernel color. Exposure to ammonia gas during storage can very quickly change the kernel color to black. Exposure of kernel to alkaline or strong acidic conditions also imparts black and deep brown colors, respectively (Kays, 1979).

### **Methods of Quality Evaluation**

Quality of agricultural commodities can be characterized, based on individual or a combination of various properties, viz. physical, mechanical, optical, sonic, electrical, electro-magnetic, thermal, hydro and aero dynamic, etc. (Gunasekaran et al., 1985; Mohsenin, 1986; Brennan et al., 1990; Chen and Sun, 1991; Thompson, 1996).

## ***Physical Properties***

Physical properties can be grouped into mass-based, size-based, shape-related, and mechanical properties. These properties generally vary with moisture content. Length, width, thickness, sphericity, geometric mean diameter, surface area, projected area, unit mass, bulk density, true density, porosity, terminal velocity, static coefficient of friction, angle of repose, firmness, etc. have been determined as potential quality indices for pumpkin seeds (Joshi et al., 1993), soybeans (Deshpande et al., 1993), cumin seed (Singh and Goswami, 1996), sunflower seeds (Gupta and Das, 1997), pearl millet (Jain and Bal, 1997), locust bean seed (Olajide and Ade-Omowaye, 1999), raw cashew nut (Balasubramanian, 2001), hazel nuts (Aydin, 2002), cotton seed (Özarslan, 2002), onion (Abhayawick et al., 2002), and African yam bean (Irtwange and Igbeka, 2002). Chen and Sun (1991) reviewed some earlier work and identified density and firmness as important quality indicators for many agricultural products.

### **Size**

Directly measured physical dimensions such as length, width, thickness, projected area, etc. and derived expressions such as roundness, geometric mean diameter, and sphericity relate to maturity and quality of many agricultural commodities (Mohsenin, 1986). Many researchers have attempted to determine distribution of these size-related properties for various commodities. Some researchers grouped this distribution for different grades of those products. Joshi et al. (1993) found that principle dimensions of randomly selected

pumpkin seed samples were normally distributed. They found significant correlation among the three principle dimensions and mass of the pumpkin seeds and kernels. Koning et al. (1994) found that the transverse cross-section of potatoes could be described by an ellipse of which the shape factor, width/height, varied between 1 and 1.5 for almost all tubers of the tested cultivars. Based on this relationship, they claimed that only one characteristic parameter, channel height, was required to grade potatoes passing through a specially designed V-channel. Gupta and Das (1997) determined coefficient of correlation for ratios of length-to-width, length-to-thickness and length-to-mass. They commented that width and thickness of sunflower seeds were closely related to length, while mass showed less association with length of seed. For the sunflower seed, kernel length-to-width ratio was found more significant than length-to-thickness and length-to-mass ratios. They reported mean equivalent diameters of 5.39 mm and 4.32 mm and mean sphericity of 0.57 and 0.53 for sunflower seed and kernel, respectively. Jain and Bal (1997) used geometric mean diameter, surface mean diameter, sphericity, and a shape factor derived from surface area and volume of pearl millet to define shape of the grain. Values of these characteristics are reported as varying in the range of 1.85 – 2.12 mm, 1.72 – 2.08 mm, 0.9374 – 0.9425, and 1.011 – 1.067, respectively for three varieties of pearl millet. Olajide and Ade-Omowaye (1999) reported geometric mean diameter and sphericity of locust bean seed as 7.47 mm and 0.69, respectively. Balasubramanian (2001) found that the three principal dimensions of raw cashew nut were normally distributed for the randomly chosen sample. He found that 52% of the nuts could be classified as medium size (length between 32 to 35 mm), 11.5% as small size

(length below 30 mm) and 36.5% as large size (length greater than 35 mm). Kernel length-to-width ratio was more significant than other dimension ratios. Raw cashew nut shell thickness had a linear relationship with moisture gain. Equivalent diameter and sphericity have been reported as 18.71 – 27.52 mm and 0.62 – 0.86, respectively for raw cashew nut and 11.82 – 19.73 mm and 0.54 – 0.81, respectively for cashew nut kernel. Aydin (2002) reported that about 70% of the tested hazel nuts had lengths ranging from 17.89 to 18.17 mm, 80% had a width ranging from 18.66 to 18.93 mm, and 80% had thickness ranging from 16.45 to 16.71 mm. Mean equivalent diameter and mean sphericity have been reported as 17.83 mm and 97.58, respectively for hazel nut and 13.38 mm and 93.57, respectively for hazel nut kernel.

### Density

The relationship between density and the quality of agricultural products has been recognized for more than a century. The density of many fruits and vegetables increases with maturity. On the other hand, certain types of damage and defects, such as frost damage in citrus, insect damage in fruits and grains, puffiness in tomatoes, bloaters in cucumbers, and hollow heart in potatoes, tend to reduce the density of the product (Chen and Sun, 1991). Kato (1997) observed that density of watermelon was related both to the degree of hollowness and the soluble solids content which could be used as a measure of sweetness. Jordan et al. (2000) related post harvest kiwifruit fruit density to dry matter and soluble solid content. McGlone et al. (2002) confirmed that density could predict dry

matter on both unripe and ripe kiwifruit and soluble solid content on ripe kiwifruit with an error around 0.5%.

### Terminal velocity

Pneumatic separation has been employed for cleaning and grading of many agricultural products. Heaton et al. (1977) reported grading and sizing with screens and blowers to separate undesired material from pecan nuts into nine sizes. Terminal velocity values for pecans could not be found in the literature, however values for many other commodities increase with higher moisture content (Singh and Goswami, 1996; Gupta and Das, 1997; Aydin, 2002; Özarslan, 2002).

### Effect of moisture content on physical and mechanical properties

Higher moisture content has been found to cause an increase in all the physical dimensions of agricultural commodities. Deshpande et al. (1993) reported that increase in moisture content of soybean from 8.7 to 25% (db) caused the three dimensions to increase by 6.12 to 11.53%. Özarslan (2002) found that sphericity of cottonseed increased from 0.626 to 0.635 with the increase in moisture content. Irtwange and Igbeka (2002) found that length, width, thickness, and equivalent diameter of 'African yam beans' increased with moisture content, while sphericity of the beans initially increased with moisture content, but later dropped.

Density has been found to decrease at higher moisture content for some crops. Joshi et al. (1993) reported a decrease from 1179 to 1070 kg/m<sup>3</sup> for pumpkin seeds for moisture content from 4 to 40% (db). Deshpande et al.

(1993) reported a decrease from 1216 to 1124 kg/m<sup>3</sup> for soybean for moisture content from 8.7 to 25% (db). Aydin (2002) reported a decrease from 727 to 624 kg/m<sup>3</sup> for hazel nut for moisture content from 2.87 to 19.98% (db). Özarlan (2002) reported a decrease from 1091 to 1000 kg/m<sup>3</sup> for cottonseed at moisture contents from 8.33 to 13.78% (db). Abhayawick et al. (2002) also reported a decrease in true density for three varieties of onion at higher moisture content. Irtwange and Igbeka (2002) found that true density of 'African yam beans' decreased from 1.326 g/cm<sup>3</sup> at 4% moisture content to 1.255 g/cm<sup>3</sup> at 16% moisture content. However, for some commodities, true density increased at higher moisture content. Singh and Goswami, 1996 (cumin seed – from 1047 to 1134 kg/m<sup>3</sup>); Gupta and Das, 1997 (sunflower seed – from 706 to 765 kg/m<sup>3</sup>, sunflower seed kernel – from 1050 to 1250 kg/m<sup>3</sup>); and Balasubramanian, 2001 (raw cashew nut – from 1201 to 1240 kg/m<sup>3</sup>) have reported such increase.

Terminal velocity has been reported to increase at higher moisture content, even when the true density of the product decreased. (Joshi et al., 1993; Singh and Goswami, 1996; Gupta and Das, 1997; Özarlan, 2002; and Aydin, 2002).

Surjadinata et al. (2001) reported that initial moisture content before freezing had a significant effect on sensory evaluation parameters and most of the instrumental texture parameters (hardness, fracturability, springiness, resilience, and chewiness).

## Methods of determining physical properties

Calipers (Joshi et al., 1993) and micrometers (Deshpande et al., 1993; Gupta and Das, 1997; Jain and Bal, 1997; Olajide and Ade-Omowaye, 1999; Balasubramanian, 2001; Aydin, 2002; and Özarlan, 2002) have been used for measuring size. Singh and Goswami (1996) used a traveling microscope to measure size of cumin seeds since it was difficult to handle such tiny seed.

Different methods have been used to determine volume to calculate true density for a product. These include: displacement of fluids/pseudofluids, empirical, and differential pressure. Heaton et al. (1982) used mustard seed displacement to determine specific gravity of pecans. Joshi et al. (1993), and Gupta and Das (1997) used an air displacement pycnometer. The water displacement method has also been used. To avoid penetration of water into the product, it can be coated with a very thin layer of water resistant material like epoxy resin adhesive (Deshpande et al., 1993). For hard-shell products the water displacement method was used without any coating (Olajide and Ade-Omowaye, 1999). Toluene displacement has been used, because the product, being lighter, does not submerge in water (Singh and Goswami, 1996; Aydin, 2002; Özarlan, 2002; Abhayawick et al., 2002). Irtwange and Igbeka (2002) used kerosene to measure volume of African yam beans. Empirical methods have been used to determine the relationship between volume and principal dimensions of the product (Jain and Bal, 1997). Vishwanathan et al. (1996) and Balasubramanian (2001) determined true density from bulk density and porosity values. Bulk density was determined by filling a known volume container with the product,



weighing the product, and then taking the ratio of mass/volume. Porosity was determined by differential pressure created by air media with and without the sample.

Nelson et al. (1992 b) commented that although equilibrium moisture contents of pecan kernels and shells differ greatly, and proportions of total nut weight represented by the kernel and shell vary significantly among cultivars, a high correlation was found between total nut moisture content and kernel moisture content. Oven drying methods under atmospheric pressure or vacuum with varying combinations of time and temperature have been used to determine moisture content. Temperature-time combinations at atmospheric pressure are:  $378 \pm 1$  K for 24 h for pumpkin seeds (Joshi et al., 1993) and cottonseed (Özarslan, 2002); 376 K for 72 h for soybean (Deshpande et al., 1993); and 403 K for 6 h for locust bean seed (Olajide and Ade-Omowaye, 1999); 403 K for 5-6 h for pecans (Surjadinata et al., 2001). For vacuum oven drying, these combinations are reported as 371 K for 5 h for pecans (Nelson and Lawrence, 1995); 343 K, under 100 mm Hg until mass of cumin seed sample was constant (Singh and Goswami, 1996); 343 K for 7 h for onion (Abhayawick et al., 2002). Balasubramanian (2001) used toluene distillation method to determine moisture content of raw cashew nut.

### Comments

Quality evaluation and separation based on physical properties is practiced extensively. Sims (1994) reported that size-based separation is used in cleaning before hulling and separation of broken and unhulled nuts from hulled

pecan meat halves. Pneumatic separation is used to remove pops, culls, shrivels, and leaves. Density-based separation is also used in water or alcohol flotation or vibrating tables to separate empty shells from shells with adhering nutmeat pieces or to separate nutmeat from insects. Readily available and less expensive machinery, ease of adjustment according to product or cultivar, higher reliability of separation, and high capacity are some of the advantages associated with separation based on physical properties. However, physical properties of whole nut have not been a reliable indicator of nutmeat quality. Biological variability does not permit a clear separation for pecan quality grades, based on individual nut physical properties. Physical properties do not account for common internal defects like insect damage, presence of insect in nut, etc. Hence non-destructive quality determination for purpose of pricing, ethical issues like presence of insects, etc. based on physical properties alone is not yet possible.

### ***Optical Properties***

The optical properties of a material are defined by the percentage of incident light that is reflected, transmitted, or absorbed by each wavelength. Birth and Norris (1958) suggested that skin color light transmittance could be used to indicate the flesh color of intact fruit. Ernest et al. (1958) observed a correlation between wavelength of peak transmittance and loss in firmness occurring during maturation and ripening. They also observed a high correlation between wavelength and soluble solid/acid content of freshly harvested fruits. Bittner and Norris (1968) used optical reflectance to evaluate maturity of fruit. Rosenthal and Webster (1973) developed an on-line system to grade apples on

the basis of light transmittance. The machine could grade two apples in one second. An air activated gate system was used to separate fruits into three groups. Light reflectance techniques have been used to detect surface defects and contamination of dried prunes (Burkhardt and Mrozek, 1973); mechanical injury, rot, molds scars, mite injury and scab on oranges (Gaffney, 1973) and tomatoes (Ruiz and Chen, 1982).

The green plants which have been irradiated give off light for considerable time after illumination. This phenomenon is known as delayed light emission (DLE). DLE is probably produced by all vegetables, fruits, and plant materials undergoing photosynthesis and can be related to chlorophyll concentration or apparent greenness of the product. Chuma and Nakaji (1976) observed an almost linear relationship between chlorophyll content of tomatoes and DLE intensity. They separated green tomatoes with high accuracy, whereas the grading of red stages was only partly successful. Chuma et al. (1977) reported grading efficiency of 54.5 to 100 % for five color grades of oranges ranging from dark green to orange. They observed negligible effect of surface treatments such as brushing, and waxing on DLE. Chuma et al. (1980) observed that ripening of banana decreased DLE. DLE decreased with sugar content and increased with firmness. Gunasekaran et al. (1985) presented a review of research work done on the optical methods of non destructive quality evaluation of agricultural and biological materials. The basic laws and interaction of light with biological material were presented with particular regard to their applicability in quality evaluation. They also presented data on optical properties of each product

serving as an index of quality. Chen and Sun (1991) reviewed near infrared analysis techniques for quality evaluation, but only for grains.

### Comments

Although, optical properties, in the visible as well as ultraviolet and infrared range, have been found to be good indicators of quality, they represent only the surface characteristics of material (shell, in case of pecan nuts). Damage to the nutmeat caused by insects or for some other reasons sometimes causes oil to exude and give a darker shine to the shell. Absence of this darkness or shine does not guarantee a clean nutmeat, and hence quality evaluation based alone on pecan shell optical properties is not a good choice.

### ***Acoustic Properties***

Many attempts have been reported to determine quality of agricultural materials based on the acoustic response generated by the product when subjected to (i) mechanical stroke/impulse or (ii) ultrasound waves (Chen and Sun, 1991). Stone et al. (1996) did not find correlation between acoustic response and destructively measured ripeness indices of watermelons. Contacting piezo-electric disk and non-contacting microphone were used to analyze acoustic resonance for firmness determination of peach (Armstrong, et.al., 1997). Spectral parameters did not have strong relationship with Effe-gi firmness or resistance to puncture determined using either instrument. However, a potential was indicated for being able to sort excessively soft, ripe or hard, immature fruit from desirable fruit with an acoustic instrument, which

would be of benefit in eliminating unmarketable fruit and providing more uniformity in pack-out. Stone et al. (1998) found a good relationship between eight-site averages of Effe-gi firmness with eight-site averages of acoustic response, but noted that the technique might not be practical for commercial implementation due to the need for fruit orientation for multiple measurements. Pearson (2000) developed an acoustic based system for sorting pistachio nuts into closed-shell and open-shell nuts. He could achieve a classification efficiency of about 98%. However, the system does not account for any quality parameter other than openings or cracks in the shell of the nut.

Cheng and Hangh (1994) detected hollow heart in potatoes and separated them from non-defective ones using ultra sound waves at 250 kHz. The amount of ultrasonic power transmitted through a potato was the basis of separation. Mizarch, et.al. (1996) used high-power, low-frequency ultrasonic excitation to determine fruit tissue properties of avocado. They observed a linear relationship between firmness and attenuation of the ultrasonic signal, thus making it possible to grade avocado. A link could be established between the ultrasonic attenuation (dB/mm) and firmness of avocado (Mizarch, et.al, 1996) and physiological indices of mangoes (Mizarch, et.al., 1997).

### Comments

Use of acoustic response properties to determine quality of food products has been less successful. Other limitations include the need for orientation and for contact between the acoustic probe and sample. The greatest limitation is that the acoustic response depends very much on the surface characteristics of

the sample, and hence cracks or damage present on the pecan shell would not allow correct quality determination.

### ***Electrical Properties***

Electrical properties of agricultural and biological materials vary widely and are dependent upon many factors relating to quality. Nelson (1973) concluded that electrical properties of agricultural material depend heavily on their moisture content and the nature of water held. He commented that chemically bound water exerts less influence on the dielectric properties than the free water in which polar molecules can orient freely with an applied electric field. Nelson (1981) reported that both dielectric constant and dielectric loss factor increased with moisture content of chopped pecans and decreased with frequency. Below 5 MHz, the slope of dielectric constant – vs – moisture content curve for pecans did not increase as markedly as for grains. At microwave frequencies (above 1 GHz) he did not find a significant relationship between dielectric constant and moisture content and between dielectric loss factor and moisture content. Nelson (1983) claimed that a linear relationship could be expected between dielectric properties of particulate materials and their densities. Stone et al. (1984) found a significant relationship between dielectric constant and moisture content for wheat at moisture content above 13%, but not below 13%. Bulk density, but not particle density of wheat had a significant effect on real permittivity (dielectric constant). Nelson (1984) defined the relationship between bulk density and dielectric properties as linear for air particle mixture of wheat and whole-wheat flour. DeVoe et al. (1985) determined that bulk density

influenced the relationship between dielectric properties and moisture content of wheat. Nelson (1991) found that measurements at single frequencies did not reveal correlations that would be useful for measuring maturity or defects in fruits and vegetables. However, he corroborated the high correlation between dielectric properties of grain and moisture content. Nelson et al. (1992 b) showed that pecan kernel moisture contents could be predicted equally well (with standard error of calibration of 0.6% of moisture content) by RF impedance measurements on kernel halves and for in-shell pecans. They used a parallel plate capacitor with pecan between the plates and microwave resonant cavity with a pecan in the resonant cavity. Lawrence et al. (1992) found that the dielectric constant of pecan kernel pieces in the frequency range from 0.1 to 110 MHz generally increased nonlinearly with increasing temperature in the range from 0 to 40 °C, and with an increasing temperature coefficient as the moisture content increased from 3.2 to 8.9%. Nelson et al. (1992 a) demonstrated that moisture content of a single kernel could be determined, based on RF impedance measurements on field corn, popcorn, peanuts, and pecans. Kraszewski and Nelson (1993) used rectangular waveguide resonant cavity to determine microwave permittivity of pecan nuts. They concluded that dielectric nature of pecan nuts is complex, since the shell and partitioning material contain three times as much water as the kernel. Nelson and Lawrence (1995) demonstrated that moisture content of individual pecan nuts could be determined rapidly and nondestructively by measuring the impedance of either intact nuts or shelled kernel halves between and in contact with parallel plate electrodes at frequencies of 1 and 5 MHz. However, they commented that best accuracies of determination

could be expected for reasonably well equilibrated nuts with respect to moisture. Schmilovitch et al. (1996) developed a prototype for online moisture measurement of individual in-shell pecan. Using parallel plate electrodes at frequencies of 1 and 5 MHz, the system could determine moisture content with standard error of 1.1% m.c., as compared with moisture contents determined by a vacuum-oven. Nelson (1999) stated that the major interest in dielectric properties was to explain the behavior of the materials when exposed to microwave or dielectric heating and their use for rapid sensing of moisture content. He introduced the concept of determining grain moisture content independent of bulk density, determining bulk density and extracting temperature information from dielectric properties as some of the potentially new applications for dielectric property data.

### Comments

Dielectric properties are quite promising in determining moisture content and bulk density of pecan. However determination of dielectric properties requires that electrodes touch the sample. Further correlating dielectric properties with other physical properties on a moisture-free basis is somewhat difficult. Use of dielectric or microwaves also poses another problem like loss of viability, etc. Nelson and Payne (1982) proposed using 40-MHz dielectric heating to control pecan weevil larvae. They could achieve complete mortality of the insect both for in-shell pecans and broken pecan kernels, but viability for germination was reduced.



## ***Electro-magnetic Properties***

Spinning protons of a material placed in a uniform magnetic field precess at a rate known as the Larmor frequency ( $\nu$ ) that is given by  $\nu = \gamma B_0$ ; where,  $\gamma$  is a constant with value dependent upon investigated nucleus and  $B_0$  is the strength of the external magnetic field. When pulsed radio frequency energy is introduced at Larmor frequency, it acts like second magnetic field perpendicular to  $B_0$ . This field changes orientation of the spinning protons from longitudinal to transverse plane, where the rotating magnetization induces an AC current (output measured as voltage signal) in a receiver coil. Thus, a signal of intensity versus frequency is recorded. Imposing a linear magnetic gradient on the external magnetic field causes the proton resonance frequency to vary, and thus the position of resonating nuclei can be determined and represented as an image (Chen, et. al, 1989; Callaghan, 1991; Clark et al., 1997). Chen and Sun (1991) and Clark et al. (1997) have reported many successful attempts at acquiring high-resolution MRIs to determine moisture content, oil content, sugar content, bruises, dry regions, watercore, worm damage, internal quality, stage maturity, etc. for various fruits and vegetables including pecan. Clark et al. (1997) commented that a compromise must be made between image resolution, product size, and image acquisition time. For example, a single image of an apple or pear at a resolution of 200 – 400  $\mu\text{m}$  (slice thickness of 3 mm) can be obtained in less than 10 min. Despite its numerous other advantages, instrument expense and long imaging time make MRI currently impractical for commercial applications of grading and sorting agricultural products.

## Theory of X-rays

Short electromagnetic waves, such as X-rays, interact with matter as if they were particles rather than waves. These particles are discrete bundles of energy and are called photons or quantum. Energy of a photon is given by  $E = h\nu$ , where  $h$  is Plank's constant ( $4.13 \times 10^{-18}$  keV.s or  $6.62 \times 10^{-34}$  joules.s), and  $\nu$  is frequency of photon wave ( $\nu = \frac{c}{\lambda}$ , where  $c$  is speed of light  $3 \times 10^8$  m/s, and  $\lambda$  is wavelength). Rearranging and substituting values of  $h$  and  $c$ , we obtain  $E = \frac{12.4}{\lambda}$  (Curry et al., 1990). The energy measurement unit for photons is the electron volts (eV). An electron volt is the amount of energy that an electron gains as it is accelerated by a potential difference of 1 V. The unit for radioactivity is Becquerel (Bq), which is  $s^{-1}$  in SI base units. The unit for absorbed dose is Gray (Gy), which is  $m^2s^{-2}$  in SI base units. Other known units for dose are Rad ( $J.kg^{-1}$ ) and Roentgen ( $A.s.kg^{-1}$  or  $Coulomb.kg^{-1}$ ).

The X-ray tube current, measured in mA, refers to the number of electrons flowing per second from the filament to the target. If a photon has 15 eV or more energy, it is capable of ionizing atoms and molecules, and it is called "ionizing radiation". An atom is ionized when it loses an electron. The region of wavelengths of X-rays is from 10 nm to 0.01 nm, and in the case of X-ray it is generally expressed as energy from 0.12 keV to 120 keV. The higher the energy, the stronger is transmittance. When an object's atomic numbers is smaller, its bulk density is lower, its thickness is thinner, and the intensity of X-ray transmitted is higher (Morita et al., 1997). Major parts of an X-ray tube are:

evacuated envelope (special glass or metal tube), heated tungsten filament or cathode, copper anode, tungsten target attached to the anode, electron focusing cup, and high voltage power supply (Curry et al., 1990).

### ***X-ray Production***

X-rays are produced when a fast moving electron, emanating from a heated cathode, impinges on a heavy metal anode. There are generally two types of X-ray emission; (i) Bremsstrahlung - A free electron is attracted to the nucleus, to conserve momentum, a photon is created with an energy dependent upon change in electron's trajectory; (ii) K-shell or characteristic X-rays – an electron from the cathode dislodges orbital electrons in the target material and produces excited atoms which stabilize by X-ray emission (Desrosier, 1960, Curry et al., 1990). Generally, less than 1 % of the energy received by the anode is converted into X-rays. The X-rays emitted from the focal spot travel in a conical beam shape through a window in the X-ray tube. Efficiency, quantity, quality, and energy of produced X-rays generally depend upon the anode material. A material with higher atomic number will produce more X-rays (Curry et al., 1990).

### ***X-ray Attenuation***

Because of high energy, x-rays can penetrate through many objects. However, there are differences in penetration due to the differences in the material properties, viz. atomic number, density, etc. (Desrosier, 1960). The photons in an X-ray beam, when passed through a body, are either transmitted,

scattered (Compton scattering) or absorbed (photoelectric collision). As a result, the energy of incident photons reduces exponentially and is given by:

$$I = I_0 e^{-\mu_m z \rho}, \quad (2.1)$$

where  $\mu_m$  is mass attenuation coefficient ( $\text{cm}^2/\text{g}$ ),  $\rho$  is material density ( $\text{g}/\text{cm}^3$ ) and  $z$  is thickness (cm) through which the X-ray passes. The mass attenuation coefficient for a material is a function of the atomic number of the absorbing material and incident photon energy. The exiting photon energy depends on material properties, including thickness. If the absorbing material consists of more than one element, the mass attenuation coefficient of the composite material will be a function of mass attenuation coefficients of individual elements and their mass fraction in the path of the photon beam.

### ***Effects of Radiation***

Desrosier (1960) names some common effects of X-rays as alteration in physical properties of material (metals can be made brittle, plastics can be made stronger; transparency of material can be altered, electrical current can be induced in some semiconductors); chemical changes (mixture of  $\text{N}_2$  &  $\text{O}_2$  gases gives nitrogen oxides, ethylene gas to polyethylene); biological effects (killing living organisms, preserving foods, medical applications such as radiation oncology). All electromagnetic radiations having energy of 15 eV or more can ionize atoms (Curry et al., 1990)

## ***X-ray Shielding***

In thicker shields, the phenomenon of buildup from scattering must be taken into account (Anon., 1994). The thicker and taller the shield, the larger the build up of scatter component. Also, the energy of the source affects the contribution of the scatter factor to the exposure range. For primary X-rays, the buildup due to shielding transmission is given as:

$$B_x = 1.67 \times 10^{-5} \frac{Hd^2}{DT}, \quad (2.2)$$

where  $B_x$  = shielding transmission,  $H$  = maximum permissible dose equivalent (mrem/h),  $d$  = distance between X-ray source and reference point (m),  $D$  = absolute dose index rate (rad m<sup>2</sup>/min), and  $T$  = area occupancy factor.

The effect of material thickness on the penetration of neutrons as a modified form of Equation 2.1 was given by Anon. (2001) as:

$$I(z) = BI_0 e^{-\Sigma_t z}, \quad (2.3)$$

where  $\Sigma_t$  is the macroscopic total cross section for neutrons, and  $B$  is build-up factor. The build-up factor could be expressed in a form of  $B(\mu z) = 1 + \mu z$  and thus:

$$I(z) = (1 + \mu z)I_0 e^{-\Sigma_t z} \quad (2.4)$$

Approximating  $\Sigma_t$  by  $\mu$  for X-rays gives

$$I(z) = (1 + \mu z)I_0 e^{-\mu z}. \quad (2.5)$$

This equation could be solved for  $z$  to obtain the thickness of shield required to reduce the radiation dose by a desired factor.

## **X-ray Imaging**

X-ray emission or absorption spectra are dependent only on atomic number and not on the physical state of the sample or its chemical composition (Desrosier, 1960). Radiography uses the difference in X-ray absorbing powers of different elements to locate position in a composite material. Positions where there are elements that strongly absorb the X-ray appear light, and positions where there are elements that do not absorb the X-rays appear dark on a film placed behind the sample (Willard et al., 1988).

In any type of X-ray imaging there are three basic elements: (i) X-ray converter, (ii) imaging medium, and (iii) casing for imaging medium. The X-ray converter, e.g. phosphor screen, stops X-rays from reaching the imaging medium and produces a visible output proportional to the incident X-ray photons. The imaging medium, e.g. photographic medium, captures the image while the casing protects the imaging medium from surrounding visible radiations. Historically, X-ray imaging has been performed on photographic plates or films (Curry et al., 1990) by subjectively identifying the feature of interest. Earlier works using digital image processing algorithms on X-ray images required scanning of X-ray films (Keagy & Schatzki, 1993). Morita et al. (1997) used a super metal image intensifier camera with a carbon plate placed on top of its CCD detector. New technology provided a line-scan X-ray machine (Kim & Schatzki, 2000), use of combination of fluoroscope, B/W digital camera, and image digitizer (Karunakaran et al., 2002), and use of image intensifier coupled to CCD camera through optical coupling and a frame grabber to digitize the image (Haff &

Slaughter, 2002). Gruner et al. (2002) identified phosphors and semiconductors as two types of X-ray converters. Important characteristics of phosphors are listed as (i) robustness and stability, (ii) X-ray stopping power, (iii) spectral matching of the light output to the next optical relay element, (iv) energy efficiency for conversion, (v) luminescent decay time and afterglow, (vi) linearity between input and output, (vii) noise, and (viii) spatial resolution across the screen. Semiconductors directly convert X-rays into electrical charge, i.e. they act both as X-ray converters and imaging medium. Some of the electronic imaging mediums identified by Gruner, et al. (2002) are vacuum tube TV cameras, CCDs, diode arrays, CIDs, and CMOS imagers.

### ***Applications***

Tollner et al. (1992) established a relation between x-ray absorption properties and dry matter content of apples. Many applications are reported using human intervention for making decisions about presence of defects (Schatzki et al., 1997; Morita et al., 1997; Haff & Slaughter, 2002). Tao & Ibarra (2000) observed that inclusions were more difficult to recognize in textured X-ray images of meat, and the errors varied with the size, shape, and thickness of the inclusions. They suggested that employing soft X-ray radiation and a high-resolution image intensifier might solve this problem. They used a computer controlled X-ray generator and a diode array for X-ray detection.

X-ray energy used to generate radiographs has been reported as 30 kVp & 4.5 mA for particle boards (Steiner et al, 1978), 25 kVp for 90 s for pistachio nuts (Keagy et al., 1996), 50 kVp and 10-13 mA for apples (Kim & Schatzki, 2000), 30

KeV and 16 mA for meat (Tao & Ibarra, 2000), 32 kVp and 3 mA for 60 s on films and 35 keV and 30 mA for 3 ms on X-ray line scan for almonds (Kim and Schatzki, 2001), 15 kVp and 65  $\mu$ A for 3-5 s for wheat (Karunakaran et al., 2002). Haff and Slaughter (2002) while using X-rays at 12 keV and 99 mA observed higher contrast wheat images and commented that the large current reduced the quantum noise.

McFarlane et al. (2000) used the contrast between image pixels to represent material and void as an indicator of image quality. They found that X-ray scatter images had a better contrast for void detection in polystyrene samples than X-ray transmission images. However, scatter images had poor signal-to-noise ratio attributed mainly to the smaller number of photon counts. Incident energy of 50 keV produced better results than 20 keV, but results did not improve at 100 keV.

### Computed Tomography (CT)

The basic principle behind computed tomography (CT) is that the internal structure of an object can be reconstructed from multiple x-ray projections of an object. Scanning a thin cross section of the body with a narrow x-ray beam and measuring the transmitted radiation with a sensitive radiation detector form the ray projections. The detector does not form the image. It merely accumulates the energy of all the transmitted photons. The numerical data from multiple ray sums are then computer-processed to reconstruct an image. Image reconstruction requires adequate non-redundant data. Analysis methods use 2-D Fourier transform or filtered back-projection to reconstruct the image. Use of CT



scanning has been reported to study insect behavior in pecans (Harrison et al., 1993) and sweet potatoes (Thai et al., 1997), search for stones in apricots (Zwiggelaar et al., 1997), study density changes in tomatoes, seek seeds in oranges and pomelos, detect defects in watermelons and cantaloupes, look for internal changes in peaches and stones in apricots (Barcelon et al., 1999 a), and quality detection of mangoes (Barcelon et al., 1999 b). X-rays for these CT scans were generated at high tube voltage, high tube current, or both. Harrison et al. (1993) used X-rays generated at 120 kVp, 33 mA for 57 s, Thai et al. (1997) used 120 kVp, 230 mA for 9 s, Zwiggelaar et al. (1997) used 25 kVp at 700 mA, Barcelon et al. (1999 b), used 150 kVp & 3 mA.

Although CT scan technique gives maximum 3-D information, it requires a narrow x-ray beam, special hardware to continuously rotate and shift the source and camera or the object, high energy X-rays, and extensive computation. For these reasons the time required for scanning an object is far more than taking one radiograph.

### ***Image Processing Algorithms***

Keagy and Schatzki (1993) considered cavities as prime indicators of infestation in wheat. The second derivative, or more generally the Laplacian,  $\frac{\partial^2}{\partial x^2} + \frac{\partial^2}{\partial y^2}$ , of the gray level intensity profile of the kernel cross-section was positive only in the region corresponding to the cavity between the insect and the kernel and at the exterior edges of the kernel itself. They added that use of the derivative assured that the result was independent of the actual intensity values.

Therefore, they proposed that if the Laplacian was computed and only the positive values were kept, the output image contained only the outline of the kernel with the interior cavities. Their algorithm used binary masking for background masking and V-shaped mask convolution for masking the kernel crease while detecting the infestation.

Keagy et al. (1995) characterized a good pistachio nut, based on X-ray images, as a bright area of nutmeat surrounded by less bright cross-section of shell. They explained that darker areas indicated space between the shell and meat and occasionally between the two nutmeat halves. The normal dark areas were generally characterized by sharp edges. In insect damaged nuts, an additional area of darkness was frequently seen corresponding to tunnels formed by the feeding insect. This effect eroded the amount of bright area and increased the amount of medium density dark area. Edges created by insect activity were generally observed to be less sharp than natural edges. Histograms of intensity and derived edge images could be used to select insect-infested nuts from good nuts. Keagy et al. (1996) first segmented pistachio nuts from the background in their X-ray image and then computed intensity histograms for each nut. They characterized histograms by number of pixels, mean intensity, variance, skewness, and kurtosis. They obtained more histogram statistics from edge image (maximum slope across each pixel), image curvature, difference of Gaussians (DOG) image, and DOG edge image (maximum slope across each pixel in DOG image). Casasent et al. (1998) found that histogram features were rotation and scale invariant. They used histogram features and applied neural network techniques to classify pistachio nuts.

Morita et al. (1997) suggested use of unsharp masking filtering to emphasize features in an X-ray image. Shahin and Tollner (1997) used an 11x11 Gaussian filter and morphological image processing to denoise the X-ray image, then binarized the image at a threshold of 150 (in 8 bit image) gray level to segment watercore in image of an apple. Shahin et al. (1999) recommended use of a Gaussian filter for noise removal in X-ray images of moving apples and onions. They did not find it necessary to the use such a filter for detection of watercore in apples due to use of morphological operations used for feature enhancement. Tollner (2002) identified defective onions using a combination of thresholding and morphological classification algorithm on commercial X-ray inspection equipment.

Kim & Schatzki (2000) used a line-scan X-ray machine to detect watercore in apples. Their algorithm consists of two stages; the first stage extracted features from the apple X-ray image, and the second stage categorized apples into different watercore levels. Accuracy of the system was measured in terms of percent correct recognition ratio, false-positive, and false-negative. The average pixel value depended on the size or thickness of the apple, since larger apples absorbed more X-rays. For this reason, their first set of features included an average pixel value and the size of whole apple estimated from the original image. The size of an apple was computed by counting the number of pixels with intensity less than a preset threshold value.

Attenuation coefficient of a material changes with thickness when measured under polychromatic X-rays (Paiva et al., 1998). Tao and Ibarra (2000) developed a thickness compensation algorithm to detect bone fractions in

poultry. The algorithm required knowledge of thickness of the material at each pixel point in the image.

Casasent et al. (2001) tried a binary watershed algorithm to segment individual pistachio nuts from a cluster and to segment nutmeat in single nut images. They achieved a segmentation of 99.3% of all nuts with only 0.25% of infested nuts being over-segmented and 0.7% of infested nuts being under-segmented after nutmeat extraction. They commented that the standard binary watershed algorithm could pose a problem of over-segmentation in images with irregular or complex boundaries.

Kim and Schatzki (2001) presented a pinhole detection algorithm for almonds which was fast enough in real time to minimize false positives. Their algorithm included the following steps: median filtering the original X-ray image to remove noise; checking intensity variation inside the almond nutmeat and marking regions with intensities not consistent with almond shape; ranking marked regions according to “deviance from the norm;” identifying germ and germ region; discarding any marked region inside the germ region; and finally, thresholding and mathematical morphological processing. Their algorithm showed 81% correct recognition and 1% false positive on film-scan images and 65% correct recognition and 9% false-positive on line-scan images. The reason for line-scan images to perform poorly could be that the resolution for film-scan images was 0.17 mm/pixel, while the same for line-scan images was 0.5 mm/pixel.

Karunakaran et al. (2002) observed that infested portions of the wheat kernel as well as the kernel crease were brighter than the endosperm, and

therefore, it was not possible to apply region-growing or edge-detection algorithms to find the infested portion. They obtained a normalized histogram of gray levels for each wheat kernel and then separated it into seven groups with 30 gray-level intervals. The histograms were used to classify the grain kernels into unique classes using PROC DISCRIM procedure (SAS®) on half the samples as a training group and the other half as a testing group. Karunakaran et al. (2002) also attempted to determine whether the insect inside the grain was alive by taking two X-ray images of the grain kernel with a time interval of 2 min, then subtracting one image from the other and counting the number of object pixels in the subtracted image. This procedure is based on the assumption that a live insect would move during the interval time.

### ***Dual Energy X-ray Measurements***

Dual-energy radiography relies on the theory of exponential attenuation of an X-ray beam when passing through a material. The relation of exponential attenuation of radiation energy (Eq. 2.1, page 29) holds true only for monochromatic X-rays. In case of polychromatic X-rays, a phenomenon called “beam hardening” (Paiva et al., 1998) causes the attenuation coefficient at a given energy level to change with thickness of material. However, if a ratio of two attenuation coefficients is considered, the thickness terms cancels out. This is the major concept behind dual-energy X-ray absorption (DEXA).

Dual-energy X-ray imaging is a method for producing images with different contrast characteristics. Two images, produced with short time between exposures, and with different contrast properties are obtained using two

exposures with different kVp, because the proportion of photoelectric absorption to Compton scattering will be different in the two situations. Using these two images makes it possible, for instance, to subtract the bone structures produced in the low-kVp image from the high-kVp image, thus generating a “soft tissue image.” The process is called “dual energy subtraction.” The subtraction will not be entirely complete, but the bone structures will be suppressed to a high degree. Inversely, visualizing high-attenuating regions can be improved by subtracting the high-kVp image from the low-kVp image. (Anon., 2003)

Mitchell et al. (1997) used medical imaging DEXA at 38 and 70 keV on three rib sections of beef and measured the ratios of attenuation coefficient as 1.2 for fat and 1.4 for 100% lean.

Rogasik et al. (1999) used dual-energy X-ray analysis on tomography images of soil to determine variations of water content, dry bulk density, and phase composition of soil at the microscale and to measure spatial distribution in naturally structured soils. Attenuation of X-rays in soil depended on volumetric fraction of the three components of soil (solids, water, and air). A linear relationship existed between the linear attenuation coefficients, as measured for defined parts of the soil in its three-phase composition (Rogasik, et al., 1999). Mitchell et al. (1998a) used DEXA to study composition of pork carcasses and to predict bone mineral content in live pigs (Mitchell et al., 1998b; 1998c; 2001).

Brienne et al. (2001) used dual-energy X-ray absorption to assess meat fat content by acquiring images at 44 and 70 keV at 0.2 mA. Buzzell and Pintauro (2003) defined ‘R-value’ for a material as the ratio of the attenuation coefficient at low-energy level to that at high-energy level.

## ***Comments***

X-ray imaging is a promising technique, because it is non-invasive, does not require a probe or device to touch the sample, and thin packaging material does not pose a barrier to taking an image. The image gives ample opportunity for subjective as well as image feature-based computer classification. Image information can also be used as radiometric information. The technique is fast and with further advances in technology, it can be economical for industrial purposes.

## **CHAPTER III**

### **MATERIALS AND METHODS**

Procedures employed to determine physical and X-ray attenuation properties are discussed in this chapter. Other related aspects, expatiated in this chapter are: development of equipment, testing of shield effectiveness, imaging, image processing algorithms, and data analysis.

#### **Determination of Physical Properties**

##### ***Sample Preparation***

Pecan nuts from four cultivars; namely 'Native - A', 'Native - B', 'Squirrels Delight', and 'Maramek' were obtained during the 2001-2002 harvesting season from research farms of Oklahoma State University, and from private and commercial pecan growers in Oklahoma. Nuts were stored in cold chambers maintained at 5 °C. Ninety nuts were randomly chosen from each lot of cultivars and numbered. From these, three groups of 30 randomly chosen nuts were formed. Group I was used for nut characteristics, group II for shell & nutmeat characteristics, and group III for moisture content determination. Each nut of group II was broken, shell and nutmeat were separated manually, weighed to determine nutmeat-to-shell ratio, and placed in numbered plastic bags. All nuts



of group I and group II (in open plastic bags) and 15 nuts from group III were then placed in a constant humidity chamber maintained at 25°C and 78% relative humidity (Rh). Samples were equilibrated in the constant humidity chamber for a period of at least 7 days. Fifteen nuts of group III were broken and used for moisture content determination. After determination of physical characteristics, these same nuts of groups I and II and remaining 15 nuts of group III were equilibrated for at least 7 days in constant humidity chamber maintained at 25°C and 40% Rh. Physical characteristics of group I and II and moisture content of group III were again determined.

### ***Size Characteristics***

Size was determined using digital calipers (Digimatic Calipers, Mitutoyo, Japan) to an accuracy of 0.1 mm. Length (L), maximum ( $D_1$ ) and minimum ( $D_2$ ) diameters around largest periphery (Fig. 3.1) were then determined, for all 30 nuts of group I, as size characteristics for whole nut. Shell thickness was determined using the same micrometer with a thickness adapter. Thickness was measured at 15 random places on shell of 12 nuts of group II. The same samples were used for thickness determination at the two Rh levels. Geometric mean diameter ( $D_e$ ) and sphericity ( $\phi$ ) of nuts were determined using the following expressions (Gupta and Das, 1997):

$$D_e = (L \cdot D_1 \cdot D_2)^{1/3} \quad (3.1)$$

$$\phi = \frac{(L \cdot D_1 \cdot D_2)^{1/3}}{L} \quad (3.2)$$

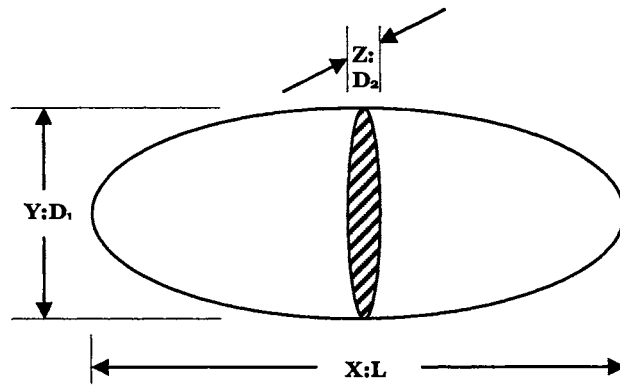


**Figure 3.1 Principal dimensions of a pecan nut in three Cartesian coordinates.**

### ***Specific Gravity***

Specific gravity of nuts, shell, and nutmeat was determined using the water displacement method. A specific gravity bottle (60 ml pycnometer) and ultra-filtered water (specific gravity 1.0) was used. Many different fluids/pseudofluids like, mustard seeds, air, toluene, and kerosene have been used to determine specific gravity of variety of commodities (Heaton et. al., 1982, Joshi, et. al., 1993; and Gupta and Das, 1997, Singh and Goswami, 1996; Aydin, 2002; Özarıslan, 2002; Abhayawick, et. al., 2002, Irtwange and Igbeka, 2002). However, water was chosen, because it is easily available, and it does not chemically react with pecans. Also, during brief submergence water did not penetrate samples, and use of the pycnometer bottle allowed submergence of sample into the fluid.

The pycnometer was filled with ultra-filtered water, capped and excess water was removed. The outside of the bottle was wiped dry and weighed ( $W_1$ , g). After recording weight in air ( $W_2$ , g), the sample was placed in an empty pycnometer bottle. The bottle was filled with ultra-filtered water, gently tapped

against a soft surface so that entrapped air, if any, came to top. The bottle was refilled, capped, and excess water was removed, then the outside of the bottle was wiped dry and weighed ( $W_3$ , g). Specific gravity of the sample (SG) was then determined by:

$$SG = \frac{W_2}{W_1 - (W_3 - W_2)}. \quad (3.3)$$

### ***Moisture Content***

Moisture content of the pecan nutmeat and shell was determined separately by the forced air oven method: keeping 5 replicates of approximately 10-g sample at 100° C for 24 h.

## **X-ray Imaging Equipment Development**

### ***Components of the Equipment***

Schematic of the equipment setup is shown in Fig. 3.2. The equipment consists of an X-ray tube that generates polychromatic X-rays, an X-ray camera, a computer, and two data acquisition and control cards for communication between equipment and computer.

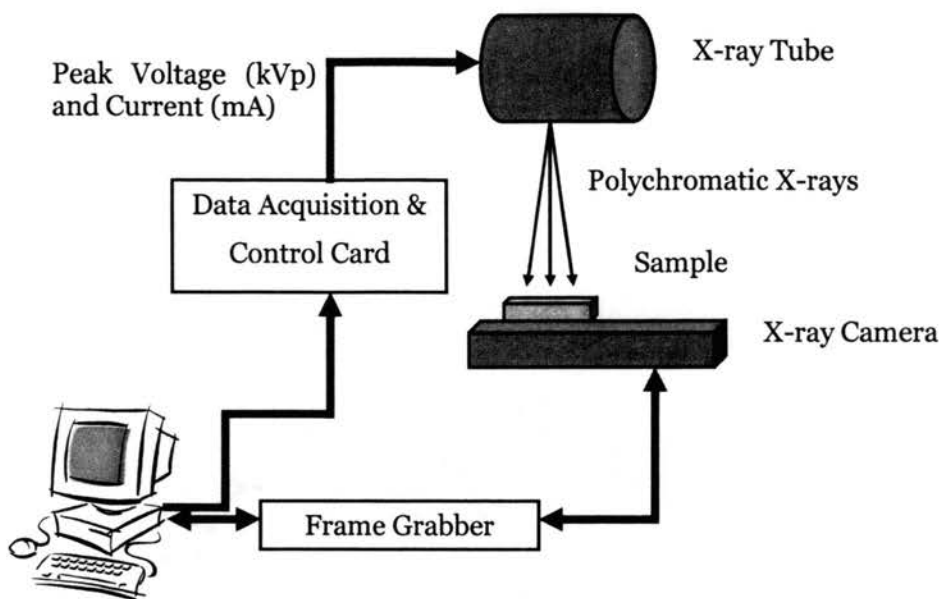


**Figure 3.2 Schematic of the equipment setup.**

### X-ray Tube

The X-ray tube (Model: XTF TM -5011, Oxford Instruments, X-Ray Technologies, Inc., Scotts Valley, CA) features are shown in Table 3.1. Figure 3.3 (courtesy <http://www.oxfordxtg.com>) shows cut-away view of the X-ray tube.

**Table 3.1 X-ray tube features**

Anode voltage	4 - 50 kV
Current	0 - 1 mA
Spot shape, Size	Oval, 76x93 $\mu\text{m}$
Cone angle	25°
Anode material	Tungsten
Window	127 $\mu\text{m}$ Beryllium
Dimensions	163.4 mm length by 69.8 mm diameter
Weight	1816 g
Maximum power	50 watts continuous

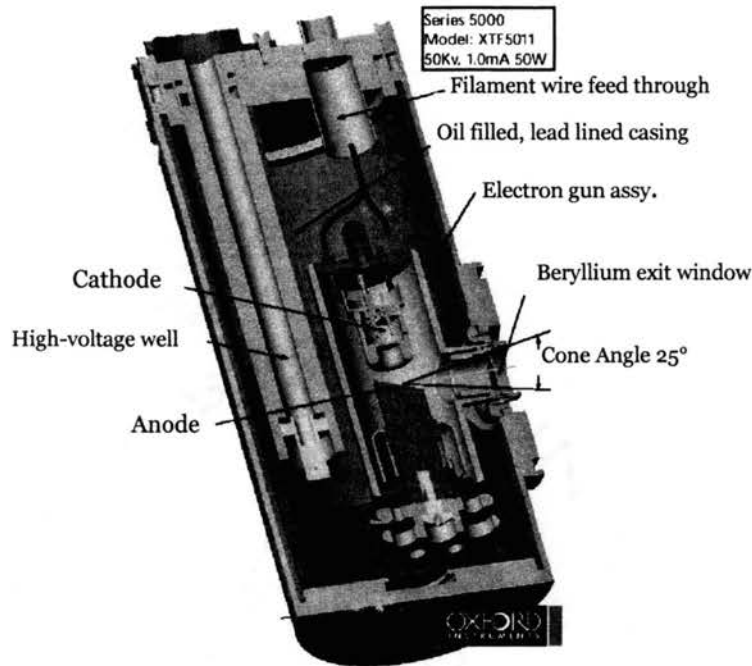


**Figure 3.3 Cut-away view of the X-ray tube.**

### X-ray Camera

The X-ray camera (Shad-o-Box™ -1024, Rad-Icon, Inc., Santa Clara, CA) is a system for high-resolution radiation imaging. The camera has a two-dimensional photodiode array containing 1024 by 1024 pixels on 48 μm centers giving a sensing area of 49.2 x 49.2 mm. A Gd<sub>2</sub>O<sub>2</sub>S scintillator screen, placed in direct contact with the photodiode array, converts incident X-ray photons to light, which in turn is detected by the photodiodes. A graphite window shields against ambient light and protects the sensitive electronics from accidental damage.

The analog signal from the photodiode sensor is digitized to 12-bit resolution in two parallel A/D channels inside the camera. Pixel clock, line-enable, and frame-enable signals are available at the connector to facilitate

acquiring the image data with a standard digital frame grabber. The camera delivers a 4000:1 dynamic range (defined as the maximum signal divided by the read noise) at a maximum frame rate of 2.7 frames per second. The camera (Fig. 3.4) operates from a standard +5V/+12V desktop power supply and consumes less than 5 W of power.

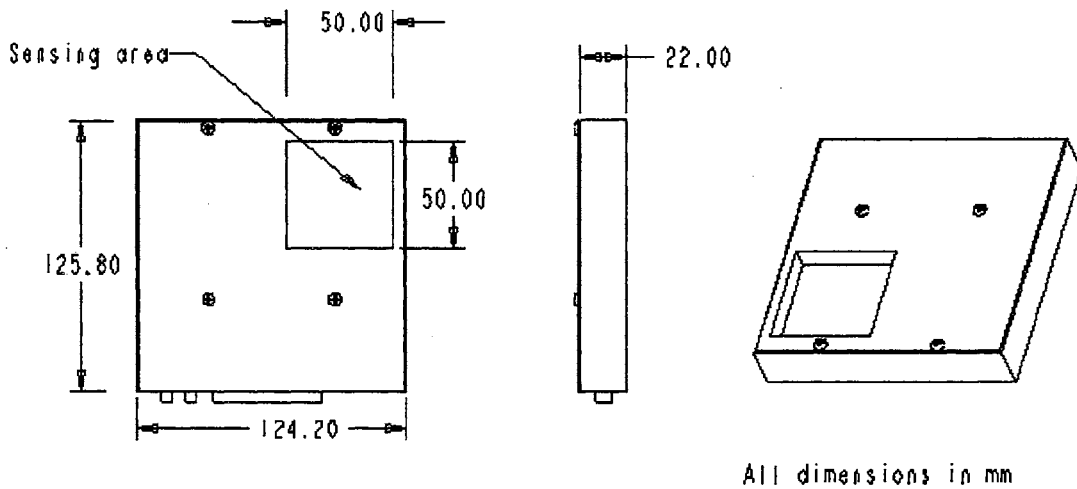


**Figure 3.4 Front, side, and isometric view of X-ray camera.**

### Computer and Communication Cards

A personal computer with Intel Pentium® III processor was used with the equipment. Signal from the photodiode sensor is acquired by the frame grabber (Imagination® PXD 1000, Imagination Corp., Beaverton, OR) mounted on this computer. A data acquisition and control card (Omega® DAQ 801 OM, Omega Engineering, Inc., Stamford, CT) was mounted on the computer for X-ray tube control.

## ***Shield Design***

X-rays in the range of 10-50 keV are about 10,000 times more energetic than visible light. Due to high energy content, the photons can penetrate many materials. This electromagnetic radiation also has ionization properties that can kill biological cells (Desrosier, 1960, Currey, et al., 1990), and hence a proper shielding is required while dealing with X-rays.

For this X-ray systems, maximum dose will be generated when the X-ray tube operates on 50 kVp and 1 mA. Shield thickness to protect against this dose was determined using two approaches.

Approach I - Incorporating buildup due to shield (Eq. 2.2) in Equation 2.1, thus Equation 2.1 becomes:

$$I = I_0(1 + B_x)e^{-\mu_m z \rho} . \quad (3.4)$$

A conservative estimate of  $B_x$  is  $1.148 \times 10^{-9}$  calculated at a distance of 0.25 m away from a source of 3 MeV, 2 mA, 1 cm diameter electron beam and area occupancy factor of 1 (Anon, 1994). Equation 3.4 was then solved for shield thickness,  $z$ .

Approach II – Using Equation 2.5 and solving for shield thickness,  $z$ .

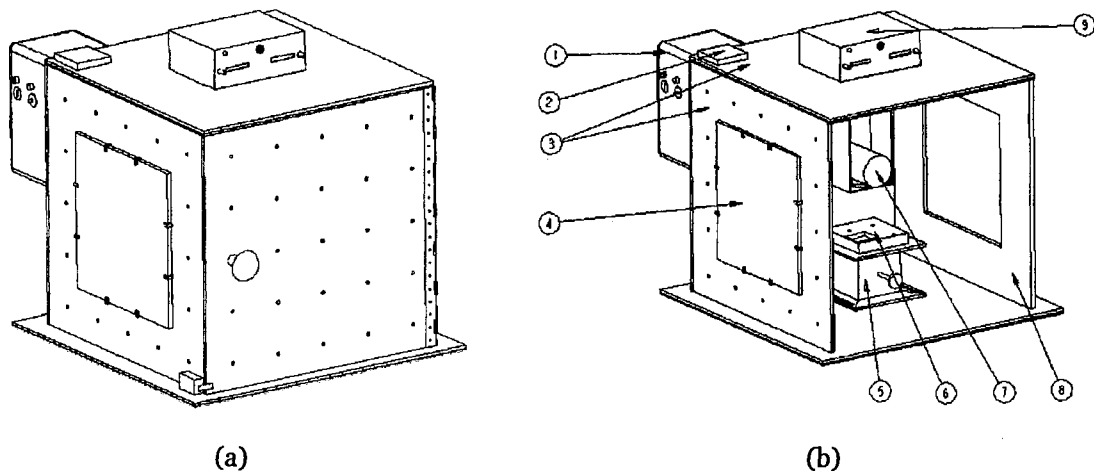
Mass attenuation coefficient of Pb for 50 keV is  $\mu_m = 6.74 \text{ cm}^2/\text{g}$  (Hubbell and Seltzer, 1995). Linear attenuation coefficient  $\mu = \mu_m * \text{Density} = 6.74 \text{ cm}^2/\text{g} * 11.35 \text{ g}/\text{cm}^3 = 76.49 \text{ cm}^{-1}$

For a 1 million times reduction of photon energy through shielding, i.e.,  $I/I_0 = 10^{-6}$ , the required thickness for lead shield was 1.805 mm (using Approach I) and 1.829 mm (using Approach II). Considering additional safety factor and

commercially available thickness of lead sheet, a value of 3.175 mm (1/8<sup>th</sup> inch) was selected for shielding.

### ***Construction of Equipment***

The box dimensions are 500 mm x 500mm x 500mm (20"x20"x20"). The box exterior is made of 6.35 mm (0.25") aluminum sheet (Fig. 3.5) lined with 3.175 mm (0.125") lead sheet on the inside. Lead provides protection against radiation while the aluminum sheet gives mechanical strength to the box. The lead and aluminum sheets were joined by making equidistant tapered holes on the aluminum sheet and then welding the lead sheet through the holes (Fig. 3.6). This way, shield thickness was not compromised. The box has two windows opposing each other for visual inspection of the sample during radiography. These windows are lead glass (300 mm x 300 mm) for x-ray shielding. A 6.35 mm (0.25") lead sheet beneath the body prevents radiation from going out the bottom. This bottom sheet is not attached to the box.



(1) Power supply system (2) Port for additional cables (3) Al sheet walls (4) Lead glass window (5) Camera stand (6) X-ray camera (7) X-ray tube (8) Lead shielding (9) Power controller

**Figure 3.5 X-ray imaging system.**



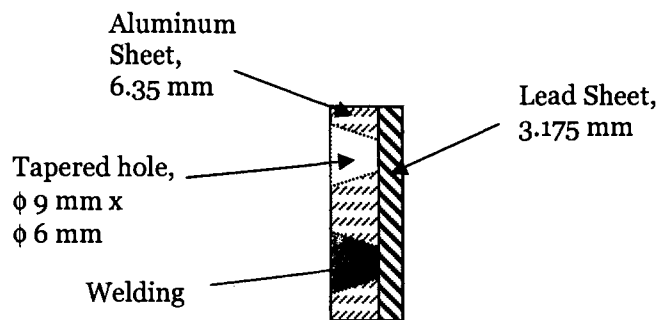
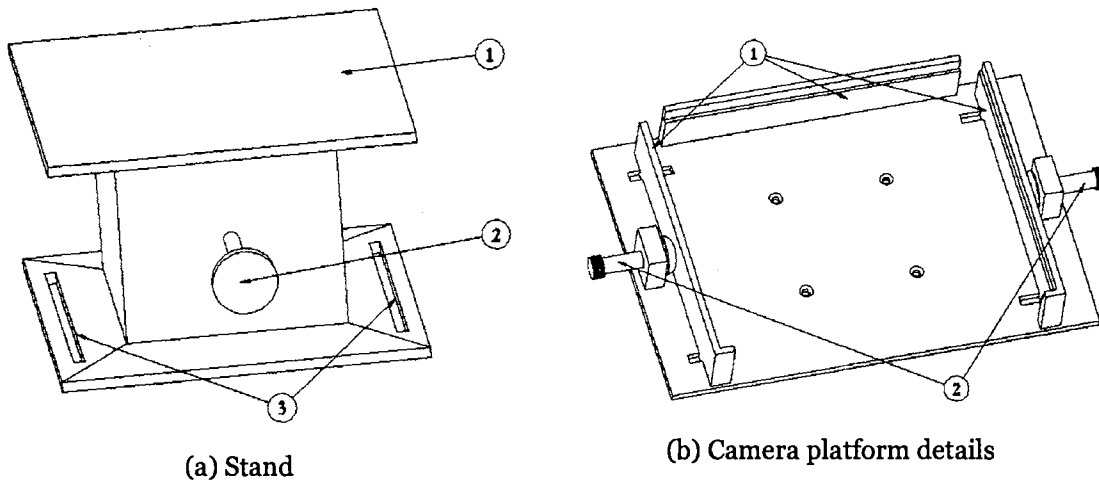


**Figure 3.6 Joining aluminum sheet with lead sheet.**

Camera support mechanism, shown in Figure 3.7 (a and b), allows camera movement in three directions.



(1) Camera platform (2) Knob to adjust height  
 (3) Slots to move camera in direction perpendicular to box door

(1) Cork lined camera support (2) Thumb screws to move camera in direction perpendicular to glass windows

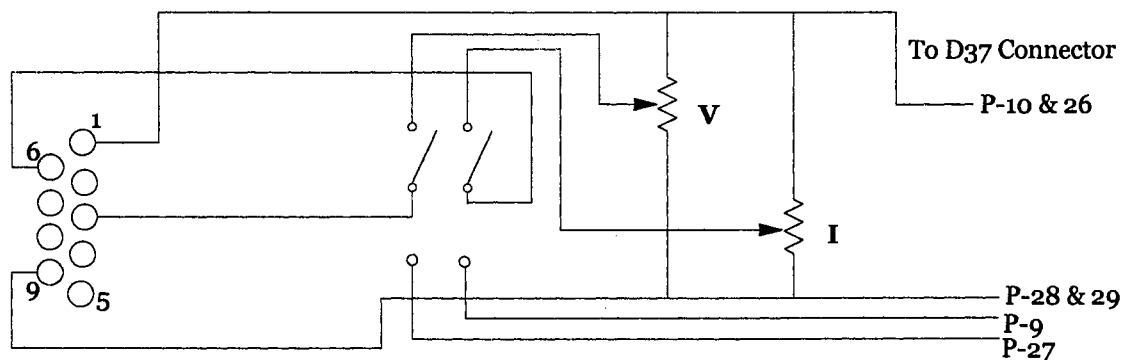
**Figure 3.7 Camera stand.**

Distance of the camera from the X-ray source can be adjusted using the knob. Position of the camera can be adjusted in the direction perpendicular to the box door by moving the assembly on slots (Fig. 3.7 a). The top of this support mechanism (Fig. 3.7 b) has three cork-lined aluminum walls, one of which is fixed and two can be moved to adjust position of camera in the direction

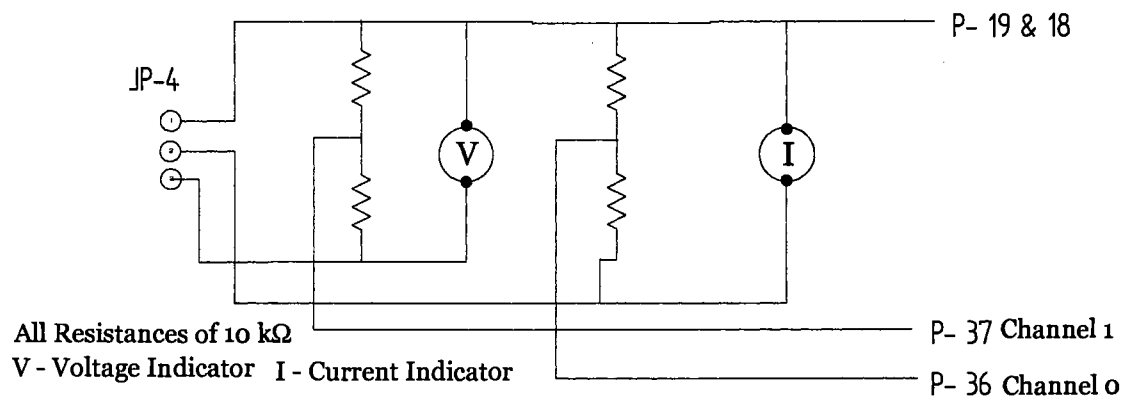
perpendicular to the box windows. Two thumb screws are rotated in opposite directions (one counterclockwise and other clockwise) to move the camera in this direction.

### ***Controls on the Equipment***

A program written in Visual Basic provided a graphic user interface for controlling the X-ray tube inputs, peak voltage, and current. Figure 3.8 shows circuits for manual and computer control.



V - Control Voltage  
I - Control Current

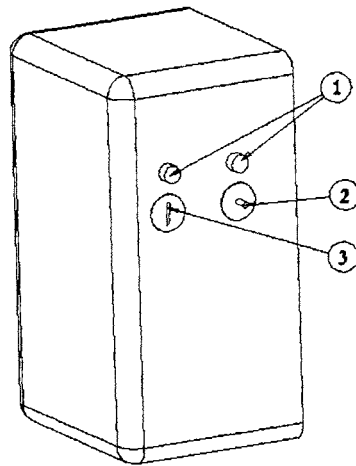


All Resistances of 10 kΩ  
V - Voltage Indicator I - Current Indicator  
P- 19 & 18  
P- 37 Channel 1  
P- 36 Channel 0

**Figure 3.8 Circuit diagram for the X-ray tube controller.**

The power circuit has been designed so that the X-ray generator will work only if all the following conditions are met: (i) main switch is ON, and (ii) 'Key switch' is switched ON using proper key, and (iii) door is shut properly, and (iv) temperature of the x-ray tube is below 55° C. A thermal switch has been mounted on the X-ray tube to cut OFF power if temperature rises above 55° C.

The power supply system (Fig. 3.9), located at the back of the shielded box converts 110 VAC to the required high voltage for the X-ray tube. Two switches and two indicator lamps are placed on this box. Current flows from the main switch to the 'key switch' to the x-ray power supply system. Therefore X-rays will not be generated unless both switches are ON. The key switch can be turned ON using its appropriate key. Indicator lamps when glowing indicate that the corresponding switch is ON.

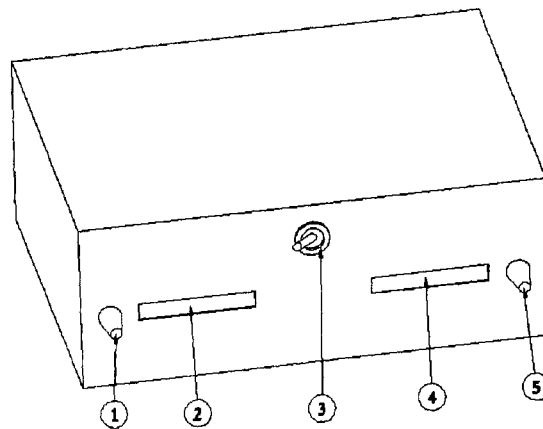


(1) Indicator lamps (2) Main switch (3) Key switch

**Figure 3.9 Power supply system.**

A power controller (Fig. 3.10), placed on top of the shielded box, is used to control the X-ray generation power and current flowing between the electrodes of the X-ray tube. The controller has a selector switch to select manual control or

remote control, two analog potentiometer displays, two rotary knobs, and a power indicator lamp. The controller selector when switched to 'Remote' takes controls from the attached computer through 'X-ray control software' and when switched to 'Manual' takes controls set by rotating the controller knobs manually. On the left side is the power controller and on the right is the current controller. The display has a needle that moves between a scale of 0 to 10, indicating the power and current. For the power, 10 represents 50 kVp while for current, 10 represent 1 mA. The potentiometer scale is linear, i.e. needle positioned at 6 indicates 30 kVp or 0.6 mA. The power controller is operational only when the X-ray tube is receiving electrical power, i.e., when X-rays are being generated.



(1) Voltage controller (2) Voltage potentiometer (3) Manual/Remote control switch (4) Current potentiometer (5) Current controller

**Figure 3.10 X-ray power controller.**

### ***Operating Procedure***

The equipment should be operated with some precautions. Only authorized persons wearing a radiation dose-monitoring badge should operate the equipment, and condition of shielding, and electrical connectors should be checked regularly.

## Camera Alignment

Camera was aligned with the X-ray beam fan to match the center of the beam with the center of image. The camera was raised to maximum possible height so that the X-ray beam fan did not cover the whole detector area and formed a nominal circular image. Position of camera was then adjusted in the two directions in the horizontal plane to match the center of this circle with the center of detector area. Distance between the X-ray tube and camera was then increased by lowering the camera until the X-ray beam fan covered the whole detector area.

## Acquiring Images

ShadoCam® (Rad-Icon, Inc., Santa Clara, CA) software was used to acquire images. The software supports image acquisition and pixel correction, offset correction, gain correction, setting frame exposure time, viewing image in different modes (continuous, single frame, average of multiple frames), setting lookup table, and storing image data in 'raw' or 'tiff' format. Pixel correction was performed using a pixel map provided by the camera manufacturer. Dark current of CCD-based detectors changes with surrounding temperature (Barna et al., 1999), therefore offset images were taken at an interval of about two minutes (for more explanation refer Kotwaliwale et al., 2003 in Appendix I). Gain or flat-field correction was applied, but not during image acquisition, and is discussed later in Image Processing section. Frame exposure time was set to 460 ms (minimum possible value). Lookup table limits were set to 0-4095, appropriate for 12-bit depth pixel intensity. Repeatability of this equipment was already

established by Kotwaliwale et al. (2003); therefore only single-frame images were acquired. Offset corrected images were saved in 'Raw' format and later processed using MATLAB (The Mathworks, Inc., Natick, MA).

### X-ray Control Software Operations

Software was developed in Visual Basic® to provide graphical user interface for controlling X-ray tube inputs, voltage and current through a data acquisition and control (DAC) card. The software accepts positive and real numbers between 0 and 50 for voltage values and between 0 and 1 for current values. The DAC card converts these digital values to analog signals of 0 to 10 V into two output channels controlling voltage and current, respectively. Performance of the software and DAC card was tested at various inputs by measuring voltage on the two output channels.

### **Testing of the Shielding**

The purpose of shielding is to protect equipment operator(s) from a harmful radiation dose. Effectiveness of shielding was determined by estimating maximum possible dose with, and without, shielding at different distances from the source and by measuring the actual dose.

### ***Theoretical Dose Rate Calculations***

Theoretical dose generated by the X-ray tube with, and without, shielding was calculated as follows. Exposure/flux rate of the X-ray tube at maximum energy, i.e. 50 keV and 1 mA was 780 R/min (7.8 Sievert/min) at 14 cm from exit

window (Boyer, 2002). Considering an isotropic point X-ray source, although this is not true, however this could be the worst condition that X-rays are emitted in all directions by same intensity. In air, exposure may be scaled by the inverse square law (Anon., 1994) and for low-energy X-rays, the absorbed dose is equal to exposure (Knoll, 1989). Therefore the absorbed dose at the proposed shield distance (25 cm from source) would be  $7.8 * \frac{(14)^2}{(25)^2} = 2.446$  Sieverts/min. Radiation energy will drop exponentially (Eq. 2.1, page 29) across the lead shield. The dose across the shield would be  $2.446 \cdot \exp(-\mu_m \cdot \rho \cdot z)$ . Mass attenuation coefficient of lead is 8.041 cm<sup>2</sup>/g, density of lead is 11.35 g/cm<sup>3</sup> (Hubbell and Seltzer, 1995). Therefore, dose coming out through 0.3 cm lead shielding would be 3.15x10<sup>-12</sup> Sieverts/min. Annual absorbed dose values at different distances from the X-ray source were calculated assuming equipment use of 600 hours per year.

### ***Actual Dose Measurement***

Actual dose was measured at 21 locations ( at three levels – bottom, half way to top and above X-ray exit window level) inside the shielded box, but not directly under the X-ray beam, and at 72 places outside the shielded box, when X-rays were emitted at 50 kVp and 1 mA (maximum possible energy for the tube). A dosimeter (Keithley 35050, Inovision Radiation Measurements, Cleveland, OH) with 150-cc ion chamber (Model 77957 H-60) was used to measure dose rate in mR/min. Minimum possible reading on the instrument was 5 μR/min. Values were converted in Sieverts/year assuming equipment use of 600 hours per year.

## Determination of Attenuation Coefficient

Pecan nutmeat was cut into uniformly thick slices using a razor saw. Ten slices of different thickness (Table 3.2) were used to determine the attenuation coefficient of pecan nutmeat of Native and Improved cultivars. Pecan shells were broken into small fragments such that the thickness of each fragment was uniform. Nine samples of varying thickness (Table 3.2) for each cultivar were used to determine attenuation coefficient of pecan shell. Each sample of pecan nutmeat and shell was placed on a 152- $\mu\text{m}$  thick polyethylene sheet over the camera so that the sample was 10 mm from the detectors and 153 mm away from the X-ray source window. Three replications were taken for each sample by placing the sample at three different places over the detector. Images of each sample were taken at eight voltage levels from 15 to 50 kVp in steps of 5 kVp and at a current at which the blank image (image without any sample) did not saturate (more details about image saturation in Kotwaliwale et al., 2003). Linear attenuation coefficient ( $\mu$ ) was calculated using Equation 2.1 (page 29) for each of the pixel points representing sample in the image. Depending on physical size of the sample, each sample covered about 7,000 to 15,000 pixels.

**Table 3.2 Thickness of pecan nutmeat and shell samples used to determine attenuation coefficient.**

Cultivar	Nutmeat slice thickness, mm	Shell thickness, mm
Native	1.6, 3.0, 3.6, 4.7, 4.7, 4.8, 7.1, 10.3, 13.8, 15.4	0.6, 0.8, 0.8, 0.9, 1.0, 1.0, 1.0, 1.1, 1.2
Improved	1.6, 2.5, 3.0, 3.7, 4.9, 5.3, 5.5, 6.2, 8.9, 15.8	0.5, 0.5, 0.5, 0.6, 0.6, 0.6, 0.8, 0.8, 0.9



### Fabrication of Pecans of Desired Quality

For development of pecan quality determination, it is imperative that samples of many possible defects should be tested using the equipment. Since finding pecans of known internal defects is difficult, it was decided to fabricate pecans. Pecan nuts of two types, Native and Improved were cut in half along the plane of the natural joint of two halves, using a razor saw. Nutmeat from cut halves was carefully removed, and nutmeat of known weight and artificially created defects, viz. holes, mechanical damage, weevil larvae, etc. were placed in the cut shell halves. These shell halves were then joined using wood glue. Defects were also created in some shells. Ten such samples, five each of Native and Improved were fabricated for X-ray imaging. Characteristics of each fabricated nut are given in Table 3.3.

**Table 3.3 Characteristics of fabricated nuts.**

<b>Sample No.</b>	<b>Nut cultivars</b>	<b>Weight nutmeat, g</b>	<b>Weight nut, g</b>	<b>Nutmeat feature</b>	<b>Shell feature</b>	<b>Insect</b>
1	Native	1.78	3.85	Good	Good	No
2	Improved	1.81	3.76	Slightly broken	Slightly broken	No
3	Native	1.10	2.73	Damaged	Crack	No
4	Improved	1.50	3.56	Pieces	Good	No
5	Native	0.62	2.29	One cotyledon	Good	No
6	Improved	1.92	3.81	Insect hole	Slight damage	Wet
7	Native	1.39	3.17	Insect hole	Good	No
8	Improved	2.48	4.94	Insect hole	Good	No
9	Native	1.36	3.04	Damaged	Good	Dry
10	Improved	1.84	3.57	Damaged	Good	Wet

## **Imaging of Pecans**

### ***Fabricated Pecans***

Images of each fabricated pecan nut were taken by placing it on a 152- $\mu\text{m}$  thick polyethylene sheet over the camera so that the sample was at 10 mm from the detectors and 153 mm away from the X-ray source window. Each sample was placed at random locations over the detectors with two orientations, i.e. with joint of two pecan halves parallel and perpendicular to the camera plane. Images were taken at eight X-ray tube voltage levels from 15 to 50 kVp in steps of 5 kVp, and five current levels, 0.1, 0.25, 0.5, 0.75, and 1.0 mA. Image integration time was 460 ms and each image was corrected by an offset image taken at each voltage level.

### ***Imaging of Unknown Samples***

Thirty pecans were selected from a lot in such a way that there were some apparently good nuts, some mechanically damaged nuts, some nuts with holes in the shell (indicating high possibility of weevil damage), and some nuts had shucks attached (indicating high probability of undeveloped or underdeveloped kernel). Shucks were removed from the nuts prior to imaging. Images were taken only at energies found appropriate in the previous experiment with fabricated nuts. Images were taken with nuts in two orientations, i.e., joint of two halves parallel and perpendicular to the camera plane. Sample location over the detectors was varied randomly for different samples and positions. Samples were

placed on a 152- $\mu\text{m}$  thick polyethylene sheet over the camera so that the sample bottom was 10 mm from the detectors and 153 mm away from the X-ray source window.

## **Image Processing**

### ***Preprocessing***

The imaging software stores image data in 12-bit depth. Images were read in image processing software MATLAB (2001) as 16-bit image matrix with the first four bits as zeros. Resolution of the recorded image was 1024x1022 pixels, however it was noticed in pre-trials that some pixels near the border were either inactive or did not respond as expected. Therefore, the central 1000 x 1000 elements of the recorded image matrix were used in further processing. A flow chart of the image preprocessing procedure is shown in Figure 3.11. Preprocessing was performed to segment the region of interest (ROI), i.e. pecan samples, from the image background. In all cases, the background was brighter than the ROI because of attenuation of X-rays by the sample. Because each sample was stationary for all the voltages and currents, the pixel map of the ROI for each sample was obtained from only one condition, i.e. 20 kVp and 1 mA. First, all pixels of the sample image (I) taken at 20 kVp and 1 mA were normalized between 0 and 1 by pixels-wise dividing by a blank image (B - image without any object in path of X-ray beam) also taken at 20 kVp and 1 mA. Ideally, all the pixels not representing the sample should have a value of one, but to account for variation in detector response, a threshold of 0.9 was used to

segment the ROI from background. A logical matrix (L) of size of the image was thus obtained wherein elements representing the sample pixel had a value of 'one' while those representing background had zero.

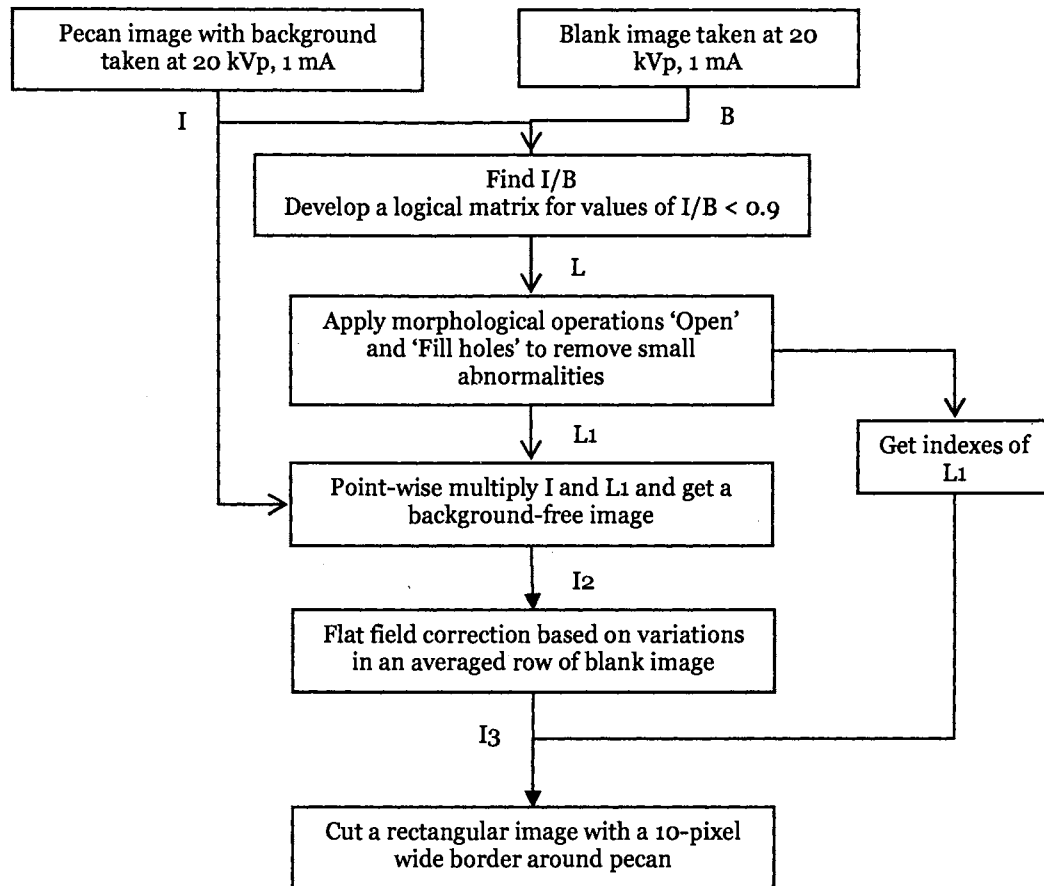


**Figure 3.11 Flow chart for X-ray image preprocessing.**

### Morphological operations

Morphological operation 'open' was applied on the matrix 'L' to remove any stray or small cluster of 'ones' from the background portion of the image. A disk-shaped structural element with 5-pixel radius was used for the 'open' operation. Morphological operation 'fillholes' removed any stray or small

clusters of 'zeros' from the ROI. Thus, a refined logical matrix 'L1' was obtained. Indices of matrix 'L1' were used for all the images of that sample taken at different voltages and currents. Point-wise multiplication of this matrix by the original image matrix produced a matrix in which all background pixels were black, i.e. their intensity value was zero, whereas all ROI pixels had the same intensity value as assigned by the camera.

### Flat-field correction

There are 1024 amplifiers in the camera, one for each column of detectors. However, due to variations among amplifier response, columns looked distinctly different from each other (Fig. 3.12).

Intensity means ( $\bar{I}_j$ ) for each column were calculated for a blank image taken at a voltage and current with which the detectors did not saturate. Flat-field correction factors ( $\bar{F}_j$ ) were calculated for each column by dividing image grand mean ( $\bar{I}$ ) by intensity means ( $\bar{I}_j$ ) for each column. Image intensity values in each row were multiplied by the respective flat-field correction factor to obtain a corrected image.

$$\bar{I}_j = \sum_i I_{i,j} / \text{Max}(i) \quad (3.5)$$

$$\bar{I} = \sum_j \sum_i I_{i,j} / (\text{Max}(i) \cdot \text{Max}(j)) \quad (3.6)$$

$$F_j = \bar{I} / \bar{I}_j \quad (3.7)$$

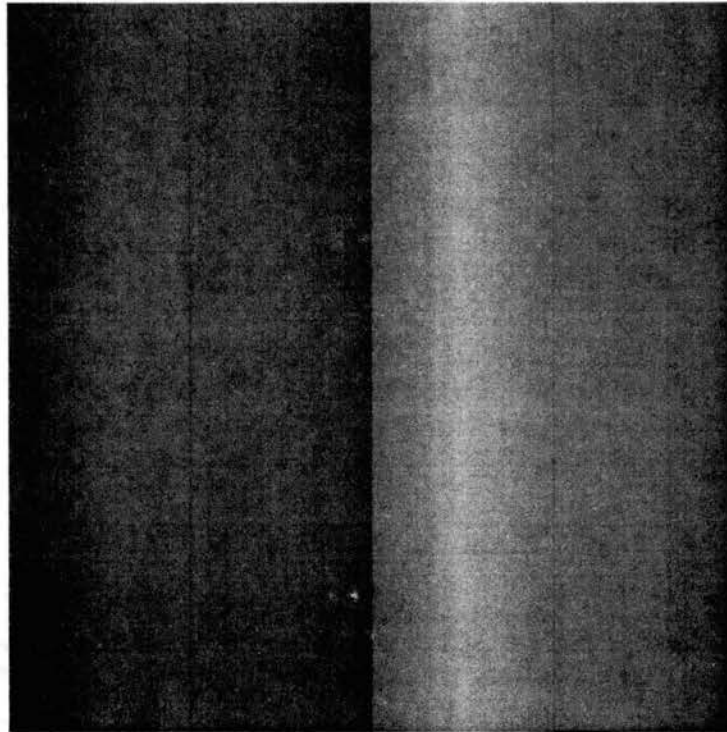


**Figure 3.12 A blank image ( $I_0$ ) taken at 50 kVp, 0.22 mA, 460 ms demonstrating detector variation.**

### ***Determination of Attenuation Coefficient***

Because the nutmeat and shell samples were small, six to nine samples could be accommodated over the detectors without touching each other. Images were preprocessed to segment the background from different ROI's. Indices of each sample were determined using 'blob analysis' with the largest 'blob' representing the background and the next six to nine 'blobs' representing each ROI. Images for determination of attenuation coefficient were obtained at X-ray energy levels for which blank images did not saturate. Therefore, intensities at each point of the respective blank images were used for ' $I_0$ ' in the Equation 2.1. Flat-field correction was not necessary for the images taken to determine

attenuation coefficient, because multiplicative correction cancels out while taking the ratio of incident and attenuated intensities ( $I/I_0$ ).

### ***Determination of Appropriate X-ray Energies for Pecan Imaging***

Low-energy X-rays were attenuated almost completely by a sample, making all pixels in the image ROI very dark. The sample was highly transparent to high-energy photons, which produced a bright image ROI. Both these conditions are undesirable because of lack of contrast between the pecan shell and nutmeat regions. All the visually 'good' images had histograms centered in the central 2/3rds region of the image dynamic range (0 to 4095). Other criteria defining good contrast are the mode and the spread of the histogram. The greater the difference between intensities at the first and second mode, the greater will be the contrast. Similarly, more spread of the histogram base represents greater image contrast.

A program was written in MATLAB (2001) to analyze all 800 images taken for 10 fabricated pecan samples at eight voltage levels and five current levels. Images were preprocessed using the algorithm explained earlier, and histograms were generated from the pixels in the ROI. The mode of the image was determined as the bin representing maximum frequency. Spread of the histogram was determined as the difference between the maximum bin and the minimum non-zero bins. The percent of the pixels representing the central 2/3rds of the histogram was calculated to determine the shift of the histogram from the center of the dynamic range (0-4095 gray levels).

## **Statistical Analysis**

Physical properties data were analyzed to test the effect of cultivar and relative humidity in storage on: (i) size characteristics of the whole pecan nut, (ii) shell thickness, (iii) specific gravity of whole nut, shell, and nutmeat, and (iv) moisture content of shell and nutmeat. The physical properties experiment was analyzed as a factorial design with cultivars and relative humidity as blocks. Data at two relative humidity levels were considered as paired.

Linear attenuation coefficients were analyzed for the effect of sample (shell and nutmeat), sample thickness, and sample cultivar. Regression coefficients were determined for a relationship between linear attenuation coefficient and sample thickness. SAS (SAS Institute, Inc., Cary, N.C.) V. 8.2 was used for statistical analysis of data.



## **CHAPTER IV**

### **RESULTS AND DISCUSSION**

#### **Physical Properties**

##### ***Moisture Content***

Mean moisture content values (wet basis) of the shell of the four varieties Native - A, Native - B, Squirrels Delight, and Maramek were found to be 10.10%, 11.77%, 11.1%, and 11.15%, respectively at 40% Rh and 16.19%, 18.54%, 17.01%, and 18.83%, respectively at 78% Rh. These values for the nutmeat of the four varieties were 3.2%, 2.68%, 2.96%, and 2.79%, respectively at 40% Rh and 5.59%, 4.87%, 4.61%, and 4.75%, respectively at 78% Rh. Effect of Rh on moisture content of the shell and nutmeat is shown in Figures 4.1 and 4.2. Statistical analysis of moisture content values reveals that shell and nutmeat moisture contents for all cultivars differ significantly between Rh 40% and Rh 78% ( $p < 0.0001$ ). Nutmeat moisture contents for both relative humidity levels and shell moisture contents at 78% Rh differ among cultivars ( $p < 0.0001$ ), while shell moisture content values at 40% Rh do not differ among cultivars ( $p < 0.1628$ ). Further analysis showed that at 40% Rh, equilibrium moisture content (EMC) values for shell as well as nutmeat were significantly different between Natives

and Improved cultivars. At 78% Rh, EMC values for both nutmeat and shell were not significantly different between Natives and Improved cultivars. This result indicates that Natives and Improved varieties have different moisture absorbing capacities. The reason might be differences in oil content and differences in shell thickness between the two types of cultivars.

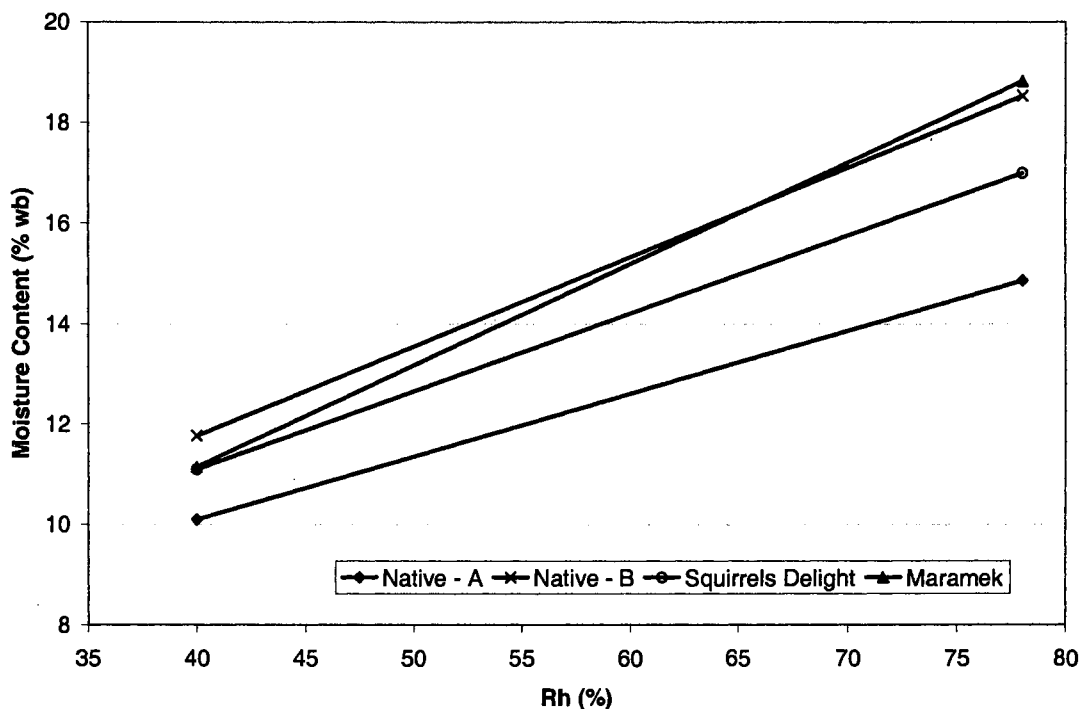


**Figure 4.1 Effect of air humidity on moisture content of shell for four pecan cultivars.**

(Each plotted point represents average of five data values)

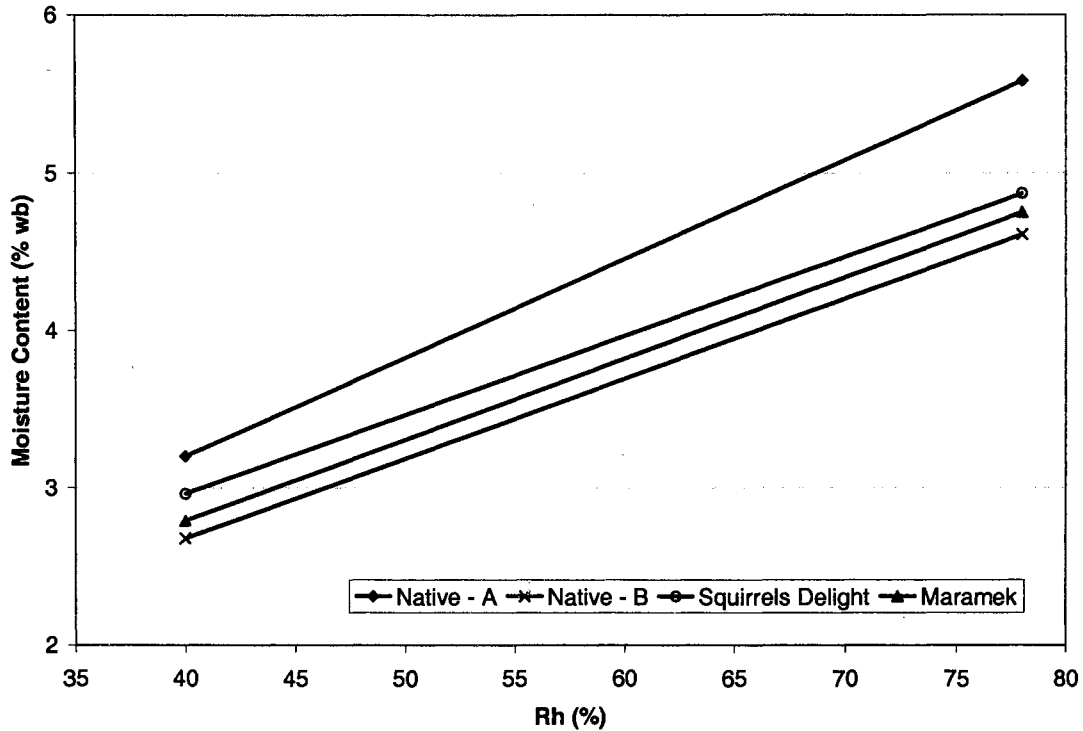


**Figure 4.2 Effect of air humidity on moisture content of nutmeat for four pecan cultivars.**

### ***Nutmeat-to-Shell Ratio (NSR)***

Mean of weight of nutmeat to shell ratios (NSR) were 0.814, 1.193, 1.035, and 1.331, respectively for 'Native - A,' 'Native - B,' 'Squirrels delight,' and 'Maramek.' The difference among cultivars was statistically significant ( $p < 0.0001$ ). Multiple comparisons showed that NSR values for each cultivar were significantly different from each other ( $p < 0.0001$ ). Weights of 100 whole nuts determined at 78% Rh were 241 g, 570 g, 473 g, and 620 g, respectively for 'Native - A,' 'Native - B,' 'Squirrels Delight,' and 'Maramek.'

## ***Principal Dimensions***

Length, maximum, and minimum diameters around the largest periphery for the four pecan cultivars equilibrated at 40% and 78% Rh are listed in Table 4.1. Mean values are plotted in Figures 4.3 and 4.4. Generally, all the dimensions were higher for pecans equilibrated at 78% Rh. The increase is more pronounced for 'Maramek,' indicating a tendency to swell more than the other cultivars. Also, 'Maramek' had a higher coefficient of variation (CV) for all the characteristics compared with those of the other cultivars. In general, CV values were less than 10%. Figure 4.5 shows frequency distributions of length, which resembles a normal distribution for all the four cultivars. Maximum and minimum diameter values along the largest periphery had similar distributions.

Pecan lengths were significantly different among cultivars and were significantly different between 40% & 78% Rh ( $p \leq 0.0223$ ) indicating that both cultivar and storage Rh significantly affect the length of the pecan nut. Statistical analysis showed that relative humidity did significantly affect diameters, while cultivar did not significantly affect maximum diameter of nut along the largest periphery. Both cultivar and Rh significantly affected minimum diameter of nut around its largest periphery.

**Table 4.1 Size characteristics of whole pecan nuts for four cultivars equilibrated at 40% and 78% Rh.**

Cultivar		Length, mm		Max. Diameter, mm		Min. Diameter, mm	
		40% Rh	78% Rh	40% Rh	78% Rh	40% Rh	78% Rh
Native - A	Mean	34.93	35.54	17.34	17.58	16.58	17.03
	CV, %	5.50	4.86	2.95	2.89	4.02	3.24
	Max	38.2	39.5	18.3	18.5	17.9	18.1
	Min	30.1	32.7	16.3	16.6	15.5	16.1
Native - B	Mean	35.17	36.12	20.28	20.78	18.28	19.29
	CV, %	5.49	5.56	3.18	3.09	12.71	3.08
	Max	38.7	39.7	21.3	21.8	20.2	20.5
	Min	31.8	32.5	18.5	18.9	10	18.1
Squirrels Delight	Mean	33.11	34.00	18.96	18.89	17.42	17.54
	CV, %	4.77	5.41	3.16	3.87	3.49	3.33
	Max	35.9	36.9	20.2	20.7	18.6	18.5
	Min	29.3	30.0	17.7	17.4	15.8	16.3
Maramek	Mean	37.92	39.13	19.68	20.42	18.35	18.60
	CV, %	9.66	9.49	7.17	7.19	8.19	7.67
	Max	44.8	45.9	23.2	23.9	20.9	21.1
	Min	31.4	32.3	17.3	17.8	15.6	16.0

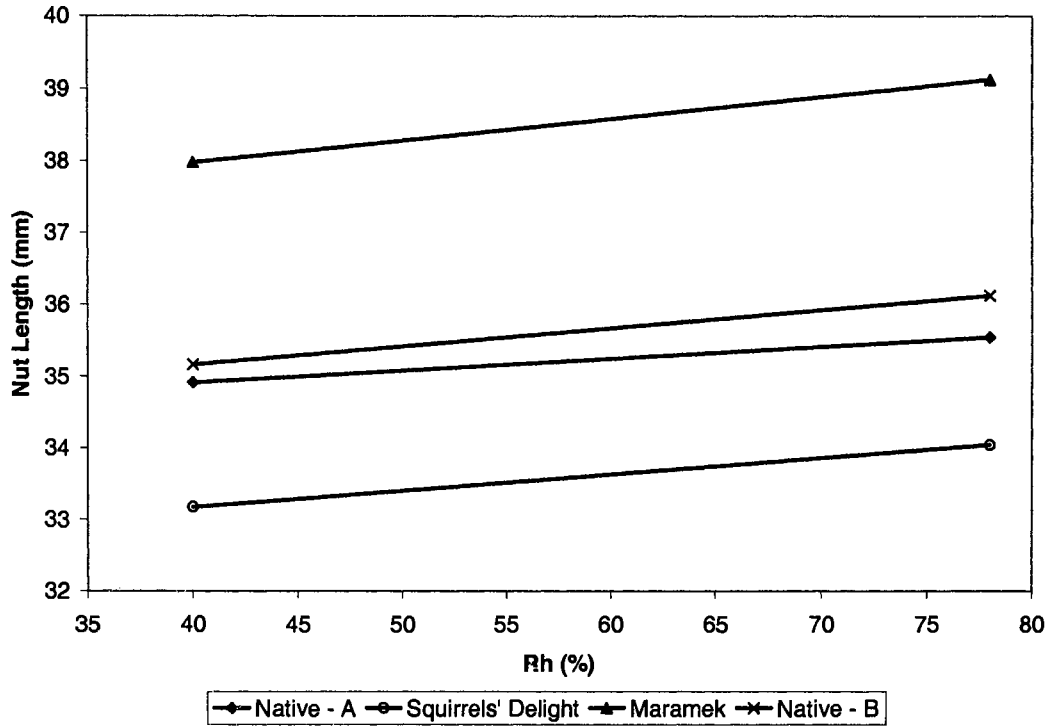


Figure 4.3 Length of whole nuts for four cultivars at two air humidities.

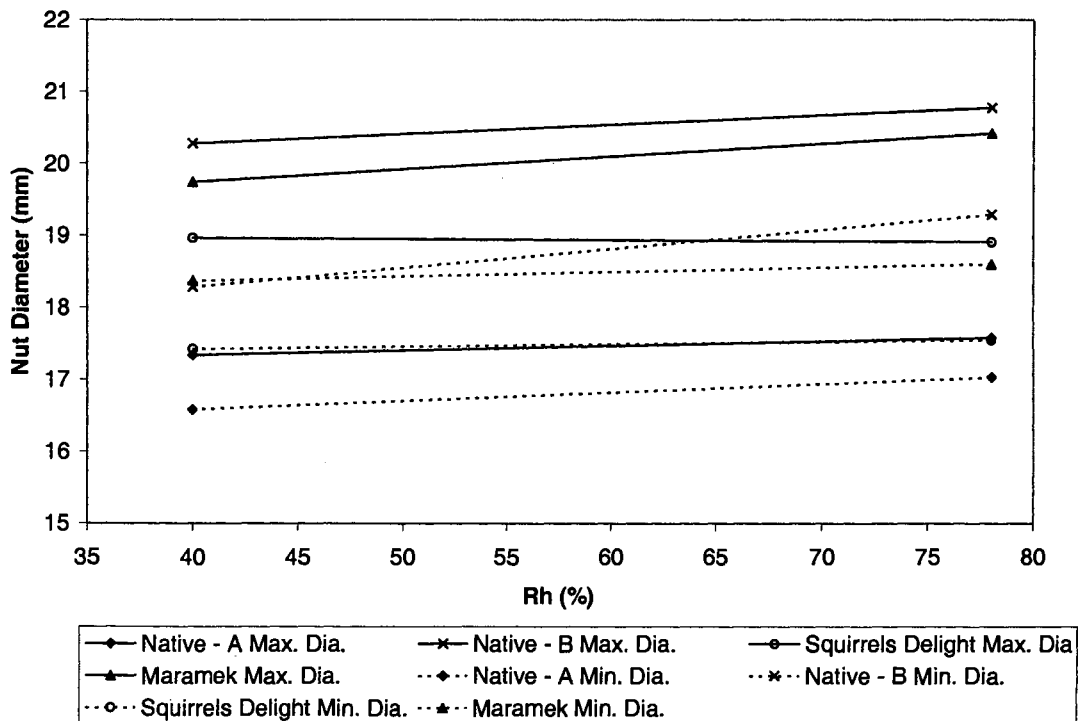
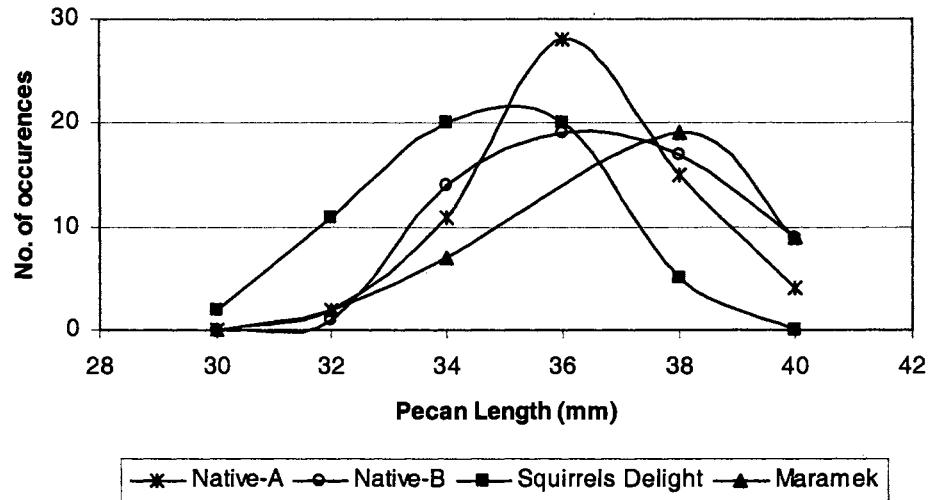


Figure 4.4 Diameter of whole nuts for four cultivars at two air humidities.



**Figure 4.5** Frequency distribution of pecan length for four cultivars.

### ***Geometric Mean Diameter (GMD) and Sphericity***

Values of geometric mean diameter (GMD) and sphericity, calculated from the principle dimensions, are presented in Table 4.2. The GMD increased for pecans equilibrated at higher humidity, which might be due to swelling of the shell at higher moisture content. However, statistical analysis showed that the increase was not significant for 'Native - A' and 'Squirrels Delight.' At both humidity levels, GMD values differed significantly among cultivars, as did sphericity values. There was no significant effect of humidity levels on sphericity of nuts, indicating that change in dimension due to humidity was not directional. The shape of pecan nuts belonging to a particular cultivar is unique. This characteristic may be seen by noting that CV values for both GMD and sphericity are lower than 10% and lower than many corresponding CV values of size characteristics. Also, these values are not as variable as those reported by

Balasubramanian (2001) for other crops like raw cashew nut (GMD 18.71 – 27.52 mm and sphericity 0.62 – 0.86).

**Table 4.2 Geometric mean diameter and sphericity of whole pecan nuts of different cultivars equilibrated at 40% and 78% Rh.**

Cultivar		GMD, mm		Sphericity	
		40% Rh	78% Rh	40% Rh	78% Rh
Native - A	Mean	21.57	21.99	0.62	0.62
	CV, %	3.45	3.04	3.30	2.94
	Max	22.85	23.35	0.65	0.66
	Min	19.67	20.72	0.56	0.58
Native - B	Mean	23.48	24.37	0.67	0.68
	CV, %	6.02	3.19	5.96	3.24
	Max	25.34	25.78	0.72	0.72
	Min	18.96	22.32	0.54	0.63
Squirrels Delight	Mean	22.21	22.41	0.67	0.66
	CV, %	3.06	3.61	3.10	2.91
	Max	23.49	24.18	0.73	0.70
	Min	20.59	20.65	0.62	0.63
Maramek	Mean	23.91	24.52	0.63	0.63
	CV, %	7.76	7.62	4.23	4.20
	Max	27.50	28.10	0.71	0.71
	Min	20.50	21.06	0.60	0.60

### **Shell Thickness**

Mean, CV, maximum, and minimum values of shell thickness observed for the four cultivars are listed in Table 4.3. Means are plotted in Figure 4.6.

**Table 4.3 Shell thickness of four cultivars at two humidity levels.**

	Native - A		Native - B		Squirrels Delight		Maramek	
	40% Rh	78% Rh	40% Rh	78% Rh	40% Rh	78% Rh	40% Rh	78% Rh
Mean, mm	0.81	0.83	0.61	0.65	0.50	0.59	0.60	0.59
CV, %	19.02	19.04	18.85	22.57	28.04	19.32	22.49	22.96
Max, mm	1.4	1.3	1.0	1.2	1.3	0.9	1.1	1.3
Min, mm	0.5	0.5	0.3	0.4	0.3	0.3	0.4	0.3



Shell thickness CV values are quite high compared with the CV values obtained from other physical characteristics. This result may be due to randomness of observations and also due to the presence of a spongy layer on the inside of shell, the thickness of which varies with location. The same reason could be given for a reduced shell thickness with increased Rh for two cultivars. Statistical analysis showed that shell thickness was significantly different among all cultivars, with Native having significantly thicker shells than Improved cultivars ( $p < 0.0001$ ). These observations are in agreement with statements made by Worley (1994 pp. 12). Humidity levels affected shell thickness significantly for only two cultivars, Squirrels Delight and Native - B ( $p < 0.039$ ).

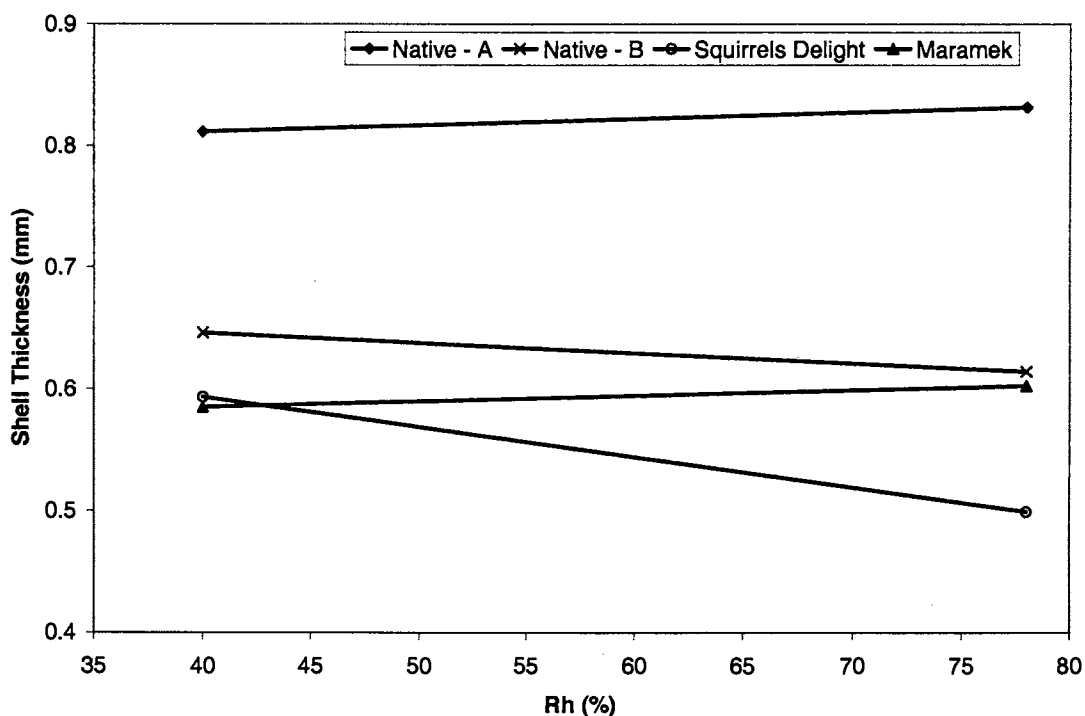


**Figure 4.6 Shell thickness of cultivars as affected by humidity.**

## ***Specific Gravity***

Table 4.4 gives basic statistics of specific gravity values for whole nut, shell, and nutmeat of four pecan cultivars equilibrated at 40% and 78% Rh.

**Table 4.4 Specific gravity values for whole nut, shell, and nutmeat of four pecan cultivars equilibrated at 40% and 78% Rh.**

Cultivar		Specific Gravity					
		Nut		Shell		Nutmeat	
		40% Rh	78% Rh	40% Rh	78% Rh	40% Rh	78% Rh
Native - A	Mean	0.878	0.880	1.109	1.098	0.933	0.937
	CV, %	2.89	2.92	6.59	5.79	2.78	2.84
	Max	0.918	0.925	1.205	1.201	0.968	0.983
	Min	0.798	0.801	0.802	0.852	0.855	0.858
Native - B	Mean	0.851	0.840	1.047	1.085	0.967	0.960
	CV, %	3.03	3.03	5.57	10.89	1.80	1.66
	Max	0.886	0.874	1.184	1.427	0.990	1.002
	Min	0.752	0.745	0.941	0.935	0.916	0.915
Squirrels Delight	Mean	0.830	0.843	1.038	1.046	0.979	0.985
	CV, %	4.33	2.72	6.49	3.99	1.95	1.67
	Max	0.871	0.886	1.276	1.1150	1.004	1.009
	Min	0.683	0.784	0.945	0.9525	0.921	0.927
Maramek	Mean	0.793	0.782	0.979	0.982	0.928	0.917
	CV, %	10.37	9.64	11.51	11.78	3.74	4.06
	Max	0.852	0.848	1.123	1.131	0.983	0.965
	Min	0.455	0.459	0.709	0.690	0.837	0.820

These measured values of nut specific gravity are in agreement with the values (reported by Heaton et al., 1982) of 0.83 to 0.86 for the 'Stuart' cultivar of pecan nuts. Figure 4.7 (a, b, c, & d) shows the effect of relative humidity on specific gravity of different components and pecan nuts of different cultivars. The shell had the highest specific gravity, followed by nutmeat for all cultivars. Even though the nut is made up of shell and nutmeat, the specific gravity of the whole

nut is less than both of these, due to the presence of air pockets between nut and shell. Statistical analyses reveal that specific gravity values of the whole nut, shell, and nutmeat at 40% & 78% Rh, are significantly different among the four cultivars ( $p < 0.0001$ ). Relative humidity has a significant effect on specific gravity of whole nut for three cultivars, but not for 'Native - A.' Shell specific gravity values were not affected by relative humidity except for 'Native - B.' Relative humidity had a significant effect on specific gravity of nutmeat for all cultivars ( $p \leq 0.0432$ ). Contrast analyses between 'Natives' and 'Improved' cultivars showed that specific gravity values at both humidity levels of both whole nuts and shells of Improved cultivars were significantly different from those of Native cultivars. ( $p < 0.0001$ ); while they were not significantly different for the nutmeat ( $p > 0.46$ ).

### **Effectiveness of Shielding**

The calculated absorbed dose at various distances from the X-ray source, with and without shielding, is shown in Figure 4.8. It is evident that a lead shield of 3.175 mm reduces the dose by about 10 log cycles to  $9.5 \times 10^{-6}$  Sieverts/yr, much below the dose limit of 0.05 Sieverts/yr permitted by the U.S. Nuclear Regulatory Commission (NIEHS., 2002).

A maximum of 6480 Sieverts/yr dose was measured inside the shielded box, but not directly under the X-ray beam. At all locations outside the shielded box where measurements were taken, no dose was detected by the instrument, indicating that actual dose escaping from the shield must be less than 0.0018 Sieverts/yr. For all practical purposes, no detectable radiation escaped the enclosure.

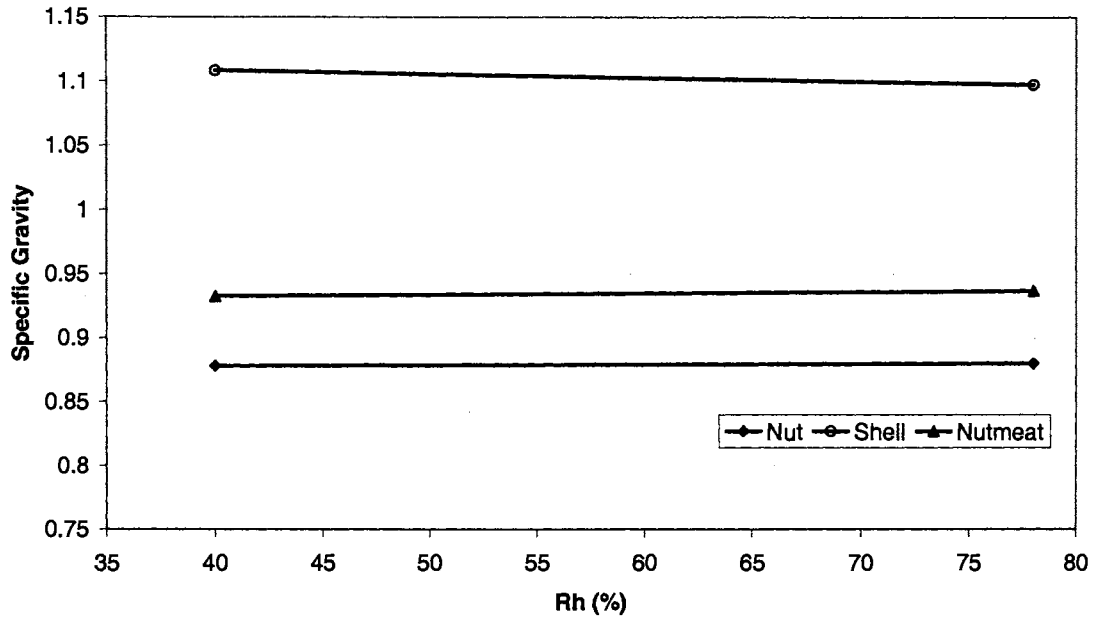


Fig. 4.7(a) Native - A.

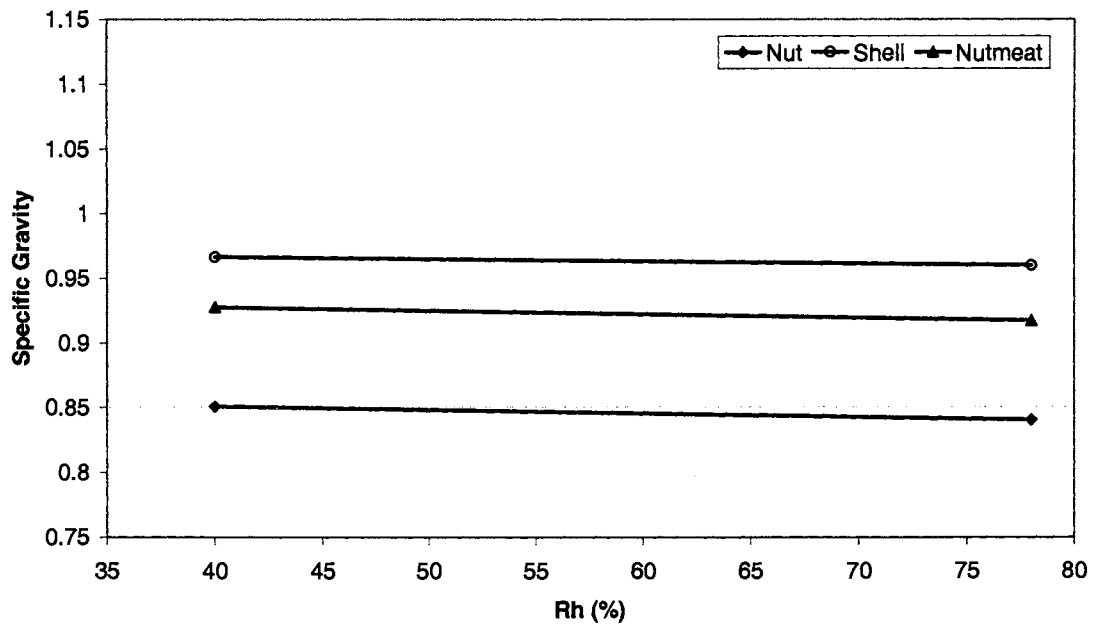


Fig. 4.7(b) Native - B.

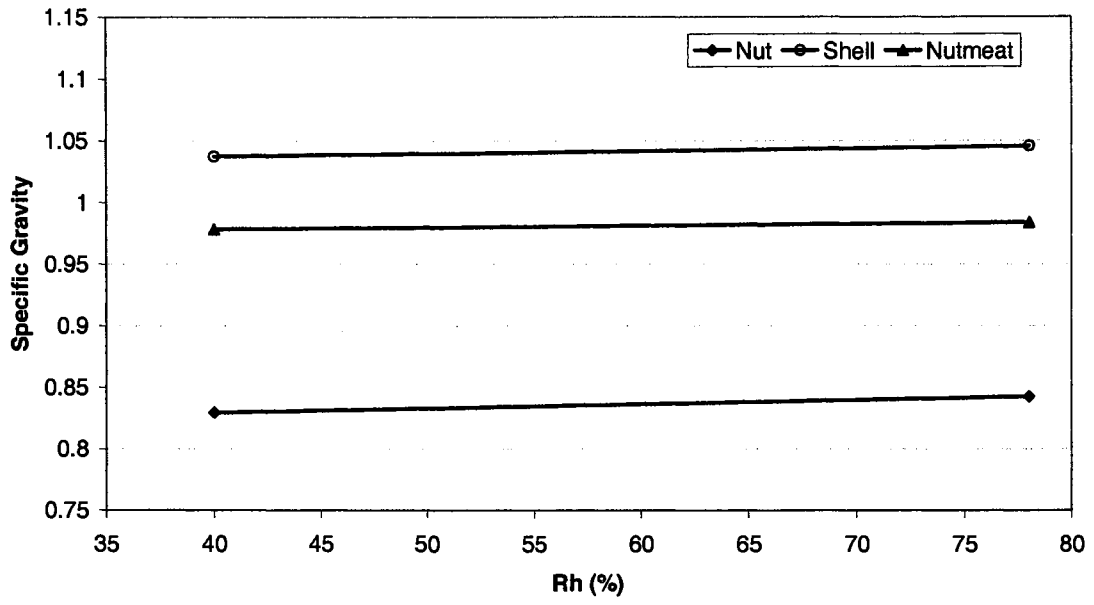


Fig. 4.7(c) Squirrels Delight.

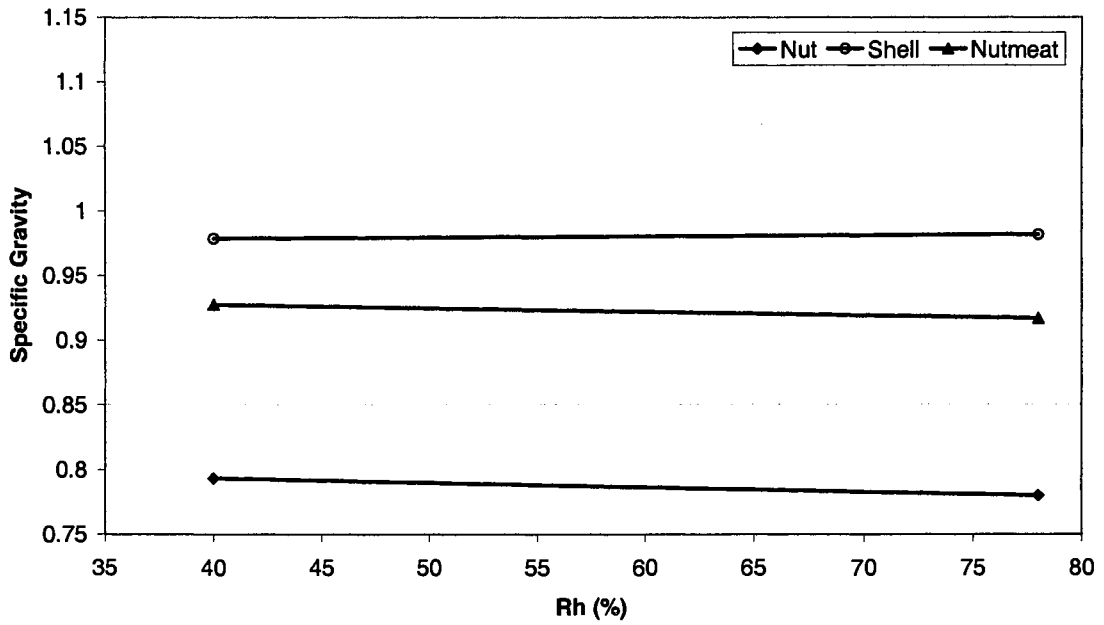
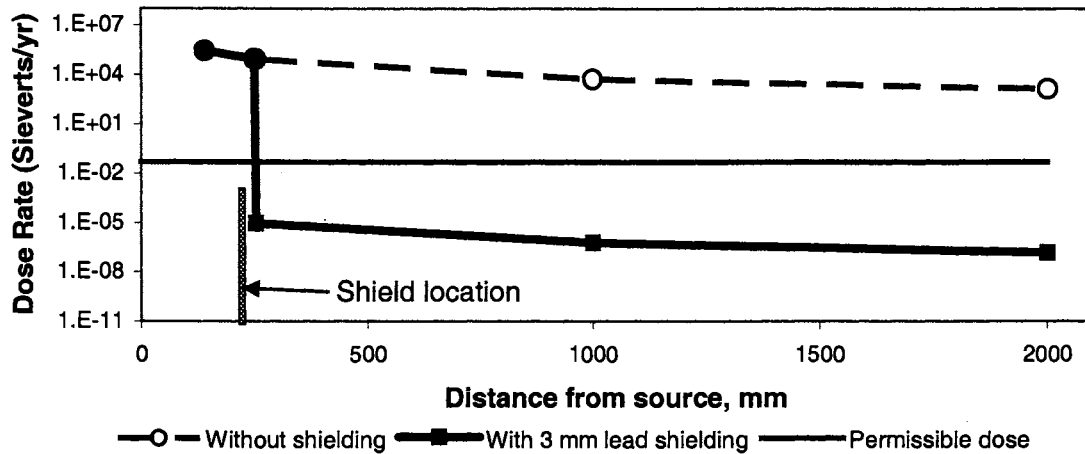


Fig. 4.7(d) Maramek.

**Figure 4.7 Specific gravity of pecan components as affected by humidity for four cultivars.**



**Figure 4.8 Variation in dose rate with distance and effect of shielding.**

### Equipment Calibration

A separate study on calibration of the equipment was undertaken. Results of that study are given in Appendix-A (Kotwaliwale et al., 2003). Detectors were found to saturate at high X-ray tube voltage and current combinations. One million regression models, one for each pixel in the image field, were therefore developed to predict pixel intensity in 12-bit intensity depth for given voltage and current values.

### Attenuation Coefficient

A linear attenuation coefficient ( $\mu$ ) is a material property obtained by multiplying mass attenuation coefficient ( $\mu_m$ ) and material density ( $\rho$ ). Values of  $\mu$  for pecan nutmeat and shell were calculated using Equation 2.1 (page 29) for each pixel in images of nutmeat and shell samples of known thickness. There were approximately 10,000 pixels in each image. Mean and CV values for the

linear attenuation coefficients are shown in Tables 4.5 and 4.6 (page 81 and 82) for pecan nutmeat and shell, respectively.

The CV values represent variations within an image and variations among three images taken at the same voltage and current conditions, but at different locations over the detector. Mean CV values due to variation in sample location over the detector were 3.23 and 3.47 % for pecan nutmeat and shell, respectively. Sample thickness did not affect the coefficient of variation among samples due to their location over the detector, which is evident from Figure 4.9. The  $R^2$  values for linear relation between thickness and linear attenuation coefficient were 0.22 and 0.10 for shell and nutmeat, respectively. Low  $R^2$  values confirm that CV values were independent from sample thickness.

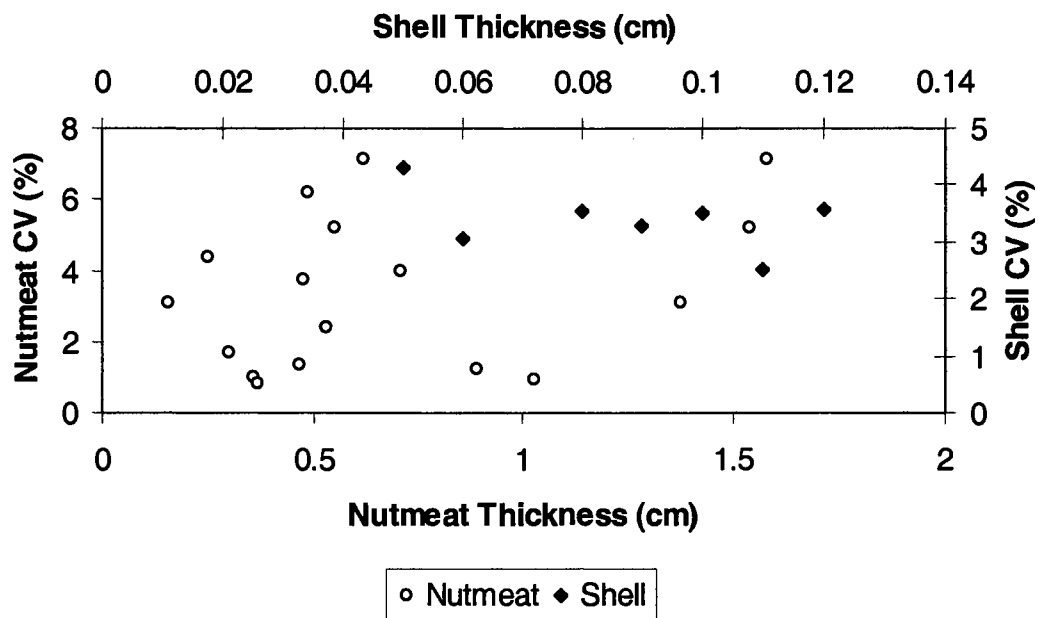


**Figure 4.9 Sample thickness vs. variation in linear attenuation coefficient of pecan nutmeat and shell.**

**Table 4.5 Mean linear attenuation coefficients ( $\mu$ ) of pecan nutmeat at different X-ray energies for two cultivars and different sample thicknesses.**

Cultivar	T*, cm	Data	Peak Voltage, kVp							
			15	20	25	30	35	40	45	50
Improved	0.16	$\mu$ , 1/cm	3.26	2.59	1.98	1.48	1.26	1.21	1.10	1.08
		CV, %	4.02	3.91	4.23	4.28	4.55	4.58	4.81	4.86
	0.25	$\mu$ , 1/cm	2.85	2.17	1.68	1.44	1.23	1.12	1.02	0.98
		CV, %	5.36	5.16	5.38	5.40	5.59	5.71	5.88	6.06
	0.30	$\mu$ , 1/cm	3.20	2.43	1.97	1.71	1.42	1.32	1.21	1.15
		CV, %	6.87	6.59	6.82	6.75	6.96	6.94	7.01	6.89
	0.37	$\mu$ , 1/cm	3.13	2.38	1.90	1.63	1.39	1.29	1.18	1.13
		CV, %	9.83	9.67	10.06	9.90	10.09	9.96	10.01	9.77
	0.49	$\mu$ , 1/cm	2.31	1.77	1.39	1.19	1.01	0.93	0.85	0.83
		CV, %	8.79	8.50	8.71	8.52	8.69	8.60	8.68	8.53
	0.53	$\mu$ , 1/cm	1.87	1.42	1.13	0.97	0.84	0.77	0.70	0.68
		CV, %	7.64	7.28	7.47	7.36	7.49	7.45	7.57	7.48
	0.55	$\mu$ , 1/cm	2.26	1.72	1.37	1.18	1.02	0.93	0.86	0.83
		CV, %	9.29	8.99	9.19	8.94	9.06	9.05	9.03	8.82
0.62	$\mu$ , 1/cm	2.11	1.58	1.27	1.08	0.93	0.86	0.78	0.75	
	CV, %	10.28	9.80	9.98	9.86	9.94	9.88	9.95	9.77	
0.89	$\mu$ , 1/cm	1.67	1.24	0.99	0.84	0.73	0.67	0.62	0.59	
	CV, %	12.58	12.00	12.13	11.98	12.14	12.06	12.20	12.05	
1.58	$\mu$ , 1/cm	1.22	0.93	0.74	0.64	0.56	0.51	0.47	0.45	
	CV, %	14.03	13.76	14.00	13.95	14.21	14.18	14.30	14.20	
Native	0.16	$\mu$ , 1/cm	2.75	2.16	1.93	1.48	-	-	-	-
		CV, %	4.43	4.08	2.72	3.40	-	-	-	-
	0.30	$\mu$ , 1/cm	2.64	2.05	1.57	1.36	1.14	1.05	0.95	0.93
		CV, %	6.07	5.81	6.02	5.90	6.02	6.04	6.20	6.20
	0.36	$\mu$ , 1/cm	2.62	2.02	1.66	1.37	1.14	1.06	1.00	0.97
		CV, %	3.09	2.88	2.88	2.57	2.04	2.11	2.28	2.42
	0.47	$\mu$ , 1/cm	2.53	1.89	1.52	1.25	1.05	1.02	0.95	0.92
		CV, %	3.33	3.43	4.05	4.04	3.14	3.08	2.59	2.62
	0.48	$\mu$ , 1/cm	2.35	1.79	1.42	1.21	1.05	0.96	0.88	0.84
		CV, %	7.94	7.57	7.65	7.46	7.52	7.45	7.51	7.48
	0.71	$\mu$ , 1/cm	2.12	1.58	1.25	1.06	0.91	0.84	0.77	0.74
		CV, %	9.75	9.41	9.61	9.48	9.53	9.41	9.40	9.25
	1.03	$\mu$ , 1/cm	1.95	1.48	1.23	1.03	0.86	0.81	0.76	0.73
		CV, %	3.69	3.36	3.30	2.70	3.56	3.68	3.31	3.28
1.38	$\mu$ , 1/cm	1.47	1.10	0.89	0.76	0.67	0.61	0.56	0.54	
	CV, %	12.28	11.69	11.74	11.63	11.88	11.82	11.93	11.74	
1.54	$\mu$ , 1/cm	1.31	0.97	0.78	0.66	0.58	0.54	0.50	0.47	
	CV, %	12.93	12.24	12.31	12.20	12.38	12.40	12.40	12.32	

\*T = Thickness



**Table 4.6 Mean linear attenuation coefficients ( $\mu$ ) of pecan shell at different X-ray energies for two cultivars and different sample thicknesses.**

Cultivar	Thickness, cm	Data	Peak Voltage, kVp							
			15	20	25	30	35	40	45	50
Improved	0.05	$\mu$ , 1/cm	6.76	5.34	4.08	3.62	3.06	2.83	2.58	2.53
		CV, %	5.66	5.49	5.57	5.56	5.62	5.81	5.95	6.19
	0.06	$\mu$ , 1/cm	6.09	4.75	3.59	3.17	2.69	2.48	2.26	2.22
		CV, %	5.53	5.41	5.54	5.48	5.53	5.76	5.89	6.08
	0.08	$\mu$ , 1/cm	6.81	5.23	4.08	3.55	3.05	2.80	2.56	2.48
		CV, %	5.40	5.20	5.32	5.23	5.34	5.38	5.46	5.56
	0.09	$\mu$ , 1/cm	5.34	4.22	3.28	2.90	2.44	2.29	2.09	2.08
		CV, %	4.46	4.22	4.37	4.42	4.65	4.59	4.70	4.77
Native	0.06	$\mu$ , 1/cm	6.84	5.29	4.19	3.64	3.17	2.89	2.65	2.52
		CV, %	4.22	4.28	4.41	4.54	4.73	5.06	5.29	5.59
	0.08	$\mu$ , 1/cm	6.44	4.96	3.83	3.34	2.83	2.61	2.38	2.33
		CV, %	6.37	6.28	6.49	6.38	6.42	6.49	6.62	6.70
	0.09	$\mu$ , 1/cm	5.89	4.60	3.57	3.12	2.66	2.46	2.25	2.20
		CV, %	4.97	4.88	5.15	5.16	5.18	5.32	5.39	5.53
	0.10	$\mu$ , 1/cm	5.35	4.08	3.07	2.67	2.22	2.05	1.85	1.83
		CV, %	6.89	6.81	7.06	6.99	7.00	7.10	7.18	7.22
	0.11	$\mu$ , 1/cm	5.48	4.18	3.31	2.86	2.42	2.22	2.02	1.96
		CV, %	6.95	6.79	6.97	6.89	7.08	7.11	7.26	7.37
	0.12	$\mu$ , 1/cm	4.99	3.87	3.01	2.62	2.20	2.04	1.86	1.82
		CV, %	6.12	5.93	6.28	6.15	6.10	6.13	6.19	6.32

Another experiment was conducted to attempt to explain the variation in attenuation coefficients due to sample location over detectors. Samples remained in position while three images were taken at eight different voltage levels (15 to 50 kVp in steps of 5 kVp). Linear attenuation coefficients and their CV were calculated at all voltages. Mean CV was 0.6%. This variation can be considered a random error; hence about 1/5th of the variation in attenuation coefficient due to sample location over detectors is due to random noise. The remaining part of the

error could be attributed to variations in detector response and the polychromatic nature of the X-ray beam as already established by Kotwaliwale et al. (2003).

It is also evident from Tables 4.5 and 4.6 that the attenuation coefficients varied with peak X-ray tube voltage (kVp) and sample thickness. Statistical analysis showed that linear attenuation coefficient decreased with higher kVp values and thickness.

At lower energies, linear attenuation coefficient is the sum of the contributions from photoelectric reactions, and Compton scattering (Curry et al., 1990). As the radiation energy, i.e. kVp, increases, the contribution of photoelectric reactions decreases as does the linear attenuation coefficient. Reduction in mass attenuation coefficient (linear attenuation coefficient x material density) with higher X-ray energy is also reported by Hubbell and Seltzer (1995) for many materials. Kotwaliwale et al., 2003 reported that kVp had a quadratic effect on X-ray image intensity. Covariance analysis of the data also supported this finding. Linear attenuation coefficients of nutmeat and shell were found to be affected significantly ( $p < 0.0001$ ) both by the first and second-order terms of kVp.

Effect of thickness on linear attenuation coefficient can be attributed to "beam hardening." Lower energy photons of a polychromatic X-ray beam are preferentially attenuated as the beam passes through a material. This effect results in an increase in the beam mean-energy as it traverses through the material, and thus the beam mean-energy transmitted through a thicker material is greater. Hence, the attenuation coefficient of material reduces with thickness. Kotwaliwale et al. (2003) demonstrated the 'beam hardening' effect for

homogeneous sheets of polystyrene. Covariance analysis of data revealed that linear attenuation coefficient of nutmeat was also affected significantly ( $p < 0.0001$ ) by the first and second-order terms of thickness. In comparison the linear attenuation coefficient of shell was affected only by the first-order terms for thickness. This difference may be due to low variability in shell thickness data (0.05 - 0.09 cm for Improved and 0.06 - 0.12 cm for Native shells).

Linear attenuation coefficient of Native pecan nutmeats was significantly lower than that of Improved cultivar pecans ( $p < 0.0001$ ) for the same material thickness. In contrast, Native shells had generally higher linear attenuation coefficients compared with shells of Improved cultivar of the same thickness. In this experiment, 'Native - A' was used to represent Natives and 'Squirrels Delight' was used to represent nutmeat of Improved cultivar. 'Maramek' was used to represent shell of Improved cultivar. It is noteworthy that nutmeat specific gravity of 'Native - A' was lower than that of 'Squirrels Delight' and shell specific gravity of 'Native - A' is higher than that of 'Maramek' (Table 4.4). This result is in agreement with Curry et al. (1990) who reported that high-density material has a higher attenuation coefficient. Linear attenuation coefficients of nutmeat and shell cannot be compared directly, since their sample thicknesses do not overlap. However, values determined by extrapolating a quadratic relationship between attenuation coefficient and thickness, indicate the linear attenuation coefficient of shell was higher than that of nutmeat at all X-ray tube voltages.

## ***Regression Equations for Attenuation Coefficient***

Regression equations of pecan nutmeat linear attenuation coefficient were modeled as a function of X-ray tube voltage and sample thickness. Initially two models were developed separately for Native and Improved cultivars, because statistical analysis of the data showed that cultivar had a significant effect on attenuation coefficient values. A general model, irrespective of cultivar, was also developed. Model parameters and their corresponding coefficients are shown in Table 4.7. All the parameters shown in Table 4.7 were statistically significant in the model with  $p < 0.0001$ . More statistical analysis of model parameters revealed that  $R^2$  values were less than 0.9 for any combination of three out of the five parameters. Excluding the  $T^2$  term from the model reduced  $R^2$  value from 0.929 to 0.894 and from 0.937 to 0.923 for Improved cultivar and combined cultivars, respectively, while it did not change the  $R^2$  value for the Native cultivar. All three models were plotted (Fig. 4.10 through 4.12) by comparing observed values and values predicted by the model.

**Table 4.7 Regression models of linear attenuation coefficient based on X-ray tube voltage and pecan nutmeat thickness.**

<b>Model</b>	<b>Intercept (A)</b>	<b>T (B)</b>	<b>T<sup>2</sup> (C)</b>	<b>V (D)</b>	<b>V<sup>2</sup> (E)</b>	<b>T·V (F)</b>
Improved cultivar	5.4881	-2.8952	0.6861	-0.1623	0.0016	0.0273
Native cultivar	4.6994	-1.2986	0.0380	-0.1467	0.0015	0.0195
Combined model	5.1160	-2.1764	0.4349	-0.1541	0.0016	0.0222

T - Sample thickness, cm

V - X-ray tube voltage, kVp

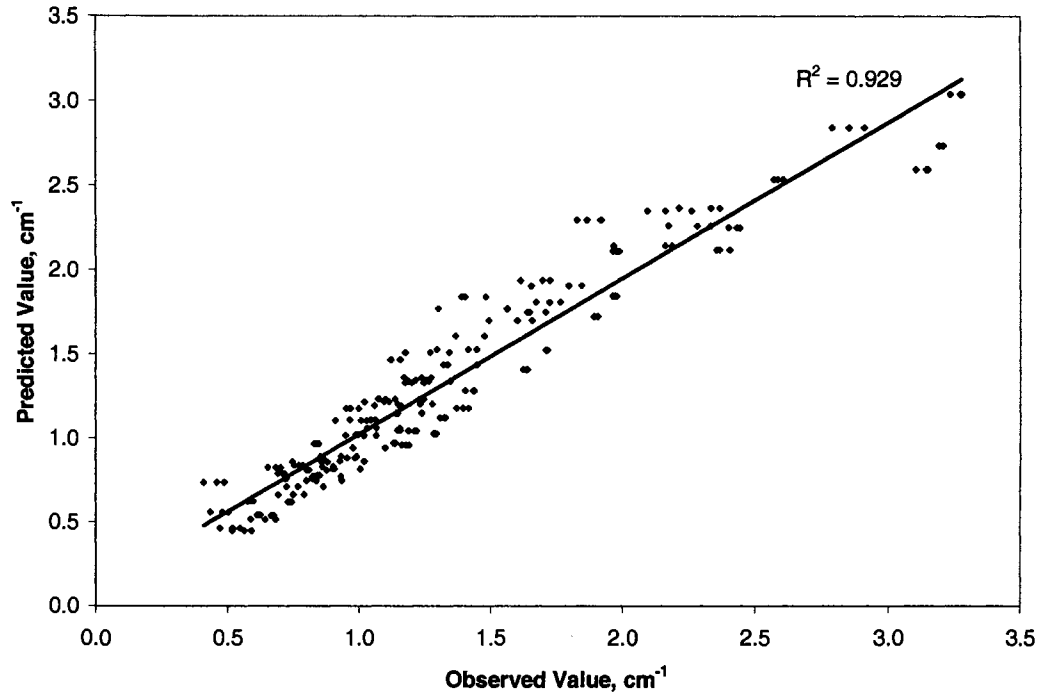


**Figure 4.10 Predicted vs. observed linear attenuation coefficients for improved cultivar 'Squirrels Delight'.**

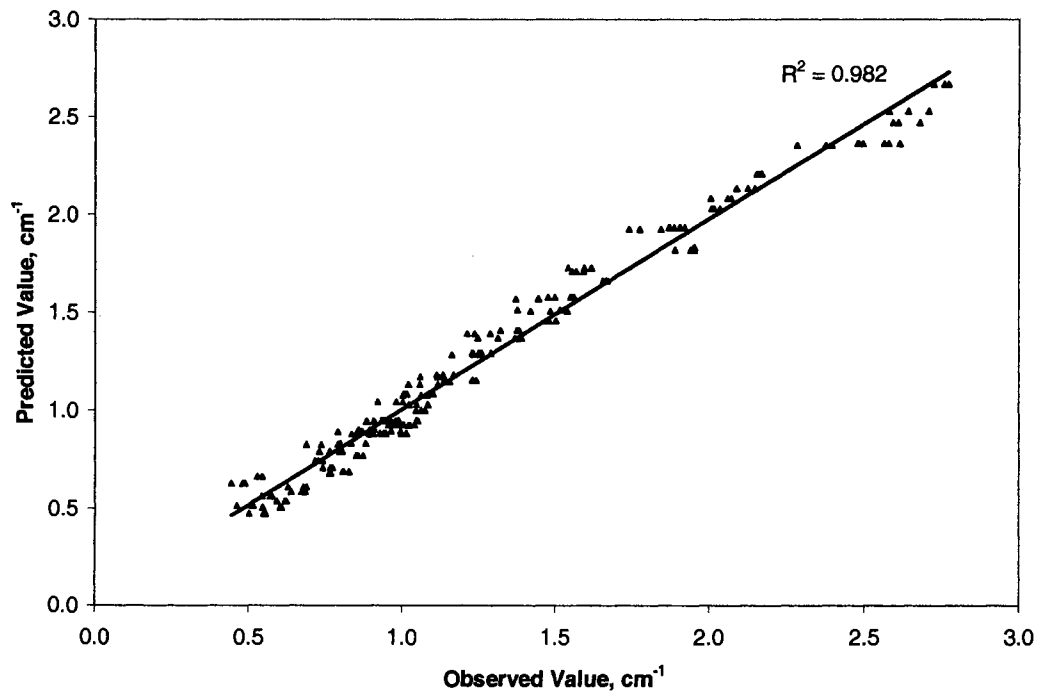


**Figure 4.11 Predicted vs. observed linear attenuation coefficients for native cultivar 'Native - A'.**

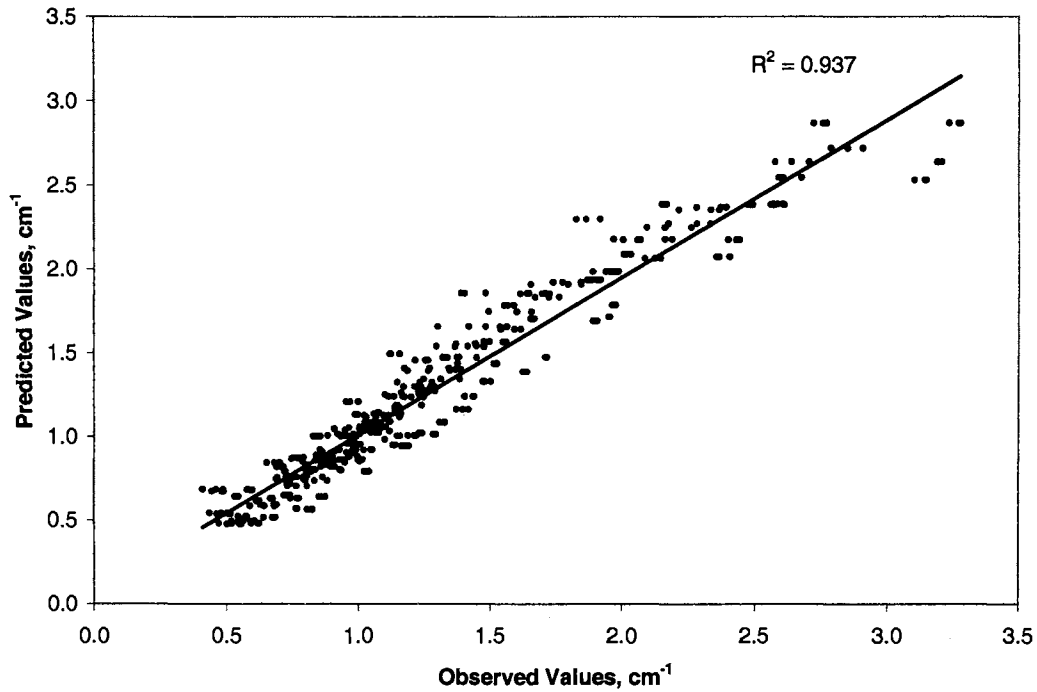


**Figure 4.12 Predicted vs. observed linear attenuation coefficients for combined model.**

### **Appropriate X-ray Energies for Good Contrast Imaging**

X-ray images of fabricated pecan samples (characteristics given in Table 3.3) were acquired at eight levels of X-ray tube voltage (15 to 50 kVp in steps of 5 kVp), five levels of current (0.1, 0.25, 0.5, 0.75, and 1.0 mA), and two orientations of nut (plane joining two pecan cotyledons horizontal or vertical). In total, 800 images were acquired. All images were pre-processed, as explained in Chapter III, and then the following features were acquired from each image to find appropriate X-ray energies for 'good' contrast: (i) percent of image pixels in central 2/3rds part of the image dynamic range (0 to 4095), (ii) variance of the pixel representing pecan in the image, (iii) spread of the histogram base (difference between minimum non-zero and maximum intensity pixels in the

image), and (iv) difference between first and second mode of image histogram. Table 4.8 shows means of percent of image pixels in central 2/3rds part of the image dynamic range for images of fabricated pecans taken at different voltages and currents.

**Table 4.8 Means of percent image pixels with intensity falling within central 2/3rds part of the image dynamic range for 10 fabricated pecan samples.**

Tube voltage, kVp	Tube current, mA				
	0.1	0.25	0.5	0.75	1
15	11.58	0.81	0.00	0.00	0.00
20	0.00	0.00	0.00	0.25	2.20
25	0.00	0.00	4.10	32.07	98.49
30	0.00	1.69	70.88	98.93	97.62
35	0.00	25.42	98.69	96.43	86.96
40	0.09	83.07	97.05	84.56	70.17
45	1.53	98.67	92.23	70.69	65.60
50	7.57	98.38	80.79	65.99	65.24

It is evident from low measurement values in Table 4.8, that none of images taken at 15 and 20 kVp gave good contrast. Also, all images taken at 0.1 mA did not give good contrast. At low X-ray energies, the histograms tended to be more left of the center, i.e. toward zero (Fig. 4.13). This result indicated that too many low-energy photons were attenuated to form a good contrast image. On the other hand, high-energy photons (e.g. at 50 kVp and 1 mA or 45 kVp and 0.75 mA) did not attenuate enough to form a contrast between different components of the pecan. The histogram of such image shifted to right (Fig. 4.14). For an image with good contrast, the pixels had intensities in the middle 2/3rds of the intensity dynamic range (0 to 4095) (Fig. 4.15). If a cutoff of 90% is assumed good, then the best combinations of voltage and current for good contrast are shown in Table 4.9.

**Table 4.9 Conditions for good contrast image.**

Voltage, kVp	25	30	35	40	45	50
Currents, mA	1	0.75, 1	0.5, 0.75	0.5	0.25, 0.5	0.25

Image variance is a good indicator of image contrast. Higher variance indicates higher contrast in the image. Table 4.10 presents means of image variance for images taken at different voltages and currents. It can be observed that voltage and current conditions for maximum variance at a given voltage (values with \* in Table 4.10) match with the conditions identified in Table 4.9 for good contrast images, except at 50 kVp.

**Table 4.10 Mean image variance for fabricated samples.**

Voltage, kVp	Current, mA			
	0.25	0.5	0.75	1.0
25	3782	17399	44380	85367*
30	10203	49694	116168	167345*
35	22686	99161	145787*	113656
40	39085	123257*	93735	67223
45	57354	103047*	66123	64842
50	72831	73062*	64612	64854

\* maximum value of variance at a given voltage, i.e. maximum for the row.



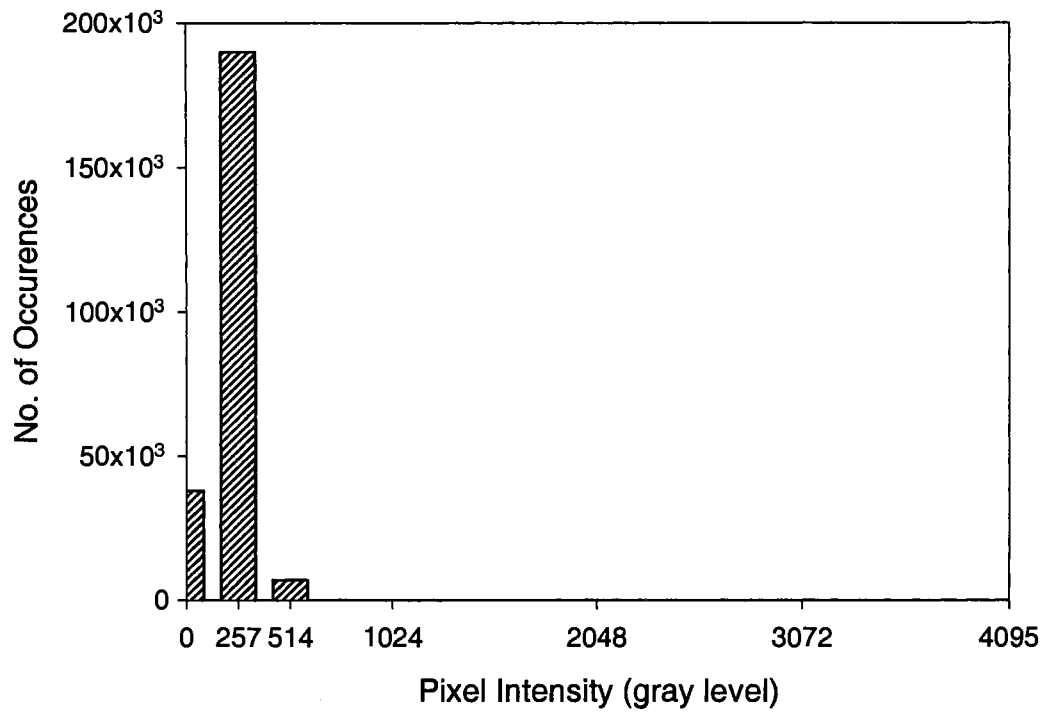


**Figure 4.13 Histogram of image taken at low X-ray power (25 kVp, 0.25 mA).**

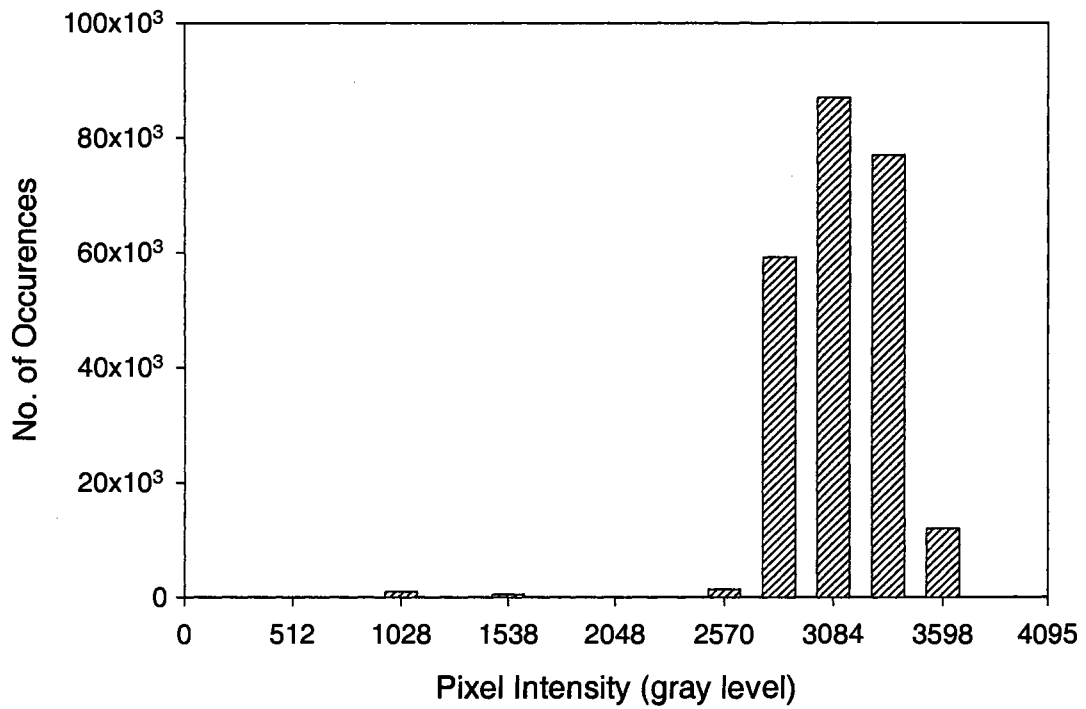


**Figure 4.14 Histogram of image taken at high X-ray power (50 kVp, 1 mA).**

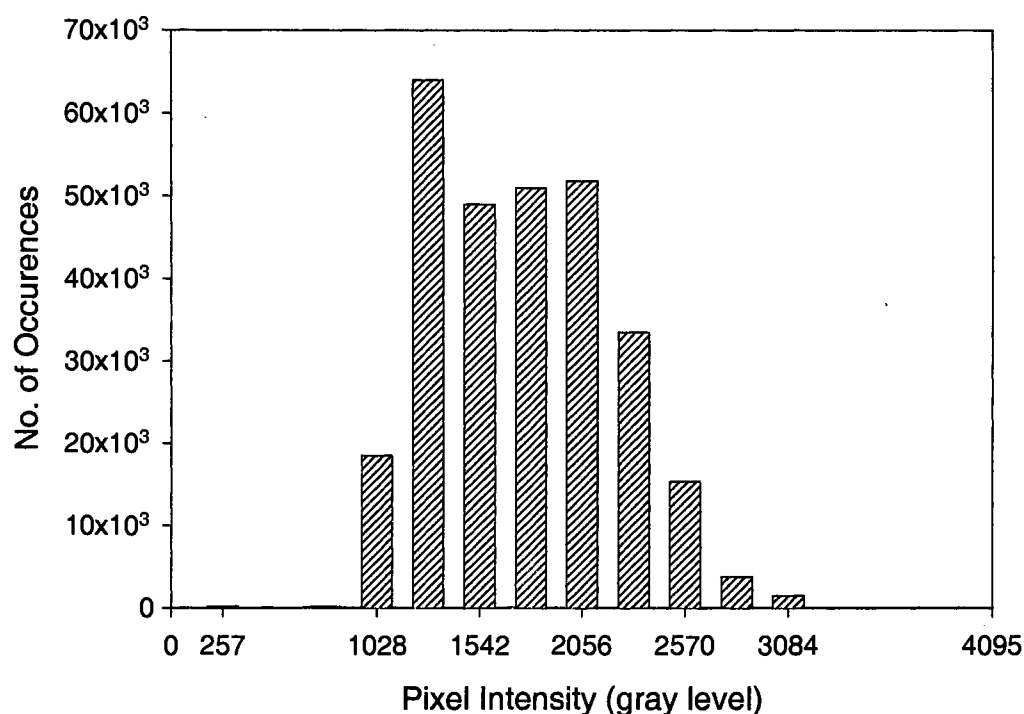


**Figure 4.15 Histogram of image acquired at a 'good' X-ray power (35 kVp, 0.75 mA).**

Out of 800 images taken, 210 were found to have good contrast, i.e. more than 90% pixels were in the central 2/3rds range of the histogram dynamic range. Table 4.11 shows the number of good images for each sample and at different X-ray energies.

**Table 4.11 Number of pecan images with more than 90% pixels having intensity in the central 2/3rds dynamic range.**

Voltage, kVp	Current, mA	Sample No.										Grand Total
		1	2	3	4	5	6	7	8	9	10	
25	1	2	2	2	2	2	2	2	2	2	2	20
	0.5	1		1		2					1	5
30	0.75	2	2	2	2	2	2	2	2	2	2	20
	1	2	2	2	2	1	2	2	2	2	2	19
30 Total		5	4	5	4	5	4	4	4	4	5	44
35	0.5	2	2	2	2	2	2	2	2	2	2	20
	0.75	2	2	2	2	1	2	2	2	2	2	19
	1	1	1		2	1	1	2		2	1	11
35 Total		5	5	4	6	4	5	6	4	6	5	50
40	0.25			2		2				1		5
	0.5	2	2	2	2	1	2	2	2	2	2	19
	0.75				2	1	1	2		1		7
	1					1						1
40 Total		2	2	4	4	5	3	4	2	4	2	32
45	0.25	2	2	2	2	2	2	2	2	2	2	20
	0.5	2	2	1	2	1	2	2		2	2	16
	0.75					1						1
	1					1						1
45 Total		4	4	3	4	5	4	4	2	4	4	38
50	0.25	2	2	2	2	2	2	2	2	2	2	20
	0.5				1	1	1	1				4
	0.75					1						1
	1					1						1
50 Total		2	2	2	3	5	3	3	2	2	2	26
Grand Total		20	19	20	23	26	21	23	16	22	20	210

Two images were taken for each sample at all energy levels. It can be observed that at energies identified in Table 4.9, out of 20 images acquired, 19 or 20 images produced good contrast, except at 45 kVp and 0.5 mA where 16 images had good contrast. A maximum of 50 images with good contrast were captured at 35 kVp, followed by 44 images at 30 kVp. Numbers of good images taken for each sample are comparable indicating that there was no bias due to sampling.

To further narrow the appropriate energies to capture a good-contrast image, the width of the histogram base (Table 4.12), and absolute difference

between the first and second mode of histogram (Table 4.13) were determined at the energies identified in Table 4.9.

**Table 4.12 Mean width of histogram base for images acquired at given X-ray energies.**

Voltage, kVp	Current, mA			
	0.25	0.5	0.75	1
25				2107.40
30			2467.20	2975.79
35		2364.40	2935.21	
40		2772.89		
45	1953.20	2923.38		
50	2210.20			

Histogram base was widest for images acquired at 30 kVp - 1 mA. Histogram base width for images acquired at 35 kVp - 0.75 mA and 40 kVp - 0.5 mA are also comparable. The difference in first and second mode also indicates that images taken at 30 kVp - 1 mA, 35 kVp - 0.75 mA, and 40 kVp - 0.5 mA were more bimodal than other images.

**Table 4.13 Mean difference in first two modes of histogram.**

Voltage, kVp	Current, mA			
	0.25	0.5	0.75	1
25				257.00
30			257.00	284.05
35		257.00	311.11	
40		284.05		
45	257.00	257.00		
50	257.00			

To verify suitability of the identified appropriate energies, 30 unknown samples were imaged at 'good' conditions as identified in Table 4.9 and Table 4.10. Parameters shown in Tables 4.8, 4.10, 4.12, 4.13 were determined for the unknown sample images and are presented in Table 4.14.

**Table 4.14 Histogram-based features for 'unknown' samples.**

<b>Imaging condition</b>		<b>Pixels with intensity in central 2/3rd range, %</b>	<b>Mean image variance</b>	<b>Mean width of histogram base, gray level</b>	<b>Mean of difference in first two modes, gray level</b>
<b>Voltage, kVp</b>	<b>Current, mA</b>				
25	1	96.39	79787	2047.43	257.00
30	0.75	99.06	106396	2398.67	257.00
30	1	98.37	151983	2775.60	274.13
35	0.75	97.41	133056	2758.47	308.40
40	0.5	97.97	111668	2625.68	278.42
45	0.5	94.49	99272	2749.90	274.13
50	0.25	98.52	64344	2111.68	257.00

It is evident that images of unknown samples, taken at all the identified X-ray energies, had good contrast. More than 90% of the pixels had intensities in the central 2/3rds range of the histogram base. Image variance values at different conditions for the unknown sample images are comparable to those for the fabricated pecans. Like the fabricated samples, the histogram base was widest for images acquired at 30 kVp - 1 mA. The histogram base width for images acquired at 35 kVp - 0.75 mA and 45 kVp - 0.5 mA are also comparable. Differences between the first and second modes also indicate that images taken at 30 kVp - 1 mA, 35 kVp - 0.75 mA, 40 kVp - 0.5 mA, and 45 kVp - 0.5 mA were more bimodal compared with other images.

### **Quality Detection from Images**

Pecan images for the fabricated samples, taken at 30 kVp and 1 mA are shown in Table B.1 (Appendix - B). Flat-field correction and contrast enhancement operations were performed on these images for better readability in print; however the contrast of the images was not modified for analysis. Even

after contrast enhancement, some features are not as distinct on hard copy print as when viewed on the computer monitor. Shape and size of nutmeat inside shell, physical damage to shell (Sample F2) and nutmeat (Samples F4 and F8), absence of nutmeat (Sample F5), and presence of weevil (Sample F6, F9, and F10) can be seen in these images.

### ***Image Segmentation***

There were four distinct segments in each image: (a) a dark area representing the shell near the edge of the pecan, (b) an area inside the shell portion with varying gray levels, representing nutmeat, (c) a central dark area in some images representing the woody separator of the pecan halves, and (d) an air gap between shell and nutmeat. Some morphological operations like image erosion and histogram-based operations to segment these portions in an image were attempted, but were not effective. Morphological operations did not succeed due to differences in shell thickness, and image histogram-based segmentation was not sufficiently robust. Segmentation was therefore done manually using the 'ROIPOLY' command of MATLAB®. Two regions of interest (ROI) were segmented for each image: (i) the region that excludes shell and central separator, thus representing nutmeat and air gap (ROI-1) and (ii) the region that represents nutmeat only (ROI-2).

### ***Determination of Damaged, Missing, and Shriveled Kernel***

It is assumed that a pecan with damaged, missing, or shriveled nutmeat will have more air gap inside the shell than a pecan having a sound kernel. The

ratio of ROI-2 to ROI-1 would therefore be higher for pecans having a sound kernel. These ratio values for the fabricated pecan nuts are shown as percent area occupied in Table C. 1 (Appendix - C).

It can be observed that the ratio of ROI-2 to ROI-1 is lower for a damaged kernel (Sample 4) and a missing kernel (Sample 5). Most values are lower than 75%, which may be because these samples were fabricated by using nutmeat that did not come from the same natural shell and thus air gaps were greater than those occurring in a complete natural sample.

As already discussed, the pixel intensity in a radiograph depends on the material density and thickness of the material. Brighter pixels represent either material having a low attenuation coefficient or less material in the path of the X-ray beam, or a combination of both. The mean pixel intensity inside the shell is therefore another feature available to identify damaged or missing nutmeat. Table C.2 (Appendix - C) shows mean and standard deviation of pixel intensity of ROI-1. Samples 3, 4, and 5 with a damaged shell and either damaged or missing nutmeat can be identified by higher mean pixel intensity values, if thresholds are fixed as shown in Table 4. 15. These values for other samples are also not low, because there were more air gaps in the fabricated samples. It is expected that the mean pixel intensity inside the shell would be lower for good natural pecans. Missing kernel in Sample 5 and a large hole in the nutmeat in Sample 8 caused high standard deviations in the pixel intensity values. Mean pixel intensity values were sensitive to X-ray viewing orientation, which is evident from the difference in values for the two orientations. However, larger damages caused an increase in intensity values, irrespective of orientation.

**Table 4.15 Threshold pixel intensity values at different X-ray energies to identify defects in pecan.**

<b>X-ray energy</b>	<b>25 kVp, 1 mA</b>	<b>30 kVp, 1 mA</b>	<b>35 kVp 0.75 mA</b>	<b>40 kVp, 0.5 mA</b>	<b>45 kVp, 0.5 mA</b>	<b>50 kVp, 0.25 mA</b>
Pixel intensity, gray level	750	1500	1800	1800	2200	1400

'Unknown' samples

Percent area occupancy (ROI-2/ROI-1\*100) was calculated for the 30 unknown samples and are presented in Table C.3 (Appendix - C). Subjective decisions made about these pecans based on their external appearance (Column 2) and a decisions based on a threshold value of 75% area occupancy (Column 5) are also presented in Table C.3. It is evident that some samples (Sample 4) which appeared good from outside were largely hollow inside due to underdeveloped nutmeat, while some samples (Samples 10 and 21), which were considered for rejection due to "shuck tight" and small insect hole had enough nutmeat inside to be accepted as good. Samples severely damaged by insects (Sample 16 through 19) and with severely underdeveloped nutmeat (Samples 11, and 13 through 15) could be easily isolated due to low percent area occupancy. A paired t-test of the data showed that orientation had a significant effect on percent area occupancy (p=0.175) and therefore decisions made only on percent area occupancy may be erroneous. It is noteworthy that this technique is based on only two-dimensional information, and the segmented nutmeat area (ROI-2) is the largest area projected by the nutmeat. In case one cotyledon of the nutmeat is considerably smaller than the other or is missing, and the X-ray image is taken with one cotyledon completely covering the other, anomalies of the smaller cotyledon



would remain undetected. A reasonably reliable decision could be made using this technique if pecan nuts are imaged in an orientation where the plane joining nutmeat cotyledons is perpendicular to the image plane. Even under this condition, the decision about quality would depend on the effectiveness of segmentation, and anomalies like insect holes and some mechanical damages may still remain undetected.

Mean and standard deviation of pixel intensity for the area inside the shell (ROI-1) for all the "unknown" pecan samples were determined (Table C.4, Appendix - C). If threshold values identified for fabricated samples are applied then Samples 4, 5, 11 through 19, and 27 can be identified as pecans with less than desired nutmeat (Fig. 4.16). Similar decisions are obtained when threshold values at other energies are applied.

Orientation of the sample did not make much difference in the decision-making results, except for Samples 1 and 3 (Fig. 4.16). If a tolerance of 40 gray-levels is allowed, then the effect of orientation was not significant on the mean pixel intensity ( $p=0.02$ ). This tolerance is less than 1% of the image dynamic range from 0 to 4095.

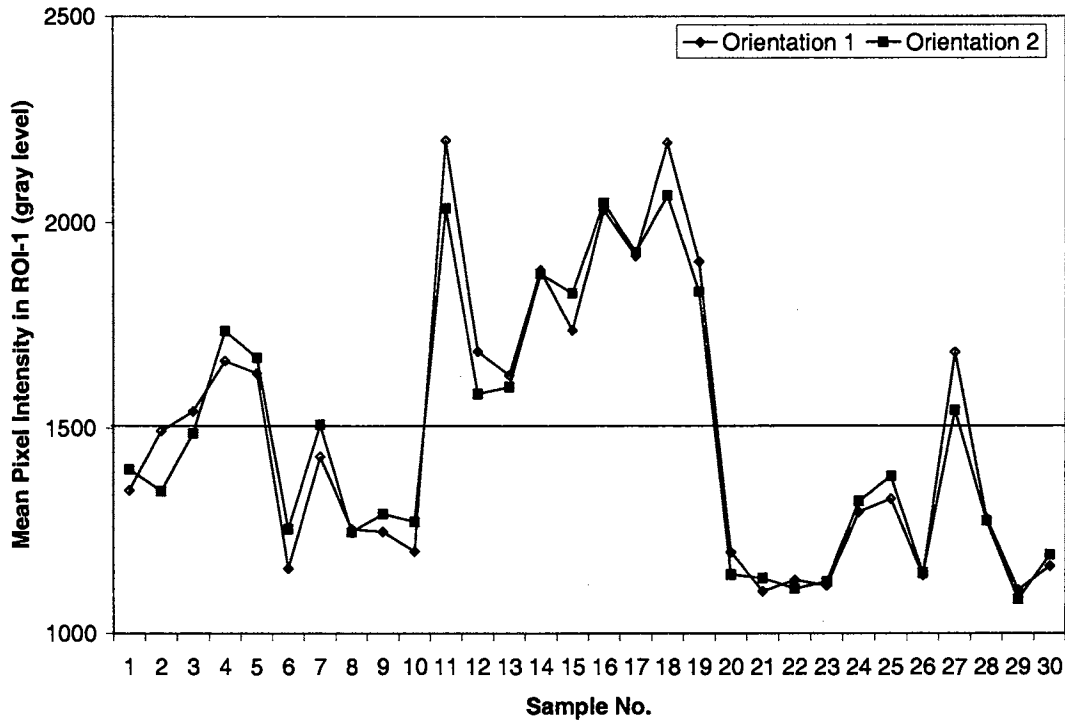


**Figure 4.16 Mean intensity based thresholding to identify damaged pecans at 30 kVp and 1 mA.**

Variations of pixel intensity from a mean of 5 x 5 neighborhood pixels were calculated for each image pixel, and a mean of these variations was found for each image. Figure 4.17 shows these mean local variations for each image taken at 40 kVp - 0.5 mA. A decision on good and inferior pecans could be made, based on a threshold value for this variation. For instance, a pecan would be rejected if the mean variation for an image taken at 40 kVp - 0.5 mA was more than 20. Similar decisions were made from images taken at other X-ray energies with their appropriate threshold values.

When decisions made on the basis of mean pixel intensity were compared with the decisions made based on percent area occupancy, 25 out of 30 had the same result. Of the five wrong decisions, four were rejected on percent area

occupancy, but accepted on mean pixel intensity. This result was because either the percent area occupancy values were near, but lower than, the threshold value, or the segmentation of nutmeat (ROI-2) was incorrect. The fifth wrong decision was for Sample 12 which was mechanically damaged. However, the damage did not cause sufficient reduction in nutmeat area and therefore percent area occupancy accepted the sample, but the mechanical damage caused a considerable increase in mean pixel intensity. A comparison of decisions based on mean pixel intensity and mean local variation showed that there were only two conflicting decisions out of 30.

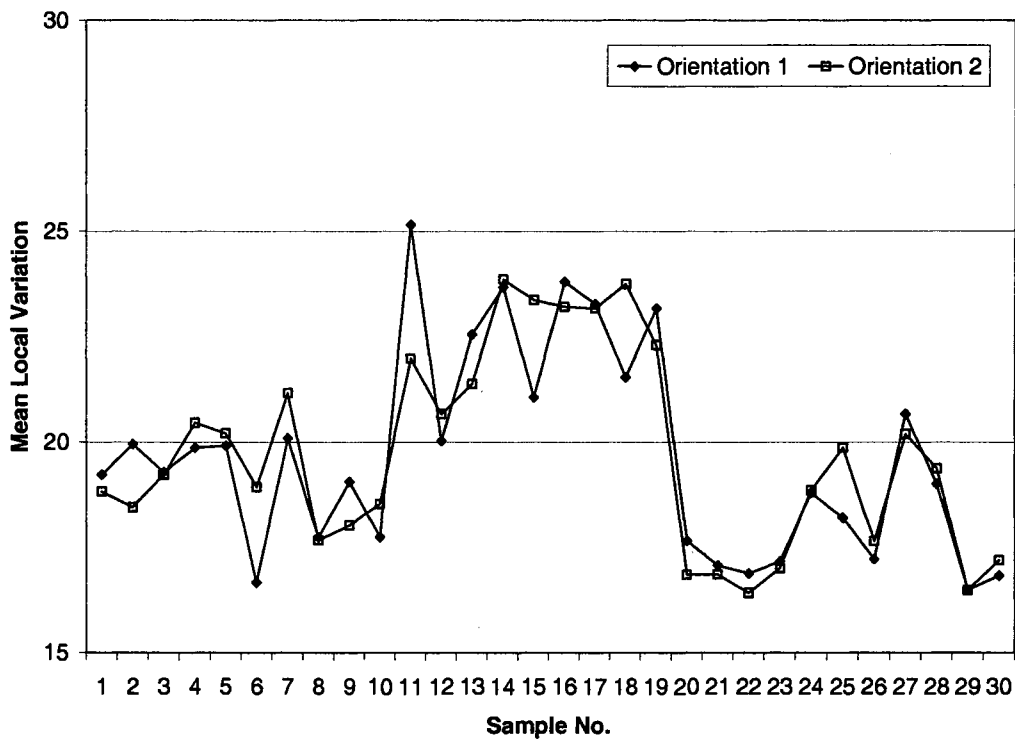


**Figure 4.17** Variation of each pixel from mean of its 5 x 5 neighborhood for image taken at 40 kVp - 0.5 mA.

## Estimation of Nutmeat Quantity

### Algorithm

Attenuation of X-ray power, given by Equation 2.1 (page 29), by the material through which the X-ray beam passes was visible as image pixel intensities. Combining  $\mu_m$  and  $\rho$  terms in Eq. 2.1 as linear attenuation coefficient  $\mu$  gives

$$I = I_0 e^{-\mu \cdot z}, \quad (4.1)$$

where  $\mu$  is linear attenuation coefficient (1/cm) and  $z$  is the material thickness (cm) through which the x-ray passes. It was assumed that for nutmeat area in pecan radiograph (ROI-2), an X-ray beam passed through two layers of shell and nutmeat. Thus rewriting Equation 4.1

$$I = I_0 e^{-(\mu_n \cdot z_n + 2 \cdot \mu_s \cdot z_s)}, \quad (4.2)$$

where,  $\mu_n$  and  $\mu_s$  are linear attenuation coefficients for nutmeat and shell and  $z_n$  and  $z_s$  are thicknesses of nutmeat and shell across the X-ray beam, respectively. It was also assumed that shell thickness and hence shell attenuation coefficient did not change for ROI-2. Because thickness of nutmeat across the X-ray beam could change considerably, the effect of beam hardening, demonstrated by Kotwaliwale et al. (2003) could not be ignored. A regression equation to estimate the attenuation coefficient of nut was therefore used as:

$$\mu_n = A + B \cdot z_n + C \cdot z_n^2 + D \cdot v + E \cdot v^2 + F \cdot z_n \cdot v, \quad (4.3)$$

where A, B, C, D, E, and F are regression coefficients given in Table 4.7, and v is X-ray tube voltage. For a known value of v, Eq. 4.3 can be rewritten as:

$$\mu_n = (A + D \cdot v + E \cdot v^2) + (B + F \cdot v) \cdot z_n + C \cdot z_n^2. \quad (4.4)$$

Combining Eq. 4.2 and 4.4 and rearranging,

$$\left( \ln \left( \frac{I}{I_0} \right) + 2 \cdot \mu_s \cdot z_s \right) + (A + D \cdot v + E \cdot v^2) \cdot z_n + (B + F \cdot v) \cdot z_n^2 + C \cdot z_n^3 = 0. \quad (4.5)$$

The positive, real roots of the cubic equation (4.5) were determined for each pixel in ROI-2 which represented nutmeat thickness for that pixel. The sum of thicknesses at all pixel points multiplied by the area of each pixel would give an estimate of nutmeat volume. Detector-to-detector distance was 48  $\mu\text{m}$ , and therefore the area represented by each pixel was 2304  $\mu\text{m}^2$ .

#### Correction for Distance and X-ray Beam Shape

The X-ray beam diverges from the anode as a cone, and therefore the angle at which a photon hits each detector of the camera varies with position of that detector as shown in Figure 4.18. Whereas the photons hit perpendicular to the detector array at its center, their angle reduces as the distance from detector array center increases. The sample projected area on the detector therefore increases. This amount of increased area depends on the distance between the sample and the detector (d), thickness of the sample, and location of sample, vis-à-vis X-ray beam angle ( $\theta$ ). The increase in dimension due to distance between sample and detectors equals  $h / (h-d)$ . All the X-ray images were taken with  $h=163$  mm and  $d=10$  mm, therefore multiplying the pixel area with  $(153/163)^2$

corrected the problem of increase in projected area due to distance between sample and detectors.

To compensate for the increase in area due to sample thickness and sample location, a matrix of 1000 by 1000 elements was created with each element having a value equal to radial distance ( $r$ , mm) between that element and center of the matrix. Values of angle ( $\theta$ ) were then calculated at each element by:

$$\theta = \tan^{-1}\left(\frac{163}{r}\right). \quad (4.6)$$

A compensation multiplier matrix was then calculated by taking sine of the angle matrix. The matrix of estimated thicknesses ( $z_n$ ) was point-wise multiplied to this correction matrix to compensate for the increase in projected area due to the conical shape of X-ray beam. Such correction is valid under an assumption that the center of the X-ray beam is aligned to the center of the detector array. Care was taken prior to imaging to ensure this alignment.

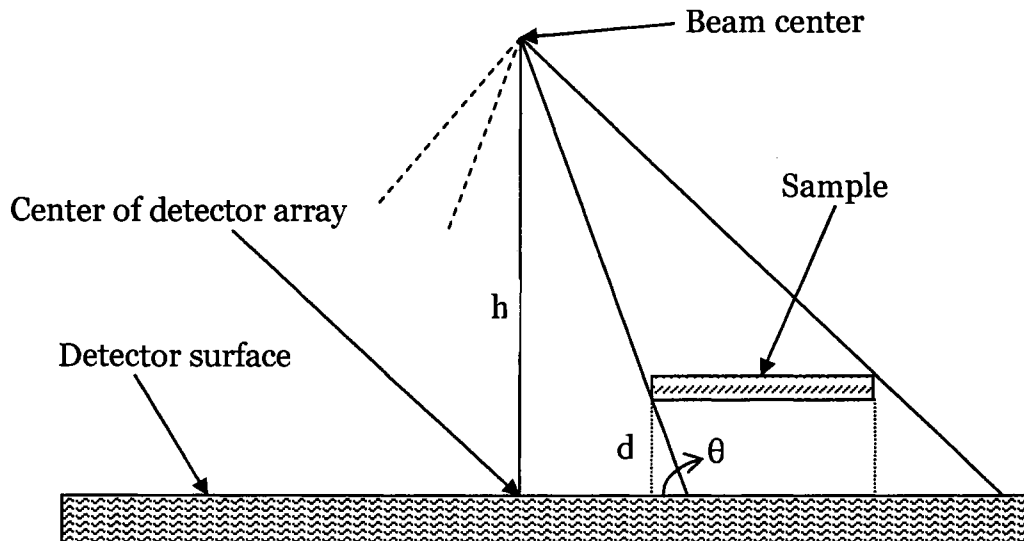


**Figure 4.18 Representation of a conical X-ray beam hitting the detector surface.**

## ***Nutmeat Weight Estimates***

The volume of nutmeat was estimated for each pecan radiographed at two orientations. Weight was estimated by multiplying the volume by mean nutmeat specific gravity of 0.95. Estimated values obtained for the fabricated nuts for two orientations and six X-ray energies are presented in Table C.5 (Appendix C). Linear correlation between actual and estimated weight values and deviations of estimates from their corresponding true values are also given. It is evident that Orientation-2 performed poorly compared with Orientation-1. Except at 50 kVp, mean deviations of estimates were positive, indicating that in Orientation – 2 values were generally overestimated. The error could be due to presence of the ‘woody separator’ between the cotyledons of the pecan nutmeat. In Orientation-2, this ‘woody separator’ was parallel to the image plane and could not be segmented from the nutmeat portion. Its presence reduced the pixel intensity in the ROI and thus increased the thickness estimates. Also, the ‘woody separator’ made the task of segmenting nutmeat from shell and air gaps difficult and might have led to segmenting an area larger than actual. This argument is supported by lower correlation coefficients obtained at Orientation – 2 than at Orientation – 1. Best estimates, with mean estimation error of -0.02 g (-1.13%), were obtained from images taken at 40 kVp and 0.5 mA in Orientation-1. At Orientation-2, images taken at 50 kVp and 0.25 mA gave best estimates with a mean error of -0.06 g (-3.66%). Overall best estimates were obtained from images taken at 45 kVp and 0.5 mA with mean errors of  $\pm 0.09$  g ( $\pm 5.8\%$ ) in the two orientations.

Estimate of weights, correlation between true and estimated weights, and means of deviation of estimates from their corresponding actual values for the "unknown" samples are given in Table C.6 (Appendix C). Again, estimates in Orientation-1 are better than estimates in Orientation-2. Correlation coefficients for the estimates with true values are lower for the "unknown" samples than for fabricated samples (Table C.5), which might be caused by shriveled and insect-damaged samples in the "unknown" lot. Weight estimates for these low-quality samples are much higher than the actual, which could be due to: (i) difference in specific gravity of actual nutmeat and shriveled, immature, and the black powdery material present due to insect damage, and (ii) error in segmentation. However, these were the samples that would be rejected, based on their percent area occupancy and mean pixel intensity values.

If the samples accepted on percent area occupancy and mean pixel intensity are considered separately, the nutmeat weight estimation error is comparable to that calculated for the fabricated samples (Table C.7). Best estimates, -0.04 g (-2.95%), were obtained from images taken at 40 kVp and 0.5 mA at Orientation-2, while at Orientation-1 best estimates were -0.09 (-4.4%) obtained from images taken at 35 kVp and 0.75 mA. Overall best estimates were obtained from images taken at 40 kVp and 0.5 mA.

### **Features Visible in Pecan X-ray Images**

Images of fabricated and "unknown" pecan samples taken at 30 kVp and 1 mA at one orientation are shown in Table B.2 (Appendix - B). Contrast of these images was enhanced for better visibility in print. Unfortunately, all features are



not always visible distinctly in print. Features visible on the computer monitor in the "unknown" samples are compared with the decisions based on percent area occupancy and mean pixel intensity in Table C.8 (Appendix - C). Almost all the quality parameters/anomalies observed in the samples after breaking them out of the shell were also observed in the X-ray images taken at energies found appropriate for good image contrast (Table 4.9). Pecans with a large amount of insect or physiological damage posed problems in segmentation, because there was very little, or virtually no, nutmeat present, and therefore in such cases the 'woody separator' of pecan cotyledons was included as nutmeat portion. This is the reason that weight estimates for nutmeat in such pecans were very high compared to the true weight of the spoiled nutmeat portion in those pecans. Only a few samples with insects inside the nut could be found. Of four such samples, pecan weevils could be clearly seen in three. High-frequency emphasis technique (Gonzalez and Woods, 2001) helped in sharpening the image and achieving better visibility of features in the image. However, techniques purely based on pixel intensity such as image histogram-based techniques and local variance for each pixel, were not successful in segmenting the pecan weevil. Visibility of features indicating quality presents an encouraging situation for development of suitable segmentation and grading algorithms in the future.

## **CHAPTER V**

### **SUMMARY AND CONCLUSIONS**

Data of the physical properties of pecan nuts (equilibrium moisture content, nut length, maximum and minimum diameters around largest nut periphery, geometric mean diameter and sphericity of whole nut, shell thickness, nutmeat-to-shell ratio, and specific gravity of whole nut, nutmeat, and shell) were obtained for four cultivars of pecans. The effects of storage relative humidity and cultivar on physical properties were determined.

Relative humidity of the environment affected equilibrium moisture content, nut length, minimum diameter of whole nut around largest periphery, geometric mean diameter, and specific gravity values for nut and nutmeat. While storage Rh affected shell thickness for some cultivars, it did not affect maximum diameter of nut around the largest periphery, sphericity of nut, or specific gravity of pecan shell.

Almost all of the physical properties varied among cultivars. Natives had thicker shells of higher specific gravity than the Improved varieties. Although nutmeat specific gravity varied among cultivars, that variation was not sufficient to differentiate between Native and Improved cultivars. Specific gravity of nutmeat was lower than specific gravity of the shell for all cultivars at equilibrium relative humidities of 40% and 78%.

A system to capture digital radiographs using soft X-rays was developed using a commercially available X-ray tube and X-ray camera. Design shielding of 3.175 mm thick lead with 6.35 mm thick aluminum was able to reduce the radiation dose by 10 log cycles and below the dose limit of 0.05 Sieverts/yr permitted by the U.S. Nuclear Regulatory Commission.

Linear attenuation coefficients of nutmeat and shell were determined at various X-ray tube voltages and sample thicknesses. The coefficients were determined from images using the equation for exponential decay of photon energy passing through a material. X-ray tube peak voltage and sample thickness inversely affected the linear attenuation coefficient of pecan nutmeat and shell. The effect of these variables on the linear attenuation coefficient was quadratic. For a given material thickness, linear attenuation coefficient was small for lower specific gravity materials. A regression equation developed to explain the effect of sample thickness, X-ray tube peak voltage, and higher order terms on linear attenuation coefficient of pecan nutmeat had  $R^2$  values of at least 0.93.

X-ray images of 10 pecan samples were acquired at eight X-ray tube voltages (15 to 50 kVp in steps of 5 kVp), five currents (0.1, 0.25, 0.5, 0.75 and 1.0 mA), and two orientations of nut (plane joining two pecan cotyledons horizontal or vertical). Image contrast in the nut region of these 800 images was determined to identify appropriate X-ray energies for imaging. Seven combinations of X-ray tube voltage and current were identified as 25 kVp - 1 mA, 30 kVp - 0.75 mA, 30 kVp - 1 mA, 35 kVp - 0.75 mA, 40 kVp - 0.5 mA, 45 kVp - 0.5 mA, and 50 kVp - 0.25 mA to obtain good contrast images of pecans. Good

imaging performance at these conditions was confirmed by capturing good-contrast images for 30 pecans with unknown internal conditions.

Without a sample present, detectors saturated at the identified combinations of X-ray tube voltage and current. Statistical models were therefore developed for the central one million pixels to predict pixel intensity at those voltages and currents. Pixel intensity ratios were found suitable for segmenting sample from the image background. Response variation among detector columns could be accommodated by flat-field correction. Pecan features such as shell, nutmeat, air gap between shell and nutmeat, defects, and presence of insects were distinctly visible in X-ray images after contrast stretching of pecan radiographs. Intensity-based approaches were, however, not successful in segmenting these features in a pecan radiograph. Two features, the area inside the shell and the area for only nutmeat were identified manually and pixel maps were stored. The ratio of areas under these two features for each pecan was a good indicator of 'nut fill.' Mean pixel intensity for the features representing the cavity inside the shell, was a good gauge for quality of nutmeat. Higher mean pixel intensity represented inferior, or no nutmeat. Nutmeat quality could also be determined by finding the mean of local variations of pixels in an image. Immature or damaged nutmeat caused higher mean variation. These indicators together were successful in finding damaged, shriveled, and missing nutmeat in a pecan, and hence could satisfactorily grade a pecan nut for acceptance or rejection.

Algorithms based on the equation for exponential decay of photon energy passing through a material were developed to estimate volume of nutmeat in the

pecan. Necessary corrections for conical shape of the X-ray beam were incorporated in the algorithms. Estimation with error less than 10% was achieved from images taken at 35 kVp - 0.75 mA, 40 kVp - 0.5 mA, and 45 kVp - 0.5 mA. Orientation of the pecan made a difference in the results in some cases. A nut oriented such that the plane joining two pecan cotyledons was perpendicular to the camera plane gave better estimates.

Manual identification of a pecan weevil in an image was easy. The area representing a weevil was darker than its surround, sometimes had a light tunnel around it, and had some regular shape. Pixel intensity based algorithms were not successful in segmenting this region, nor were algorithms based on high-frequency emphasis.

### **Challenges for Future**

Variations in physical properties among cultivars indicate a need for collection of more data of physical properties of more pecan cultivars. X-ray images could be used to define some shape and size features of pecan shell and nutmeat for these cultivars.

Attenuation properties of nutmeat and shell were determined using a polychromatic X-ray source. These values should not change for different X-ray tubes producing X-rays from a tungsten anode, however, this needs to be confirmed. Attenuation coefficients should also be determined for a monochromatic X-ray source so that the data could be used for dual-energy X-ray analysis. Techniques like taking a ratio of images obtained at two energies might merit consideration.

Segmentation efforts based purely on individual pixel intensity did not perform well. These efforts can be considered as only an initial attempt and as potential for other more complex approaches based on area features, texture features, and combinations of spatial and frequency based features. Advanced approaches for segmentation might also be able to identify weevils in pecans. Efforts could also be devoted to identifying damage from invasive insects such as the stink bug.

Decisions on accepting or rejecting a pecan based on percent area occupancy, mean pixel intensity, and mean local variations were made manually. Neural network or fuzzy logic algorithms could be developed to make decisions based on collective information about these features.

All the algorithms related to images were developed using MATLAB®. Converting 'raw' image to the required format and execution of program loops required 8 to 10 seconds to process an image. Image processing time could be reduced using more efficient programming techniques and languages.

This research has found that combined knowledge of physical and X-ray attenuation properties can lead to a feasible technique for non-destructive quality evaluation of nutmeat in 'in-shell' pecans. Based on this knowledge, development of a prototype to grade and/or sort pecans appears to be technically feasible.

## REFERENCES

- Abhayawick, L., J.C. Laguerre, V. Tauzin, and A. Duquenoy. 2002. Physical properties of three onion varieties as affected by the moisture content. *Journal of Food Engineering* 55(3):253-262.
- Anonymous. 1979. Pecan grading guidelines ... An aid to marketing. *Pecan South*. 6(6):22-27.
- Anonymous. 1994. Radiation protection training manual and study guide for radiation producing devices. Available at: <http://www.inform.umd.edu/CampusInfo/Departments/EnvirSafety/rs/prod/tmsgrp/d/device.html#toc>. Accessed 18 June 2003.
- Anonymous. 2001. Material attenuation of neutrons. Available at: <http://engphys.mcmaster.ca/~garlandw/ep4u4/nuclear/4u4nuclab-1.pdf>. Accessed 18 June 2003.
- Anonymous. 2003. Dual energy digital imaging. Available at: <http://www.amershamhealth.com/medcyclopaedia/Volume%20I/DUAL%20ENERGY%20DIGITAL%20IMAGING.asp>. Accessed 18 June 2003.
- Armstrong, P.R., M.L. Stone, and G.H. Bruswitz. 1997. Peach firmness determination using two different nondestructive vibrational sensing instruments. *Transactions of the ASAE*. 40(3):699-703.

- Aydin, C. 2002. Physical properties of hazel nuts. *Biosystems Engineering*. 82(3):297-303.
- Balasubramanian, D. 2001. Physical properties of raw cashew nut. *J. agric. Engng. Res.* 78(3):291-297.
- Barcelon, E.G., S. Tojo, and K. Watanabe. 1999 a. X-ray computed tomography for internal quality evaluation of peaches. *J. agric. Engng. Res.* 73(4):0323-0330.
- Barcelon, E.G., S. Tojo, and K. Watanabe. 1999 b. Relating X-ray absorption and some quality characteristics of Mango fruit (*Mangifera indica* L.). *J. Agric. Food Chem.* 47:3822-3825.
- Barna, S.L., M.W. Tate, S.M. Gruner, and E.F. Eikenberry. 1999. Calibration procedures for charge-coupled device x-ray detectors. *Review of Scientific Instruments.* 70(7): 2927-2934.
- Birth, G.S. and K.H. Norris 1958. An instrument using light transmittance for non destructive measurement of fruit maturity. *Food Technology.* 12:592-595.
- Bittner, D.R., and K.H. Norris. 1968. Optical properties of selected fruits vs maturity. *Transactions of the ASAE.* 11(4):534-536.
- Boyer, B.W. 2002. Personal communication. Oxford Instruments, X-Ray Technologies, Inc., Scotts Valley, CA.
- Brennan, J.G., J.R. Butters, N.D. Cowell, and A.E.V. Lilley. 1990. *Food Engineering Operation IIIrd Edition*. Elsevier Applied Science. London and New York.



- Brienne, J.P., C. Denoyelle, H. Baussart, and J. D. Daudin. 2001. Assessment of meat fat content using dual energy X-ray absorption. *Meat Science*. 57: 235-244.
- Burkhardt, T.H., and R.F. Mrozek. 1973. Light reflectance as a criterion for sorting dried prunes. *Transactions of the ASAE*. 16(4):683-685.
- Buzzell, P. and S. Pintauro, 2003. Dual energy X-ray absorptiometry. Department of food sciences and nutrition. University of Vermont. Available at <http://nutrition.uvm.edu/bodycomp/dexa/>. Accessed on January 6, 2003.
- Callaghan, P.T. 1991. *Principles of Nuclear Magnetic Resonance Microscopy*. Clarendon Press, Oxford.
- Casasent, D., A. Talukder, P. Keagy, and T. Schatzki. 2001. Detection and segmentation of items in X-ray imagery. *Transactions of the ASAE*. 44(2):337-345.
- Casasent, D.A., M.A. Sipe, T.F. Schatzki, P.M. Keagy, and L.C. Lee. 1998. Neural net classification of X-ray pistachio nut data. *Lebensm.-Wiss. u.-Technol.* 31(2):122-128.
- Chen, P., and Z. Sun. 1991. A review of non-destructive methods for quality evaluation and sorting of agricultural products. *J. agric. Engng. Res.* 49(2):85-98.
- Chen, P., M.J. McCarthy, and R. Kauten. 1989. NMR for Internal quality evaluation of fruits and vegetables. *Transactions of the ASAE*. 32(5):1747-1753.

- Cheng, Y. and C.G. Haugh. 1994. Detecting hollow heart in potatoes using ultrasound. *Transactions of the ASAE*. 37(2):217-222.
- Chin, K.L. and W.A. Young. 1980. Hormonal changes in developing and dehiscing pecan shucks. *Hortscience*. 15(4):522-523.
- Chuma, Y. and K. Nakaji. 1976. Optical properties of fruits and vegetables to serve the automatic selection within the packing house line (4) - Delayed light emission as a means of automatic selection of tomatoes. *J. Soc. Agric. Mach., Jap.* 38(2): 217-224.
- Chuma, Y., K. Nakaji, and M. Ohura. 1980. Maturity evaluation of bananas by delayed light emission. *Transactions of the ASAE*. 23(4): 1043.
- Chuma, Y., K. Sein, S. Kawaro, and K. Nakaji. 1977. Delayed light emission as a means of automatic selection of a Satsuma oranges. *Transactions of the ASAE*. 20(5): 996-1000.
- Clark, C.J., P.D. Hockings, D.C. Joyce, and R.A. Mazucco. 1997. Application of magnetic resonance imaging to pre- and post-harvest studies of fruits and vegetables. *Postharvest Biology and Technology*. 11:1-21.
- Curry, T.S. III, J.E. Dowdey, and R.C. Murry Jr. 1990. *Christensen's Physics of Diagnostic Radiology- 4th ed.* Williams and Wilkins, Baltimore.
- Deshpande, S.D., S. Bal, and T.P. Ojha. 1993. Physical properties of soybean. *J. agric. Engng. Res.* 56(2):89-98.
- Desrosier, N. W. 1960. *Radiation technology in food, agriculture, and biology.* Westport, Conn., Avi Pub. Co.

- DeVoe, D.R., G.H. Brusewitz, and M.L. Stone. 1985. Quantitative importance of bulk density when using dielectric measurements to predict percent moisture of hard red winter wheat (Density effect on dielectric properties of wheat). *Summer Meeting American Society of Agricultural Engineers*. ASAE paper No. 85-3027.
- Erickson, M.C. 1994. Methods of measurement of Pecan quality. In *Pecan Technology* ed. C. R. Santerre. Chapman & Hall New York. pp. 111-133.
- Ernest, J.V., G.S. Birth, A.P. Sidwell, and C. Golumbic. 1958. Evaluation light transmittance techniques for maturity measurement of two varieties of prune type plums. *Food Technology*. 12(11):595-599.
- Gaffney, J.J. 1973. Reflectance properties of citrus fruits. *Transactions of the ASAE*. 16(2):310-314.
- Gonzalez, R.C. and R.E. Woods. 2001. *Digital Image Processing - Second Edition*. Prentice Hall, Upper Saddle River, NJ.
- Gruner, S.M., M.W. Tate, and E.F. Eikenberry. 2002. Charged couple device area X-ray detectors. *Review of Scientific Instruments*. 73(8):2815-2842.
- Gunasekaran, S., M.R. Paulsen, and G.C. Shove. 1985. Optical methods for nondestructive quality evaluation of agricultural and biological materials. *J. agric. Engng. Res.* 32(3):209-241.
- Gupta, R.K., and S.K. Das. 1997. Physical properties of sunflower seeds. *J. agric. Engng. Res.* 66(1):1-8.

- Haff, R.P., and D.C. Slaughter. 2002. X-ray inspection of wheat for granary weevils. Real time digital imaging vs. film. *ASAE paper No. 026093*. American Society of Agricultural Engineers, St. Joseph, Mich.
- Harris, M.K., B.L. Cutler, and D.R. Ring. 1986. Pecan nut loss from pollination to harvest. *Journal of Economic Entomology*. 79(6):1653-1657.
- Harrison, R.D., W.A. Gardner, W.E. Tollner, and D.J. Kinard. 1993. X-ray computed tomography studies of the burrowing behavior of fourth-instar pecan weevil (Coleoptera:Curculionidae). *Journal of Economic Entomology*. 86(6):1714-1719.
- Heaton, E.K., A.L. Shewfelt, A.E. Badenhop, and L.R. Beuchat. 1977. Pecans: Handling, storage, processing and utilization. *Georgia Agricultural Experimentation Station Bulletin 197*. University of Georgia/ College of Agriculture.
- Heaton, E.K., J.W. Daniell, and L.C. Moon. 1982. Effect of drip irrigation of pecan quality and relationship of selected quality parameters. *Journal of Food Science*. 47(4):1272-1275,1279.
- Hubbell, J.H. and Seltzer, S.M. 1995. Tables of X-ray mass attenuation coefficients and mass energy absorption coefficients 1 keV to 20 MeV for elements Z=1 to 92 and 48 additional substances of dosimetric interest. *NISTIR 5632*. National Institute of Standards and Technology. US Department of Commerce.

- Irtwange, S.V., and J.C. Igbeka. 2002. Some physical properties of two African yam bean (*Sphenostylis stenocarpa*) accessions and their interrelation with moisture content. *Applied Engineering in Agriculture*. 18(5):567-576.
- Jain, R.K., and S. Bal. 1997. Properties of pearl millet. *J. agric. Engng. Res.* 66(2):85-91.
- Jordan, R.B., E.F. Walton, K.U. Klages, and R.J. Seelye. 2000. Postharvest fruit density as an indicator of dry matter and ripened soluble solids of kiwifruit. *Postharvest Biology and Technology*. 20:163-173.
- Joshi, D.C., S.K. Das, and R.K. Mukherjee. 1993. Physical properties of pumpkin seeds. *J. agric. Engng. Res.* 54(3):219-229.
- Karunakaran, C., D.S. Jayas, and N.D.G. White. 2002. Soft X-ray Inspection of wheat kernels infested by *Sitophilus oryzae*. *ASAE paper No. 023132*. American Society of Agricultural Engineering.
- Kato, K. 1997. Electrical density sorting and estimation of soluble solids content of watermelon. *J. agric. Engng. Res.* 67:161-170.
- Kays, S.J. 1979. Pecan kernel color changes during maturation, harvest, storage and distribution. *The Pecan Quarterly*. 13(3):5-12.
- Keagy, P.M., and T.F. Schatzki. 1993. Machine recognition of weevil damage in wheat radiographs. *Cereal Chemistry*. 70(6):696-700.
- Keagy, P.M., B. Parvin, and T.F. Schatzki. 1995. Machine recognition of navel orange worm damage in x-ray images of pistachio nuts. In *Proceedings of SPIE-The International Society for Optical Engineering*, 2345:192-203.

- Keagy, P.M., B. Parvin, and T.F. Schatzki. 1996. Machine recognition of navel orange worm damage in X-ray images of pistachio nuts. *Lebensmittel-Wissenschaft + Technologie (Food Science + Technology)*. 29(1&2):140-145.
- Kim, S., and T.F. Schatzki,. 2000. Apple water-core sorting system using X-ray imagery: I. Algorithm development. *Transactions of the ASAE*. 43(6):1695-1702.
- Kim, S., and T.F. Schatzki. 2001. Detection of pinholes in almonds through x-ray imaging. *Transactions of the ASAE*. 44(4):997-1003.
- Knoll, GF. 1989. *Radiation Detection and Measurement – 2<sup>nd</sup> edition*. John Wiley & Sons, New York.
- Koning, C.T.J. de, L. Speelman, and H.C.P. de Vries. 1994. Size grading of potatoes: Development of a new characteristic parameter. *J. agric. Engng. Res.* 57(2):119-128.
- Kotwaliwale, N., J. Subbiah, P.W. Weckler, G.H. Brusewitz, and G.A. Kranzler. 2003. Development and calibration of a soft X-ray digital imaging system. *Unpublished research paper, copy at Appendix A*.
- Kraszewski, A., and S. Nelson. 1993. Microwave permittivity of pecan nuts. *Journal of Microwave Power and Electromagnetic Energy*. 28(3):165-173.
- Lawrence, K.C., S.O. Nelson, and A.W. Kraszewski. 1992. Temperature dependence of the dielectric properties of pecans. *Transactions of the ASAE*. 35(1):251-255.

- Maness, N., and G.H. Brusewitz. 2000. Drying, handling and storage of pecans. *Unpublished article.*
- MATLAB. 2001. MATLAB. Ver. 6.1.0.450 Rel. 12.1. Natick, M.A.: The Mathworks, Inc.
- McFarlane, N.J.B., C.R. Bull, R.D. Speller, G.J. Royle, and K.R.A. Johnson. 2000. The potential for Compton scattered X-rays in food inspection: The effect of multiple scatter and sample inhomogeneity. *J. agric. Engng. Res.* 75(3):265-274.
- McGlone, V.A., R.B. Jordan, R. Seelye, and P.J. Martinsen. 2002. Comparing density and NIR methods for measurement of kiwifruit dry matter and soluble solid content. *Postharvest Biology and Technology.* 26:191-198.
- Mitchell, A. D., M. B. Solomon and T. S. Rumsey. 1997. Composition analysis of beef rib sections by dual-energy x-ray absorption. *Meat Science.* 47(1-2):115-124.
- Mitchell, A.D., A.M. Scholz, V.G. Prusel, and C.M. Evok-Clover. 1998a. Compositional analysis of pork carcasses by dual energy X-ray absorptiometry. *Journal of Animal Science.* 76(8):2104-2114.
- Mitchell, A.D., A.M. Scholz, and J.M. Conway. 1998b. Body composition analysis of pigs from 5 to 97 kg by dual energy X-ray absorptiometry. *Applied Radiation Isotopes.* 49(5-6):521-523.
- Mitchell, A.D., A.M. Scholz, and J.M. Conway. 1998c. Body composition analysis of pigs by dual energy X-ray absorptiometry. *Journal of Animal Science.* 76(9):2392-2398.

- Mitchell, A.D., A.M. Scholz, and V.G. Pursel. 2001. Total body and regional measurements of bone mineral density in pigs by dual energy X-ray absorptiometry. *Journal of Animal Science*. 79(10): 2594-2604.
- Mizarch, A., N. Galili, S. Gun-mor, U. Flitsanov, and I. Prigozin. 1996. Models of ultrasonic parameters to assess avocado properties and shelf life. *J. Agric. Engng Res*. 65(4):261-267.
- Mizarch, A., U. Flitsanov, and V. Fuchs. 1997. An ultrasonic nondestructive method for measuring maturity of mango fruit. *Transactions of the ASAE*. 40(4):1107-1111.
- Mohsenin, N.N. 1986. *Physical properties of plant and animal materials*. G&B Scientific Publishers, NY.
- Morita, K., S. Tanaka, C.N. Thai, and Y. Ogawa. 1997. Development of soft X-ray imaging for detecting internal defects in food and agricultural products. *Proc. Sensors for nondestructive testing: Measuring quality of Fresh Fruits & Vegetables- Florida (Feb 18-21, 1997)*:305-315.
- Nascenzi, N. 2000. Aw, shucks – In nutshell, pecans pitiful. *Tulsa World* dt. November 10, 2000.
- Nelson, S.O. 1973. Electrical properties of agricultural products – A critical review. *Special Publications SP-05-73*. American Society of Agricultural Engineers.
- Nelson, S.O. 1981. Frequency and moisture dependence of the dielectric properties of chopped pecans. *Transactions of the ASAE*. 24(6):1573-1576.



- Nelson, S.O. 1983. Observations on the density dependence of dielectric properties of particulate materials. *Journal of Microwave Power*. 18(2):143-152.
- Nelson, S.O. 1984. Density dependence of the dielectric properties of wheat and whole-wheat flour. *Journal of Microwave Power*. 19(1):55-64.
- Nelson, S.O. 1991. Dielectric properties of agricultural products – Measurement and applications. *IEEE Transactions on Electrical Insulation*. 26(5):845-869.
- Nelson, S.O. 1999. Dielectric properties measurement techniques and applications. *Transactions of the ASAE*. 42(2):523-529.
- Nelson, S.O., and J.A. Payne. 1982. RF dielectric heating for pecan weevil control. *Transactions of the ASAE*. 25(2):456-458,464.
- Nelson, S.O., and K.C. Lawrence. 1995. Nondestructive moisture determination in individual pecans by RF impedance measurements. *Transactions of the ASAE*. 38(4):1147-1151.
- Nelson, S.O., Chari V.K. Kandala, and K.C. Lawrence. 1992 a. Moisture determination in single grain kernels and nuts by RF impedance measurements. *IEEE Transactions on Instrumentation and Measurement*. 41(6):1027-1031.
- Nelson, S.O., K.C. Lawrence, and A.W. Kraszewski. 1992 b. Sensing moisture content of pecans by RF impedance and microwave measurements. *Transactions of the ASAE*. 35(2):617-623.

- NIEHS. 2002. Permissible exposure levels. Available at: <http://www.niehs.nih.gov/odhsb/radhyg/radguide/sectxi.htm>. Accessed 24 April 2003.
- Olajide, J.P., and B.I.O. Ade-Omowaye. 1999. Some physical properties of locust bean seed. *J. agric. Engng. Res.* 74(2):213-215.
- Özarslan, C. 2002. Physical properties of cotton seed. *Biosystems Engineering.* 82(2):169-174.
- Paiva, R.F.D., J. Lynch, E. Rosenberg, and M. Bisiaux. 1998. A beam hardening correction for X-ray microtomography. *NDT & E International*, 31(1):17-22.
- Pearson, T. 2000. Detection of pistachio nuts with closed shells using impact acoustics. *ASAE paper No. 003068*. 2000 ASAE Annual International Meeting, Milwaukee, Wisconsin, USA.
- Reid, J.T., and E.K. Heaton. 1977. The effect of mechanical harvesting and cleaning operations on shell-breaking and nutmeat quality of pecans. *Transactions of the ASAE.* 20(2): 623-625.
- Rogasik,H., J.W. Crawford, O. Wendroth, I.M. Young, M. Joschko and K. Ritz. 1999. Discrimination of Soil Phases by Dual Energy X-ray Tomography. *Soil Science Society of America Journal.* 63:741-751.
- Rosenthal, R.D., and D.R. Webster. 1973. On line system sorts fruit on basis of internal quality. *Food Technology.* 27(7):52-60.
- Ruiz, M. and P. Chen. 1982. Use of the first derivative of spectral reflectance to detect mold on tomatoes. *Transactions of the ASAE.* 25(3):759-762.

- Santerre, C.R. 1994. Pecan composition. In *Pecan Technology* Ed. C.R. Santerre. Chapman & Hill, NY. PP 98-110.
- SAS. 1990. SAS. Ver. 6a. Cary, N.C.: SAS Institute, Inc.
- Schatzki, T.F., R.P. Haff, R. Young, I. Can, L-C. Le, and N. Toyofuku. 1997. Defect detection in apples by means of X-ray imaging. *Proc. Sensors for nondestructive testing: Measuring quality of Fresh Fruits & Vegetables-Florida* (Feb 18-21, 1997):161-171.
- Schmilovitch, Z., S.O. Nelson, C.V.K. Kandala, and K.C. Lawrence. 1996. Implementation of dual frequency RF impedance technique for on-line moisture sensing in single in-shell pecans. *Applied Engineering in Agriculture*. 12(4):475-479.
- Shahin, M.A., and Tollner, E.W. 1997. Detection watercore in apples using X-ray linescans feature extraction and classification. *Proc. Sensors for nondestructive testing: Measuring quality of Fresh Fruits & Vegetables-Florida* (Feb 18-21, 1997):389-400.
- Shahin, M.A., E.W. Tollner, and S.E. Prussia. 1999. Filter design for optimal feature extraction from X-ray images. *Transactions of the ASAE*. 42(6):1879-1887.
- Sims, K.A. 1994. Mechanization of post harvest pecan processing. In *Pecan Technology* Ed. C.R. Santerre. Chapman & Hill, NY. PP 68-86.
- Singh, K.K., and T.K. Goswami. 1996. Physical properties of cumin seed. *J. agric. Engng. Res.* 64(2):93-98.

- Stein, L. 1980. Maintaining the quality of pecans with storage. *The Pecan Quarterly*. 14(4):12-17.
- Steiner, P.R., L.A. Jozsa, M.L. Parker, and S. Chow. 1978. Application of X-ray densitometry to determine density profile in waferboard: Relationship of density to thickness expansion and internal bond strength under various cycles. *Wood Science*. 11(1):48-55.
- Stone, M.L., G.H. Brusewitz, and D.R. DeVoe. 1984. Variation in dielectric properties of wheat. *ASAE Paper No. 84-3547*. Winter Meeting American Society of Agricultural Engineers.
- Stone, M.L., P.R. Armstrong, D.D. Chen, G.H. Brusewitz, and N.O. Maness. 1998. Peach firmness prediction by multiple location impulse testing. *Transactions of the ASAE*. 41(1):115-119.
- Stone, M.L., P.R. Armstrong, X. Zhang, G.H. Brusewitz, and D.D. Chen. 1996. Watermelon maturity determination in the field using acoustic impulse impedance technique. *Transactions of the ASAE*. 39(6):2325-2330.
- Surjadinata, B.B., Brusewitz, G.H., and Bellmer, D. 2001. Pecan texture as affected by moisture content before freezing and thawing rate. *J. Food Process Eng.* 24(4):253-272.
- Tao, Y., and J.G. Ibarra. 2000. Thickness-compensated X-ray imaging detection of bone fragments in deboned poultry-Model analysis. *Transactions of the ASAE*. 43(2):453-459.

- Thai, C.N., E.W. Tollner, K. Morita, and S.J. Kays. 1997. X-ray characterization of sweet potato weevil larvae development and subsequent damage in infested roots. *Proc. Sensors for nondestructive testing: Measuring quality of Fresh Fruits & Vegetables- Florida* (Feb 18-21, 1997):361-368.
- Thompson, A.K. 1996. *Post Harvest Technology of Fruits and Vegetables*. Blackwell Science Ltd. Oxford, London, Cambridge(USA).
- Tollner, E.W. 2002. Classification of onions based on internal defects using commercial X-ray inspection equipment. *ASAE paper No. 026092*. American Society of Agricultural Engineers, St. Joseph, Mich.
- Tollner, EW; YC Hung; BL Upchurch; and SE Prussia. 1992. Relating X-ray absorption to density and water content in apples. *Transactions of the ASAE*. 35(6):1921-1928.
- USDA. 2002 a. Nuts, pecans (1). USDA National Nutrient Database for Standard Reference. Available at: [http://www.nal.usda.gov/fnic/cgi-bin/list\\_nut.pl](http://www.nal.usda.gov/fnic/cgi-bin/list_nut.pl). Accessed May 23, 2003.
- USDA. 2002 b. *Fruit and Tree Nuts Yearbook - summary*. Available at: <http://ers.usda.gov/publications/fts/Yearbook02/FTS2002s.txt>. Accessed May 23, 2003.
- USDA. 2003. *Noncitrus fruits and Nuts - 2002 preliminary summary*. United States Department of Agriculture. National Agricultural Statistics Service. Fr Nt 1-3(03). Also available at: <http://usda.mannlib.cornell.edu/reports/nassr/fruit/pnf-bb/ncit0103.pdf>. Accessed on May 12, 2003.

- Verma, B.P., E.K. Heaton, and A. Zaltman. 1985. Mechanization of some pecan harvesting processes. *ASAE paper No. 85-3047*. American Society of Agricultural Engineers, St. Joseph, Mich.
- Viswanathan, R., P.T. Palaniswamy, L. Gothandapani, and V.V. Sreenarayanan. 1996. Physical properties of neem nut. *J. agric. Engng. Res.* 63(1):19-26.
- Wagner, A. 1980. Pecan Storage : An important post harvest practice in preventing nut damage. *Pecan South*. September:40-43.
- Willard, H.H., L.L. Merritt Jr., J.A. Dean, and F.A. Settle, Jr. 1988. *Instrumental Methods of Analysis (7th Edition)*. Wadsworth Publishing Company, California.
- Wood, B.W., J.A. Payne, and L.J. Grauke. 1994. An overview of the evolution of the US pecan industry. In *Pecan Technology* Ed. C.R. Santerre. Chapman & Hill, NY. PP 1-11.
- Worley, R.E. 1994 a. Pecan production. In *Pecan Technology* Ed. C.R. Santerre. Chapman & Hill, NY. PP 12-38.
- Worley, R.E. 1994 b. Pecan physiology and composition. In *Pecan Technology* Ed. C.R. Santerre. Chapman & Hill, NY. pp 39-48.
- Zwiggelaar, R., C.R. Bull, M.J. Mooney, and S. Czarnes. 1997. The detection of "soft" materials by selective energy Xray transmission imaging and computer tomography. *J. agric. Engng. Res.* 66(3):203-212.

## **APPENDICES**

Appendix - A -- Development and Calibration of a Soft X-Ray Digital  
Imaging System for Agricultural products

Appendix - B -- X-ray Images of Pecans

Appendix - C -- Features detected from X-ray images for quality detection

Appendix - D -- Photographs of the equipment

Appendix - E -- Computer programs

## **APPENDIX - A -- DEVELOPMENT AND CALIBRATION OF A SOFT X-RAY DIGITAL IMAGING SYSTEM FOR AGRICULTURAL PRODUCTS**

(Only portion on calibration presented here)

Nachiket Kotwaliwale, ASAE Member, Graduate Student, Jeyamkondan Subbiah, ASAE Member, Research Engineer, Paul R. Weckler, ASAE Member, Assistant Professor, Gerald H. Brusewitz, ASAE Fellow, Regents Professor, and Glenn A. Kranzler, ASAE Fellow, Professor, Department of Biosystems and Agricultural Engineering, Oklahoma State University, Stillwater, OK.

Developed X-ray imaging system was calibrated to study X-ray attenuation of agricultural products and relate it to product quality. Calibration procedure of the equipment is discussed in this paper.

### **Materials and Methods**

#### ***System Calibration and Testing***

Calibration addressed the effect on detector response (X-ray image intensity) of: (a) the instrument characteristics, viz., dark current (camera) and polychromatic X-rays (source tube); and (b) the input variables, viz., signal integration time, X-ray tube current, and X-ray tube voltage. Images were captured with the camera placed 153 mm from the X-ray source and quantized at 8-bit depth for analysis. Only the central 1000 x 1000 pixels were used in this



study because some pixels near the border were either dead or did not receive X-ray photons as expected. Images were analyzed using MATLAB (The Mathworks, Inc., Natick, MA), and all statistical analyses were conducted in SAS (SAS Institute, Inc., Cary, N.C.).

### Dark Current

The detector array accumulates some signal even when not exposed to X-ray radiation. This effect is due to dark current (leakage) in the photodetector. Thermally generated charge is the main source of dark current in the photodetector arrays (Barna et al., 1999). Images generated by the photodetector consist of the signal due to dark current in addition to the signal generated by incident X-ray energy. Therefore, the dark current image (or offset image) must be deducted from all the images to obtain the net signal due to X-rays. To eliminate the effect of ambient temperature on signal or detector response, an offset image was acquired just before acquisition of each image used in the calibration study.

### Flat-Field Correction

Non-uniformities in pixel response, phosphor scintillator, optical coupling, and transmission cause variation in response across the face of the detector (Gruner et al., 2002). Flat-field correction, also known as gain correction, is commonly employed to overcome these abnormalities and is multiplicative in nature (Barna, et al., 1999). The primary research interest was in calculating the attenuation coefficient, which is calculated from the ratio of two

intensities,  $I$  and  $I_0$ . This multiplicative correction cancels out during division, and therefore flat-field correction was not employed on images used in this study.

### Effect of Equipment Variables

To determine the effect of X-ray tube current on image detector response, images were acquired at currents from 0.1 to 1 mA in steps of 0.1 mA for voltages from 12.5 to 22.5 kVp in steps of 2.5 kVp, and from 25 to 50 kVp in steps of 5 kVp. Detectors saturated at high voltages and currents (Ref. Section ahead – Development of Model) therefore, a suitable uniform material was placed over the detector array for voltages above 25 kVp such that the detectors did not saturate at 1 mA for that particular voltage. The lowest available integration time of 460 ms was used.

To study the effect of X-ray tube voltage on image detector response, blank images were acquired at currents from 0.2 to 1 mA in steps of 0.1 mA for voltages from 12.5 to 22.5 kVp in steps of 2.5 kVp. From 25 to 50 kVp in steps of 5 kVp, images were acquired at current levels of 0.25, 0.50, 0.75, and 1.00 mA with a suitable uniform material placed over detector so that the detectors did not saturate at 50 kVp for that particular current. Signal integration time was set to 460 ms.

To test the effect of signal integration time, images were acquired at 460, 640, 820, and 1000 ms for eight different combinations of voltage and current. A uniform material, if required, was placed over the detector, to prevent saturation at 1000 ms.

### Repeatability of the System

Imprecision is defined as lack of repeatability in the system. It consists of: (a) variability of the X-ray source tube in producing the desired quantity and quality of X-ray photons, and (b) variability in response of photodiode arrays to X-rays. An experiment was set-up as a factorial design with four levels of integration time (460, 640, 820, and 1000 ms), two levels of voltage supplied to tube (30, 50, kVp), and three levels of current supplied to tube (0.3, 0.6, and 0.9 mA). At each condition, if required, the X-ray beam was filtered using a uniform material to avoid image saturation. Three replicates were collected. Standard deviation of gray level at each pixel for three replicates was calculated. Mean of standard deviation of gray level of all one million detectors (pixels) was reported as the imprecision of the system at that condition.

### Development of Model

Blank images were acquired when no material was between the detector and X-ray tube. Blank images taken at different voltages and currents represent incident X-ray intensity ( $I_0$ ) at that condition.  $I_0$  is required to calculate attenuation coefficient. Detector response increases with increasing voltage, current, or integration time, but reaches a limit after which an increase in any of these factors does not increase detector response. Figure A.1 shows saturation of detectors at higher voltages and currents at 460-ms integration time. Detector saturation complicates calculation of attenuation coefficient. For instance, at 50 kVp and 1 mA we should capture a good quality image of an agricultural product. Such an image would represent transmitted X-ray intensity ( $I$ ) at 50 kVp and 1

mA. However, because of detector saturated at that condition, estimating  $I_0$  is erroneous, and hence calculations of the attenuation coefficient would be incorrect. Therefore, calibration equations were developed to explain the relationship between voltage, current, and blank image intensity at 460 ms integration time. Detectors did not saturate at 1 mA and 460-ms for voltages below 25 kVp. Therefore, images were acquired at voltages from 25 to 50 kVp at intervals of 1 kVp, and at 10-15 different current levels, chosen to avoid detector saturation. In total, 897 images were acquired to develop the model. The developed statistical model can be used to estimate extrapolated image intensity at higher voltages and currents, where detectors normally saturate. Because detector-to-detector variation was quite high, (Fig. A.2), calibration equations were developed for each of the 1 million pixels.

To validate the developed statistical models, new blank images were acquired under conditions different from those with which the model was developed. Conditions were selected to avoid detector saturation. At each voltage from 25-50 kVp in steps of 1 kVp, one validation image was acquired.

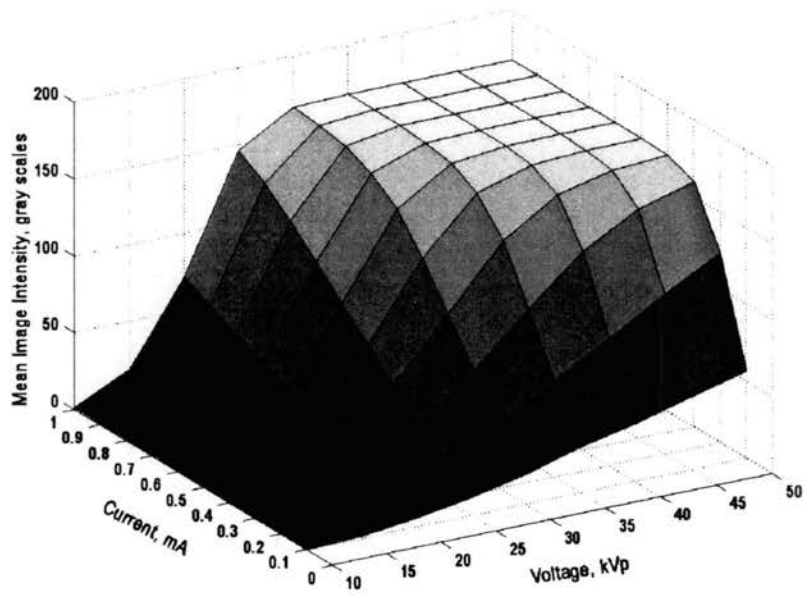


**Figure A.1** Detector saturation at higher voltages and currents at 460 ms.

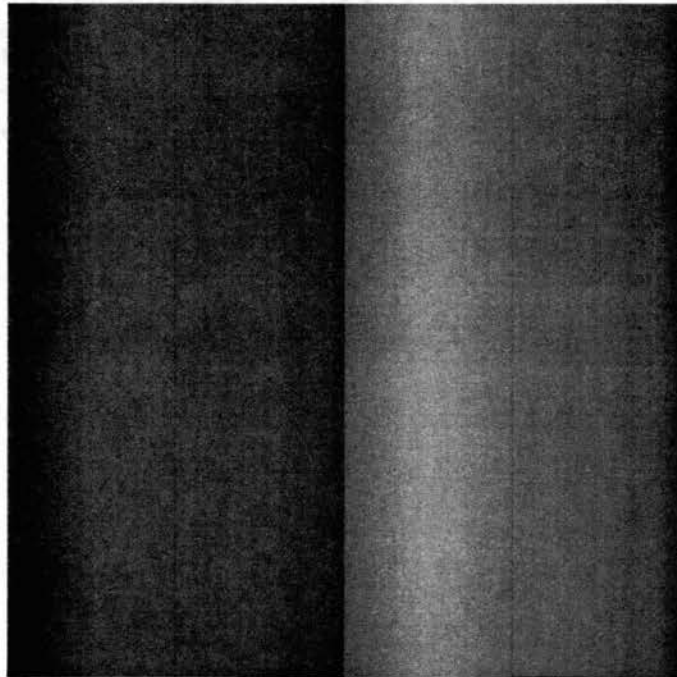


**Figure A.2** Blank image ( $I_0$ ) taken at 50 kVp, 0.22 mA, 460 ms demonstrating detector variation.

## Beam Hardening

Attenuation coefficient is a material property and therefore does not vary with the thickness of a material for monochromatic radiations of any given energy. Under polychromatic X-rays, the attenuation coefficient of a material varies with thickness. During the trajectory through the material, lower energy X-ray photons are first preferentially attenuated as a result the spectrum of polychromatic radiation changes continuously, shifting towards higher mean energy (Paiva et al., 1998). If the results are interpreted with monochromatic approximation, the attenuation decreases as polychromatic X-rays passes through the material. This effect is known as “beam hardening”. To demonstrate this effect of “beam hardening”, polystyrene sheets of thickness from 0.08 to 6.03 cm (22 levels) were used to predict mass attenuation coefficient ( $\text{cm}^2/\text{g}$ ). Polystyrene was selected, because its density and atomic number are similar to biological materials (McFarlane, et al., 2000). Images were obtained at 460-ms signal integration time, at 15 to 50 kVp, and at three currents chosen such that the histogram distribution fell within the dynamic range of mean image intensities between 80 and 170 gray level. Blank images captured to develop statistical model were used for incident energy without attenuation ( $I_0$ ), wherever possible. Otherwise,  $I_0$  for the conditions were estimated from the developed model.

## Results and Discussion

### ***Calibration***

#### Effect of X-ray Tube Current

Figure A.3 shows the scatter plot of current versus intensity at voltages from 12.5 kVp to 22.5 kVp. Intensity is linearly related to current with  $R^2$  values of linear fit are above 0.99. Note that plots are for blank images, and thus the positive effect of voltage on intensity can also be seen. Scatter plots of current versus intensity at voltages from 25 to 50 kVp are shown in Figure A.4. However, voltage curves cannot be compared to each other, as different filtration materials were used to avoid detector saturation. For instance, 0.127 mm mild steel sheet was used at 50 kVp whereas 3.175 mm LDPE and 4.76 mm HDPE sheet were used at 30 kVp. The filtration materials were selected such that the intensity at the highest current (1 mA) was in the range of 120-160 gray level. Despite filtration, at each voltage linear effect of current on intensity was eminent. The linear relationship between current and image intensity is in agreement with the literature (Curry et al., 1990, Gambaccini et al., 1996).

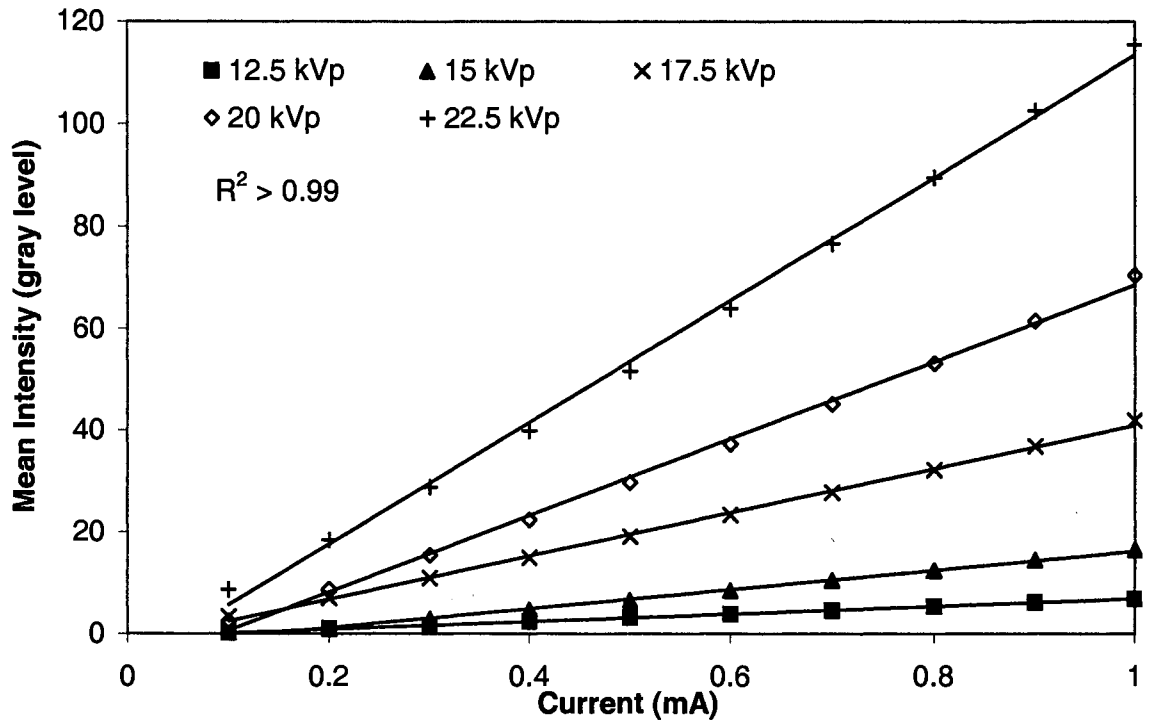


Figure A.3 Effect of current on intensity at lower voltages for blank images.

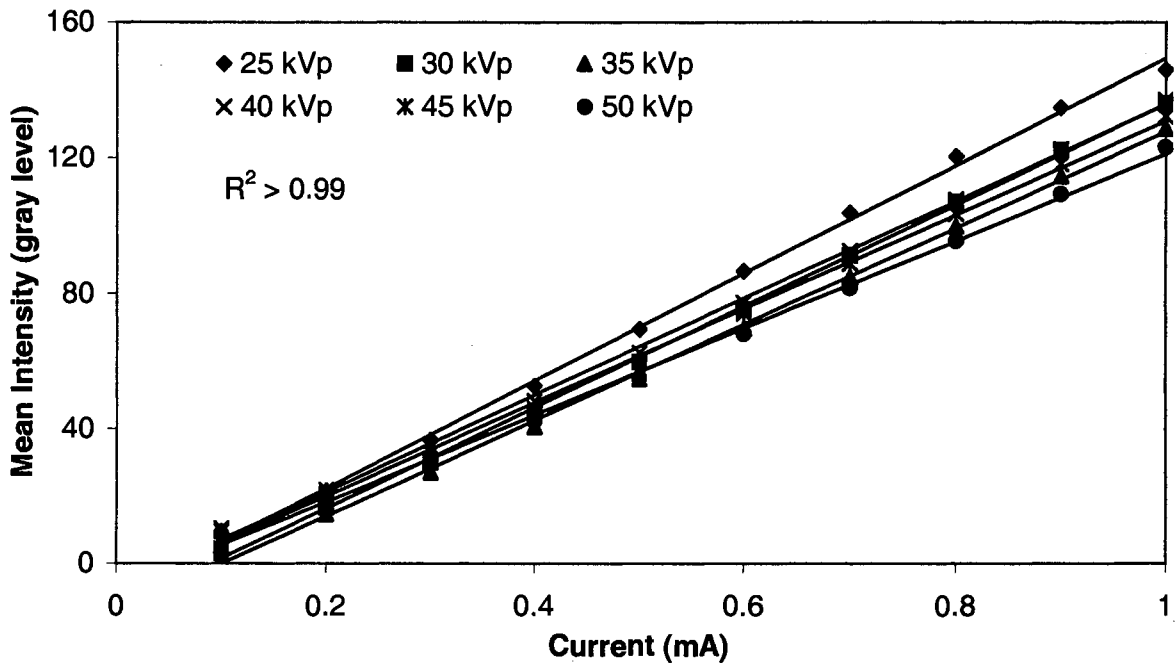


Figure A.4 Effect of current on intensity at higher voltages for images with filtered X-ray beam.



## Effect of X-ray Tube Voltage

The effect of voltage on intensity of blank images at voltages from 12.5 kVp to 22.5 kVp is presented in Figure A.5. Voltage showed a quadratic relationship with intensity. Peak voltage determines the maximum energy of the X-ray photons. In addition, higher voltage also increases the number of X-ray photons by increasing the electron cloud near the anode. Therefore, X-ray intensity increases as the square of the kilovoltage (Curry et. al., 1990). Regression models were constructed with intensity as dependent variable and voltage and square of voltage as independent variables. At lower currents (0.1 to 0.3 mA) the square of the voltage does not have a significant effect on intensity. At higher current ( $\geq 0.4$  mA), the intensity depends on the square of the voltage. Adjusted  $R^2$  values greater than 0.94 were obtained at various currents. Data at voltages higher than 22.5 kVp is not shown in Figure A.5, because images at these voltages were taken with the X-ray beam filtered differently to avoid detector saturation and to keep the signal level high enough to detect. However, when analyzed for individual currents, at lower current (0.25 mA), the voltage-squared term was not significant. At higher currents ( $\geq 0.50$  mA), the intensity was dependent on square of the voltage. Adjusted  $R^2$  values greater than 0.99 were obtained at all currents. The quadratic effect of voltage on intensity holds only for the unfiltered X-ray beam (Krestel, 1990). The beryllium window in the X-ray tube and filters used to avoid detector saturation can be identified as reasons for lack of a quadratic relation at lower currents. At higher currents the photon flux density was sufficient to show a significant quadratic relationship.

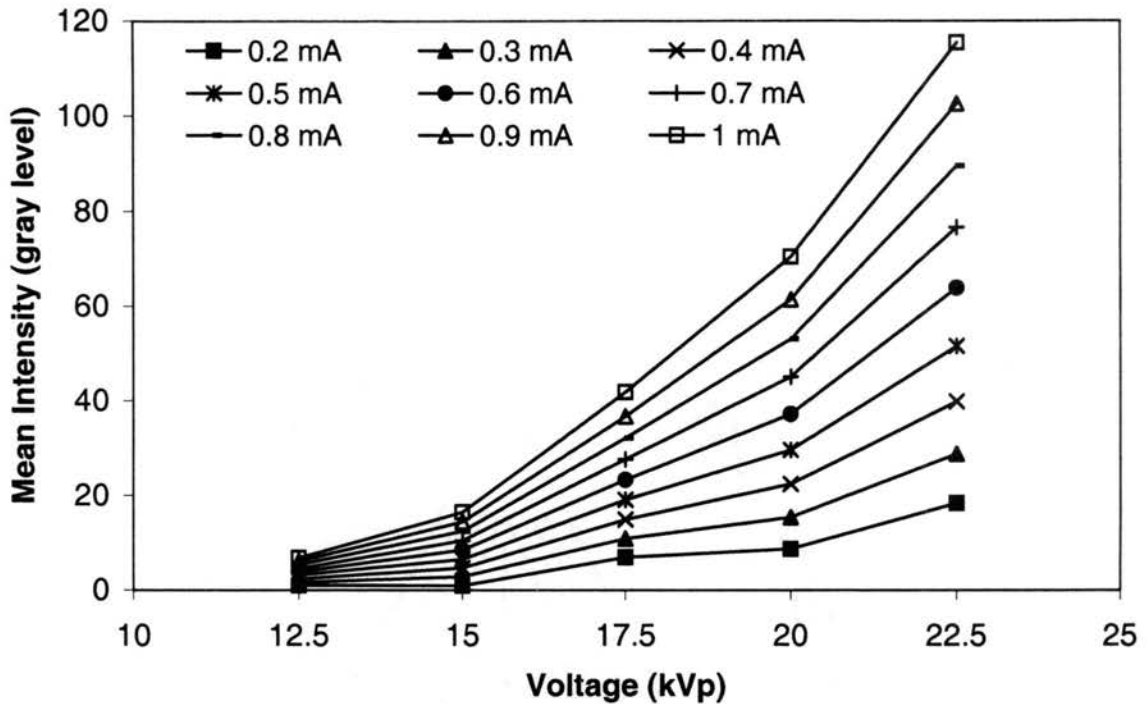


Figure A.5 Effect of voltage on intensity of blank images at various currents.

Effect of Integration Time

The effect of integration time on the mean image intensity is shown in Figure A.6.  $R^2$  values of more than 0.99 were observed, indicating that the response varied linearly with signal integration time. Gambaccini et al., (1996) reported the cumulative effect of current and integration time to be linear on X-ray image intensity. Some deviations in linearity at high voltage levels can be attributed to detector saturation. Increasing integration time not only increases signal level but also increases dark current level. Detectors tend to saturate at longer integration times, causing a decrease in the net signal. Figure A.7 shows this saturation effect for images taken at 15 kVp and 1 mA at different integration times. Integration times above 1500 ms result in loss of information and at 5000 ms both dark current and signal become saturated and hence the net signal drops

to zero. The integration time limit for detector saturation would be different for different voltages.

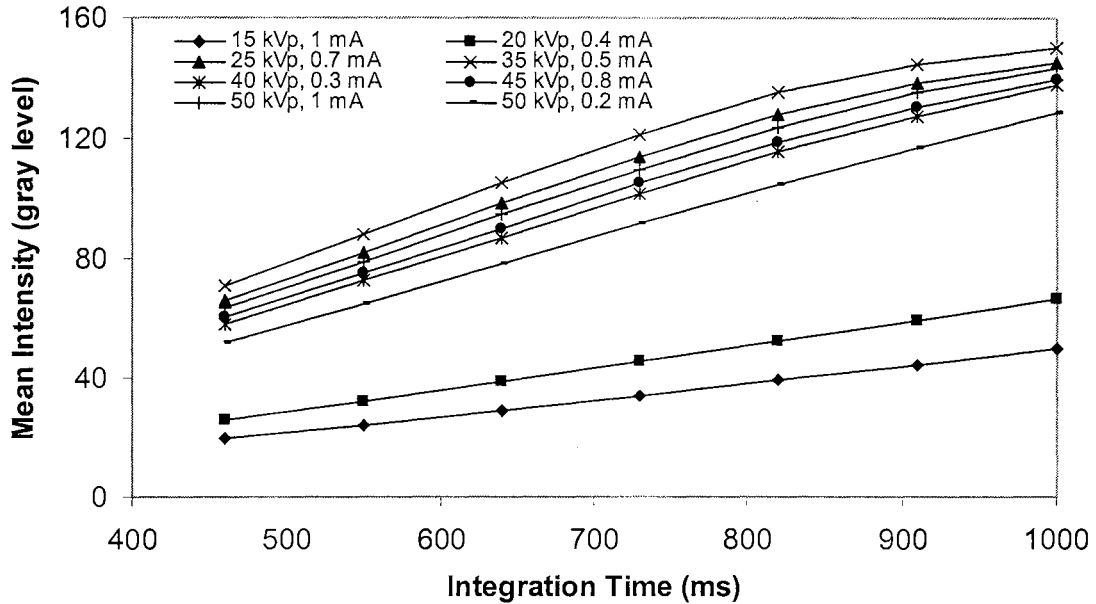


Figure A.6 Effect of integration time on the mean image intensity for eight different combinations of voltage and current.

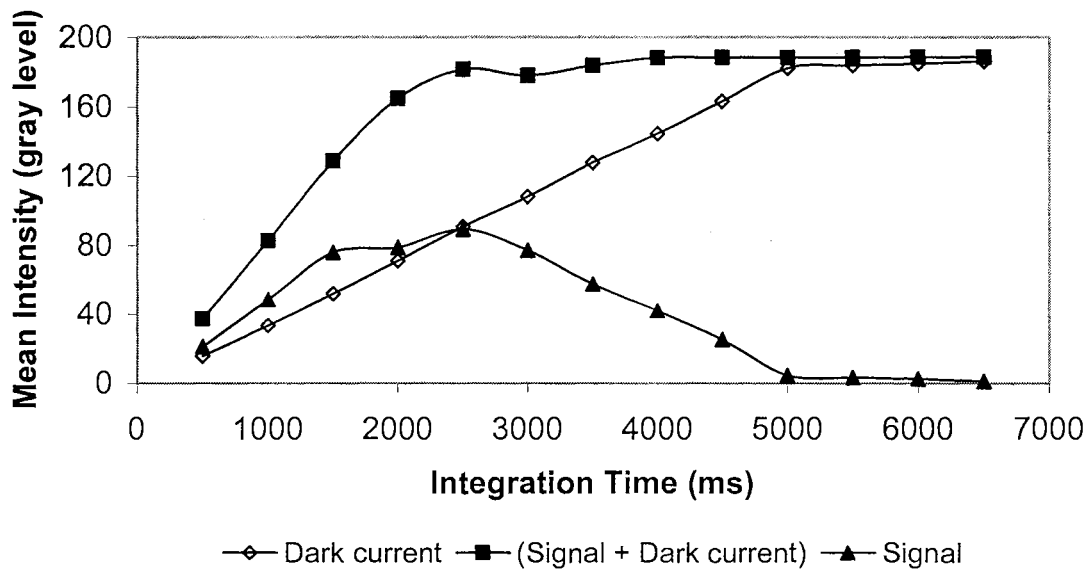


Figure A.7 Saturation in dark current and signal due to increase in integration time.

## Imprecision

System imprecision indicated by the mean standard deviation, ranged from 0.41 to 3.52 gray level with a mean of 1.63. All combinations of two-way interaction of three factors were not significant at 95% level of significance. All factors, voltage ( $p=0.15$ ), current ( $p=0.22$ ), and integration time ( $p=0.23$ ) did not have significant effect on the imprecision of the system. This result implies that the imprecision of the system is stable with respect to all input variables. The mean imprecision of 1.63 gray level is relatively insignificant compared to dynamic range (0-255 gray level).

## Statistical Model

Statistical regression models were developed using data from blank images where detectors did not saturate. These models can be used to predict incident intensity at conditions in which detector saturation occurs. Because intensity is directly proportional to current (Fig. A.3 and A.4) and proportional to the square of the voltage (Fig. A.5), the following model was first evaluated.

$$I_o = A + B \cdot i + C \cdot v^2 \quad (A-1)$$

where:  $I_o$  is pixel intensity, A, B, and C are regression coefficients,  $i$  is current and  $v$  is tube voltage. When this model was applied, the adjusted  $R^2$  value was only 0.68.

Because the intensity was linearly related to current, separate regression models were developed for each voltage level from 25-50 kVp in steps of 1 kVp. The statistical model evaluated was:

$$I_{o(v)} = A_v + B_v \cdot i \quad (A-2)$$

The  $R^2$  values were greater than 0.99 for all models. The slope ( $B_v$ ) in Equation 7 was linearly related to voltage (Fig. A.8), as given by:

$$B_v = C + D \cdot v \quad (A-3)$$

By combining Equations A-2 and A-3, a single model was obtained to estimate pixel intensity ( $I_o$ ) for all voltages (kVp) and currents (mA).

$$I_o = A + C \cdot i + D \cdot i \cdot v \quad (A-4)$$

Coefficients A, C, and D were calculated for each of the one million pixels from 897 images captured for model development.

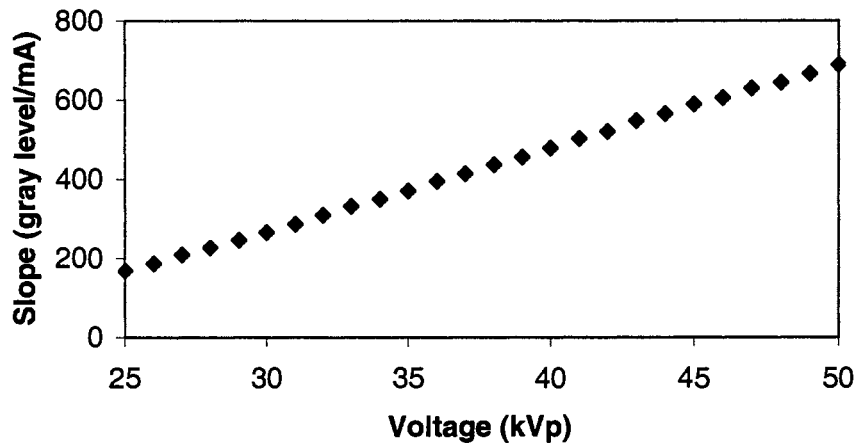


**Figure A.8 Relationship between voltage and slope of the linear current model.**

#### Evaluation of Statistical Models

The developed model (Eq. A-4) was used to predict intensity of blank images at conditions under which the model was developed. Mean absolute deviation of the predicted intensity from observed intensity values was 1.18 gray level. The predicted intensity versus observed intensity for different voltages and currents is shown in Figure A.9. Adjusted  $R^2$  value was higher than 0.99 for a linear fit. The plot shows a slight sigmoid shape indicated that higher-order

terms of  $(v \cdot i)$ ,  $i$ ,  $v$  could improve the degree of fit. Including higher-order coefficients did not improve the  $R^2$  value nor the distribution residuals. The validation error was 2.72 gray level. Errors are of the order of system imprecision (1.62 gray level), indicating the models are adequate for practical purposes.

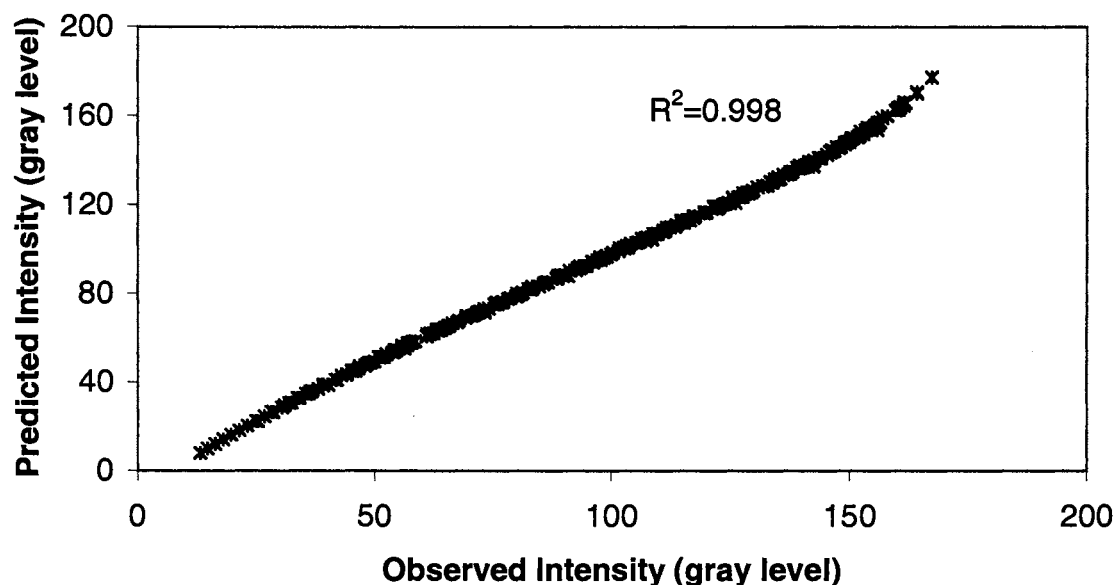
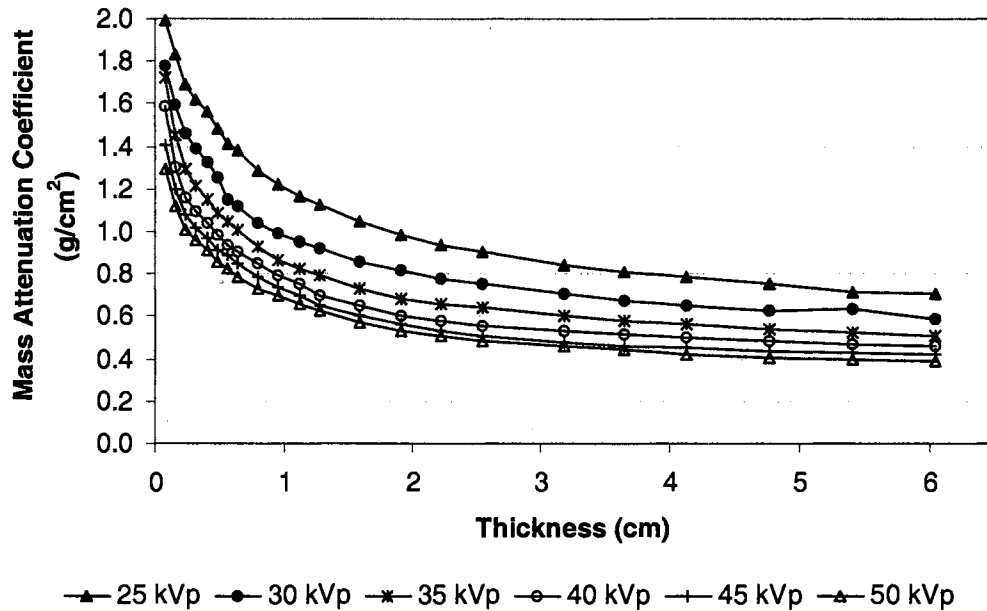


Figure A.9 Evaluation of model (Eq. A-4) for calibration images.

### Beam Hardening

The measured mass attenuation coefficient of the polystyrene decreased with the thickness of polystyrene (Fig. A.10). This is due to “beam hardening” of polychromatic X-rays produced by the source tube. At a given thickness, mass attenuation coefficients were less for higher voltages (Fig. A.10) as also reported by Curry et al. (1990) and Hubbell and Seltzer (1995). A sharp drop in attenuation coefficient values is evident at lower thickness. However, the drop decreased with thicker material. The attenuation coefficient values will drop

until the polychromatic X-ray beam becomes effectively monochromatic, i.e. the mean energy of the beam reaches the applied peak voltage.



**Figure A.10 Beam hardening in polystyrene at different X-ray energies**

### Conclusions

Calibration of a soft X-ray imaging system for agricultural products was presented in this study. Repeatability of the system was established. Effect of X-ray imaging variables (X-ray tube voltage, current, integration time), inconsistencies in X-ray source and detectors and product thickness on the image pixel intensities was discussed in detail. An attempt was also made to deal with detector saturation at higher voltages and currents. The following conclusions can be drawn from this study:

- X-ray tube current is linearly related to detector response, while X-ray voltage has a quadratic relationship.

- The signal integration time has a linear effect on detector response; however high integration times can saturate the detector.
- System imprecision ranged from 0.41 to 3.52 gray level with a mean of 1.63.
- Statistical models developed to estimate incident intensity ( $I_0$ ) at higher voltages and currents (at which sensors saturate) were successful with  $R^2 > 0.99$ , prediction error = 1.18 gray level, and validation error = 2.72 gray level. Error was of the order of system imprecision (1.62 gray level).
- Attenuation coefficient for a material changes with material thickness due to beam hardening effect.

## REFERENCES

- Barcelon, E.G., S. Tojo, and K. Watanabe. 1999. X-ray computed tomography for internal quality evaluation of peaches. *J. agric. Engng. Res.* 73(4):323-330
- Barna, S.L., M.W. Tate, S.M. Gruner, and E.F. Eikenberry. 1999. Calibration procedures for charge-coupled device x-ray detectors. *Review of Scientific Instruments.* 70(7): 2927-2934.
- Boyer, B.W. 2002. Personal communication. Oxford Instruments, X-Ray Technologies, Inc., Scotts Valley, CA.
- Chen, P. and Z. Sun. 1991. A review of non-destructive methods for quality evaluation and sorting of agricultural products. *J. agric. Engng. Res.* 49:85-98.
- Curry, T.S., J.E. Dowdey, and R.C. Murry, Jr. 1990. *Christensen's Physics of Diagnostic Radiology- 4th Ed.* William & Wilkins, Media, PA.



- Desrosier, N.W. 1960. *Radiation Technology in Food, Agriculture, and Biology*. Westport, Conn., AVI Pub. Co.
- Gambaccini, M., A. Taibi, A. Del Guerra, M. Marziani, and A. Tuffanelli. 1996. MTF evaluation of a phosphor-coated CCD for x-ray imaging. *Phys. Med. Biol.* 41:2799-2806.
- Gruner, S.M., M.W. Tate, and E.F. Eikenberry. 2002. Charge-coupled device area x-ray detector. *Review of Scientific Instruments.* 73(8):2815-2842.
- Haff, R.P. and D.C. Slaughter. 2002. X-ray inspection of wheat for granary weevils. Real time digital imaging vs. film. *ASAE paper No. 026093*. American Society of Agricultural Engineers, St. Joseph, Mich.
- Hubbell, J.H. and Seltzer, S.M. 1995. Tables of X-ray mass attenuation coefficients and mass energy absorption coefficients 1 keV to 20 MeV for elements Z=1 to 92 and 48 additional substances of dosimetric interest. *NISTIR 5632*. National Institute of Standards and Technology. US Department of Commerce.
- Karunakaran, C., D.S. Jayas, and N.D.G. White. 2002. Soft X-ray Inspection of wheat kernels infested by *Sitophilus oryzae*. *ASAE Paper No. 023132*. American Society of Agricultural Engineers, St. Joseph, Mich.
- Keagy, P.M. and T.F. Schatzki. 1993. Machine recognition of weevil damage in wheat radiographs. *Cereal Chemistry.* 70(6):696-700.
- Keagy, P.M., B. Parvin, and T.F. Schatzki. 1995. Machine recognition of navel orange worm damage in x-ray images of pistachio nuts. *Proceedings of SPIE-The International Society for Optical Engineering.* 2345:192-203.

- Kim, S. and T.F. Schatzki. 2000. Apple water-core sorting system using X-ray imagery: I. Algorithm development. *Transactions of the ASAE*. 43(6):1695-1702.
- \_\_\_\_\_. 2001. Detection of pinholes in almonds through x-ray imaging. *Transactions of the ASAE*. 44(4):997-1003.
- Krestel, E. 1990. *Imaging Systems for Medical Diagnosis: Fundamentals and Technical Solutions - X-Ray Diagnostics - Computed Tomography - Nuclear Medical Diagnostics - Magnetic Resonance Imaging - Ultrasound Technology*. John Wiley & Son Ltd. PP 69.
- Mathworks. 2001. MATLAB. Ver. 6.1.0.450 Rel. 12.1. Natick, M.A.: The Mathworks, Inc.
- McFarlane, N.J.B., C.R. Bull, R.D. Speller, G.J. Royle, and K.R.A. Johnson. 2000. The potential for Compton scattered X-rays in food inspection: The effect of multiple scatter and sample inhomogeneity. *J. agric. Engng. Res.* 75(3):265-274.
- Paiva, R.F.D., J. Lynch, E. Rosenberg, and M. Bisiaux. 1998. A beam hardening correction for X-ray microtomography. *NDT & E International*. 31(1):17-22.
- SAS. 1990. SAS. Ver. 6a. Cary, N.C.: SAS Institute, Inc.
- Schatzki, T.F., R.P. Haff, R.Young, I. Can, L.C. Le, and N. Toyofuku. 1997. Defect detection in apples by means of X-ray imaging. *Transactions of the ASAE*. 40(5):1407-1415.

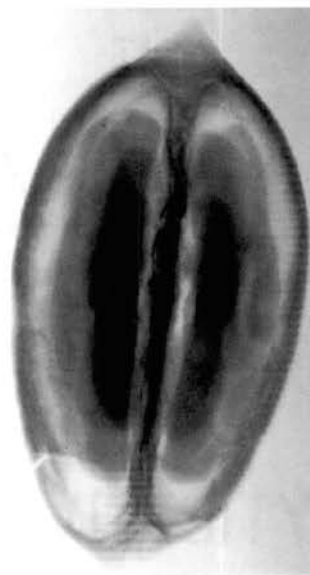
- Siemens. 2001. Simulation of X-ray spectra. Available at: <http://www.med.siemens.com/med/rv/spektrum/mamIn.asp>. Accessed on: 29 May 2003.
- Steiner, P.R., L.A. Jozsa, M.L. Parker, and S. Chow. 1978. Application of X-ray densitometry to determine density profile in waferboard: Relationship of density to thickness expansion and internal bond strength under various cycles. *Wood Science*. 11(1):48-55.
- Tao, Y. and J.G. Ibarra. 2000. Thickness-compensated X-ray imaging detection of bone fragments in deboned poultry - Model analysis. *Transactions of the ASAE*. 43(2):453-459.
- Thomas, P., A. Kannan, V.H. Degwekar, and M.S. Ramamurthy. 1995. Non-destructive detection of seed weevil-infested mango fruits by X-ray imaging. *Postharvest Biology and Technology*. 5(1-2):161-165.
- Tollner, E.W. 2002. Classification of onions based on internal defects using commercial X-ray inspection equipment. *ASAE paper No. 026092*. American Society of Agricultural Engineers, St. Joseph, Mich.

## APPENDIX - B -- X-RAY IMAGES OF PECANS

These images were taken at 30 kVp, 1 mA. Most of these images were taken with the plane joining two pecan halves perpendicular to the camera plane. Integration time was 460 ms and offset correction was performed with an offset image taken immediately preceding the pecan image.



Sample F-1



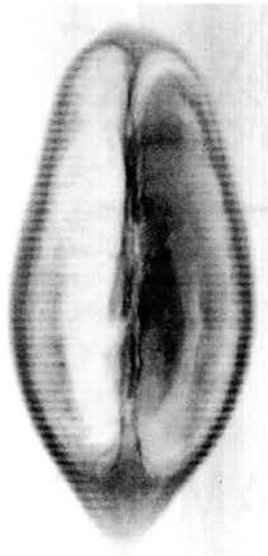
Sample F-2



Sample F-3



Sample F-4



Sample F-5



Sample F-6



Sample F-7



Sample F-8



Sample F-9

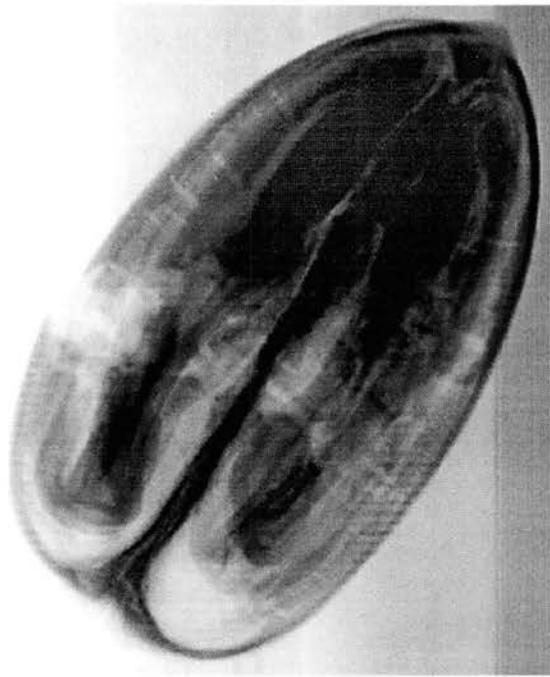


Sample F-10

**Figure B.1 X-ray images of fabricated pecans at one orientation.**



Sample U-1



Sample U-2



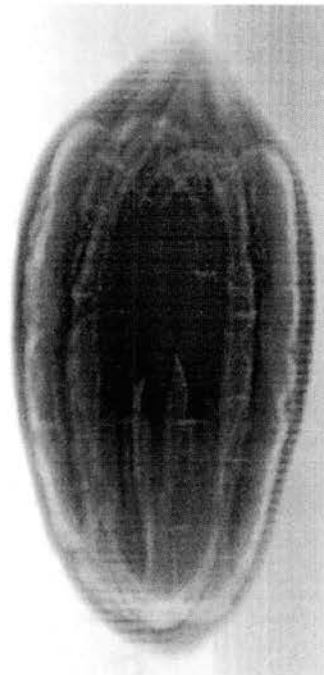
Sample U-3



Sample U-4



Sample U-5



Sample U-6



Sample U-7



Sample U-8





Sample U-9



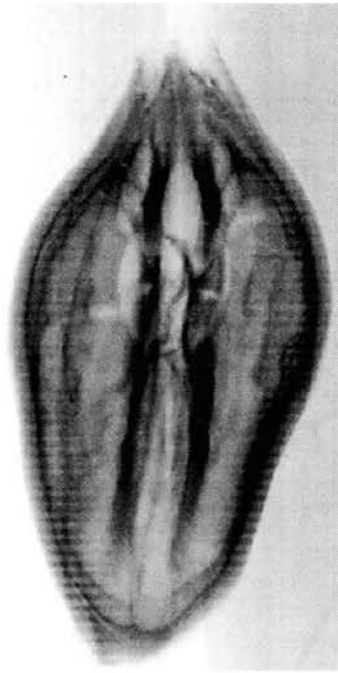
Sample U-10



Sample U-11



Sample U-12



Sample U-13



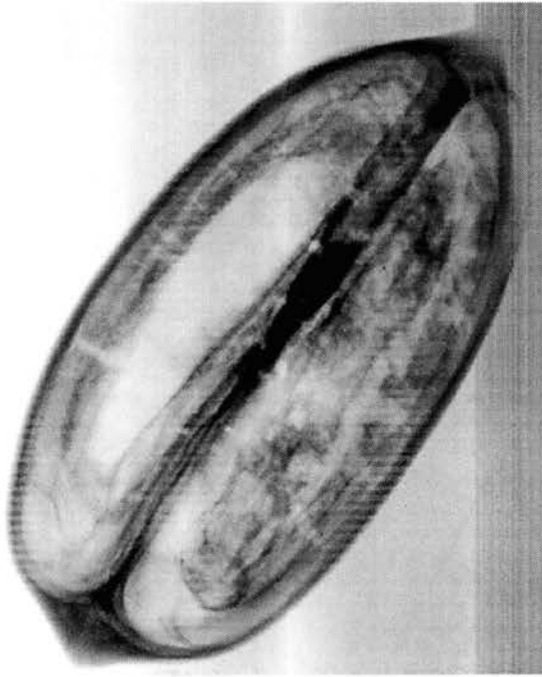
Sample U-14



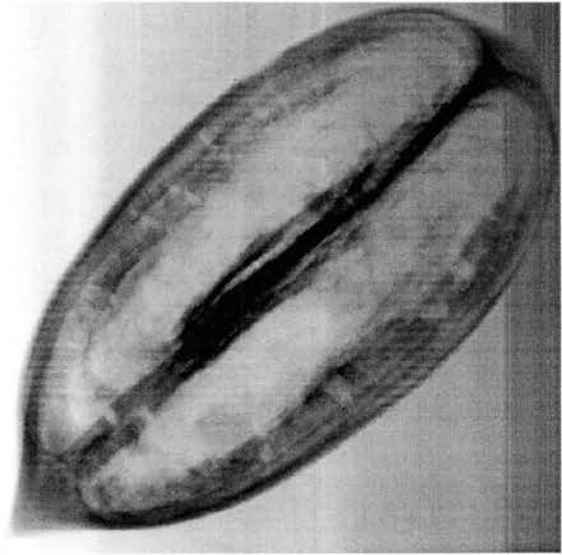
Sample U-15



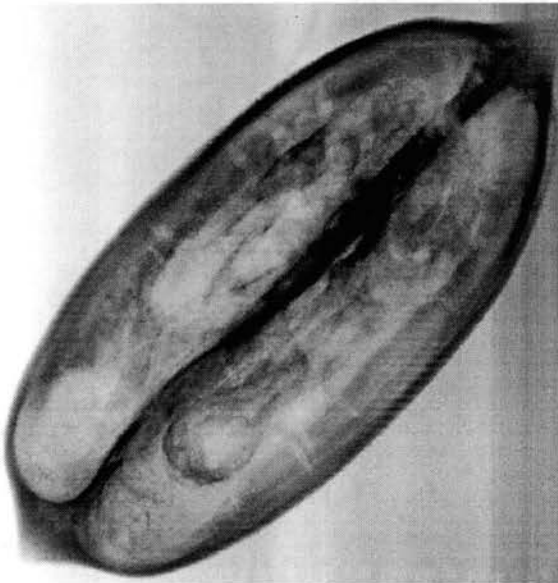
Sample U-16



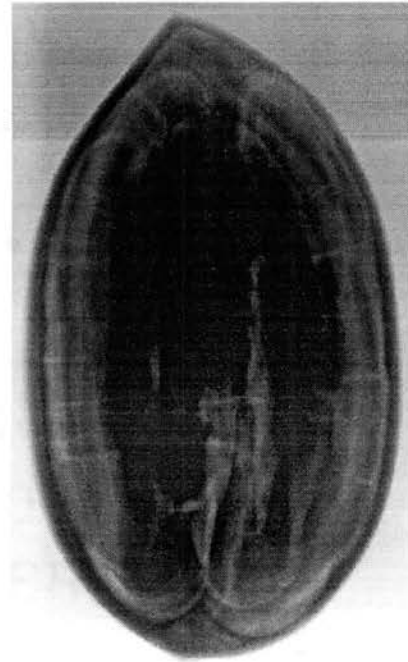
Sample U-17



Sample U-18



Sample U-19



Sample U-20



Sample U-21



Sample U-22



Sample U-23



Sample U-24



Sample U-25



Sample U-26



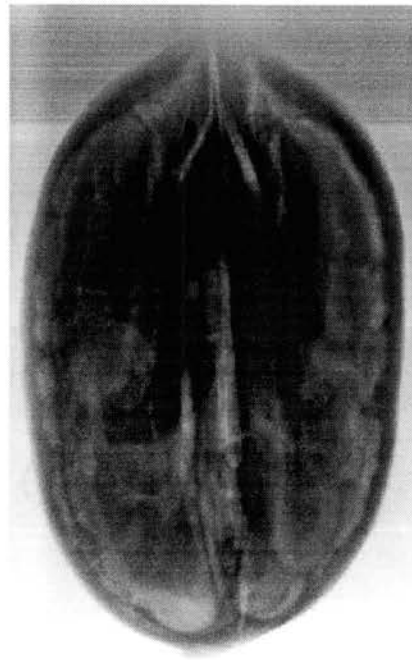
Sample U-27



Sample U-28



Sample U-29



Sample U-30

**Figure B.2 X-ray images of 'unknown' pecans at one orientation.**

**APPENDIX - C -- FEATURES FROM X-RAY IMAGES FOR QUALITY  
DETECTION**

**Table C.1 Nutmeat features and percent area occupied by nutmeat inside  
shell for fabricated pecans.**

<b>Sample</b>	<b>Nutmeat feature</b>	<b>Orientation</b>	<b>Percent area occupied by the nut<sup>§</sup></b>
1	Good	1	79.79
		2	76.79
2	Slightly broken	1	72.56
		2	63.79
3	Surface Damaged	1	65.08
		2	89.52
4	Broken pieces	1	62.80
		2	55.98
5	One side part	1	34.96
		2	54.51
6	Insect hole with insect	1	76.36
		2	81.10
7	Tiny Insect hole	1	68.67
		2	59.69
8	Insect hole	1	95.92
		2	82.82
9	Insect hole with insect	1	68.11
		2	69.42
10	Insect hole with insect	1	71.34
		2	68.43

(§= ROI-2/ROI-1\*100)

**Table C.2 Mean and standard deviation of pixel intensity of ROI-1 for fabricated pecan samples.**

Sample No.	Actual wt., g	Nutmeat feature	25 kVp		30 kVp		35 kVp		40 kVp		45 kVp		50 kVp	
			Mean	STD	Mean	STD	Mean	STD	Mean	STD	Mean	STD	Mean	STD
<b>Orientation 1</b>														
1	1.78	Good	651	215	1390	415	1706	483	1600	443	2117	508	1281	341
2	1.81	Slightly broken	700	250	1453	453	1735	475	1604	422	2098	463	1250	304
3	1.10	Surface Damaged	1014	189	2019	288	2337	269	2171	256	2669	216	1704	200
4	1.50	Broken pieces	780	268	1592	458	1890	469	1754	431	2254	440	1372	329
5	0.62	One cotyledon	1181	428	2172	550	2411	475	2281	474	2611	375	1822	406
6	1.92	Insect present	714	183	1483	332	1782	358	1663	329	2154	359	1319	259
7	1.39	Tiny Insect hole	685	117	1440	217	1744	238	1631	220	2136	253	1297	177
8	2.48	Insect hole	705	307	1444	510	1724	516	1618	475	2071	480	1288	367
9	1.36	Insect present	683	155	1441	303	1745	338	1618	309	2150	364	1269	239
10	1.84	Insect present	645	157	1361	285	1651	301	1531	260	2036	294	1192	181
<b>Orientation 2</b>														
1	1.78	Good	702	185	1501	343	1828	371	1713	337	2261	382	1370	258
2	1.81	Slightly broken	639	173	1353	329	1639	356	1519	318	2023	363	1189	236
3	1.10	Surface Damaged	893	183	1794	317	2096	328	1931	307	2434	316	1496	245
4	1.50	Broken pieces	647	155	1369	273	1665	281	1548	242	2049	268	1211	170
5	0.62	One cotyledon	956	258	1878	408	2165	395	1993	380	2474	348	1533	305
6	1.92	Insect present	688	269	1412	468	1687	482	1570	438	2036	455	1231	328
7	1.39	Tiny Insect hole	660	132	1391	253	1690	282	1574	257	2085	305	1237	199
8	2.48	Insect hole	709	234	1472	414	1771	435	1660	401	2145	424	1324	311
9	1.36	Insect present	687	173	1440	323	1738	348	1606	311	2124	352	1250	230
10	1.84	Insect present	690	191	1438	352	1727	375	1596	335	2100	370	1244	248



**Table C.3 Percent area occupied by the nut inside shell of natural pecans and decision based on a threshold value of 75% for 'unknown' samples.**

<b>Sample</b>	<b>Condition appearing from outside</b>	<b>Orientation</b>	<b>Percent area occupied by the nut<sup>s</sup></b>	<b>Decision</b>
1	Good	1	84.87	Accept
		2	82.06	
2	Mechanical and apparent insect damage	1	83.46	Accept
		2	89.68	
3	Good	1	78.01	Accept
		2	87.14	
4	Good	1	67.56	Reject
		2	70.41	
5	Mechanical damage	1	76.33	Reject
		2	74.35	
6	Good	1	93.09	Accept
		2	84.98	
7	Good	1	87.44	Accept
		2	83.35	
8	Good	1	96.95	Accept
		2	90.54	
9	Shuck tight	1	91.47	Reject
		2	62.38	
10	Shuck tight	1	89.96	Accept
		2	75.96	
11	Shuck tight and apparently hollow	1	24.36	Reject
		2	1.24	
12	Mechanical damage and oil stain	1	75.30	Accept
		2	78.87	
13	With shuck	1	41.67	Reject
		2	65.57	
14	Shuck tight	1	27.81	Reject
		2	3.47	
15	Shuck tight	1	64.33	Reject
		2	31.24	
16	Insect hole	1	54.86	Reject
		2	12.30	
17	Insect hole	1	8.80	Reject
		2	5.98	
18	Insect hole	1	0.08	Reject
		2	1.24	

Sample	Condition appearing from outside	Orientation	Percent area occupied by the nut <sup>§</sup>	Decision
19	Insect hole	1	7.00	Reject
		2	19.90	
20	Good	1	84.62	Accept
		2	85.66	
21	Insect hole and oil stain	1	80.69	Accept
		2	89.84	
22	Good	1	76.63	Accept
		2	83.43	
23	Insect hole	1	78.80	Reject
		2	69.72	
24	Insect hole and oil stain	1	83.70	Reject
		2	65.55	
25	Oil stain	1	73.85	Reject
		2	76.79	
26	Insect hole and oil stain	1	59.65	Reject
		2	81.51	
27	Insect hole	1	24.76	Reject
		2	38.25	
28	Good	1	86.47	Accept
		2	81.88	
29	Oil stain	1	94.08	Accept
		2	89.76	
30	Good	1	88.54	Accept
		2	84.61	

(§ = ROI-2/ROI-1\*100)

**Table C.4 Mean and standard deviation of pixel intensity inside the shell of pecan for 'unknown' pecan samples.**

Sample No.	Condition without breaking the nut	25 kVp		30 kVp		35 kVp		40 kVp		45 kVp		50 kVp	
		Mean	STD	Mean	STD	Mean	STD	Mean	STD	Mean	STD	Mean	STD
<b>Orientation 1</b>													
1	Good	649	255	1348	408	1617	397	1519	356	1968	349	955	224
2	Mechanical and apparent weevil damage	730	301	1494	498	1772	494	1650	437	2122	449	1281	305
3	Good	775	403	1542	620	1803	594	1687	540	2132	525	1310	385
4	Good	845	402	1665	607	1936	581	1798	524	2270	510	1385	375
5	Mechanical damage	839	355	1635	498	1898	457	1770	424	2226	372	1374	325
6	Good	541	132	1158	229	1421	232	1347	205	1766	206	1071	147
7	Good	703	193	1431	281	1688	251	1586	237	1971	182	1253	187
8	Good	593	136	1255	243	1532	259	1440	226	1901	264	1138	157
9	Shuck tight	580	123	1249	215	1540	219	1452	190	1942	203	1148	135
10	Shuck tight	561	125	1201	225	1477	237	1392	206	1852	230	1103	145
11	Shuck tight + apparently hollow	1204	298	2200	402	2419	356	2251	335	2618	306	1720	244
12	Mechanical damage and oil stain	894	335	1687	406	1932	337	1807	332	2224	223	1415	279
13	With shuck	799	166	1630	276	1929	273	1785	236	2280	234	1375	161
14	Shuck tight	986	299	1885	427	2140	376	1992	355	2410	278	1524	259
15	Shuck tight	896	173	1739	241	1976	205	1850	194	2197	167	1450	149
16	Insect hole	1064	202	2031	304	2291	290	2112	256	2539	277	1611	179
17	Insect hole	987	181	1920	275	2188	253	2023	228	2455	219	1553	162
18	Insect hole	1229	280	2195	345	2389	298	2238	285	2566	263	1736	222

Sample No.	Condition without breaking the nut	25 kVp		30 kVp		35 kVp		40 kVp		45 kVp		50 kVp	
		Mean	STD	Mean	STD	Mean	STD	Mean	STD	Mean	STD	Mean	STD
19	Insect hole	969	233	1905	369	2188	354	2015	311	2491	317	1538	212
20	Good	551	130	1199	245	1486	265	1400	231	1880	276	1106	163
21	Insect hole	512	116	1103	209	1371	221	1301	194	1743	216	1040	139
22	Good	525	167	1131	296	1395	305	1322	268	1756	287	1058	191
23	Insect hole	514	96	1117	175	1390	186	1318	163	1776	186	1051	117
24	Insect hole	613	138	1297	240	1579	246	1482	215	1951	228	1171	152
25	Oil stain	633	131	1328	229	1611	239	1506	207	1979	232	1181	143
26	Insect hole	530	107	1142	200	1416	218	1336	187	1800	227	1061	128
27	Insect hole	839	224	1686	361	1970	348	1828	308	2294	303	1411	216
28	Good	612	125	1281	217	1558	224	1464	195	1920	209	1155	136
29	Oil stain	512	94	1106	168	1371	177	1300	156	1733	172	1041	113
30	Good	539	146	1164	267	1438	287	1360	251	1813	297	1081	178
<b>Orientation 2</b>													
1	Good	686	263	1400	404	1670	388	1567	350	2012	338	1232	261
2	Mechanical and apparent weevil damage	650	256	1347	376	1623	370	1524	332	1986	340	1202	250
3	Good	726	290	1488	483	1768	484	1646	423	2125	446	1279	296
4	Good	908	390	1738	568	1984	519	1852	481	2274	414	1435	354
5	Mechanical damage	864	361	1673	524	1930	480	1800	444	2242	384	1396	331
6	Good	585	147	1255	268	1546	283	1454	242	1947	277	1145	165
7	Good	729	193	1510	331	1811	326	1680	283	2200	278	1295	192
8	Good	585	123	1248	220	1527	229	1435	201	1903	218	1134	144
9	Shuck tight	607	144	1292	263	1579	280	1484	244	1961	285	1171	170

Sample No.	Condition without breaking the nut	25 kVp		30 kVp		35 kVp		40 kVp		45 kVp		50 kVp	
		Mean	STD	Mean	STD	Mean	STD	Mean	STD	Mean	STD	Mean	STD
10	Shuck tight	602	142	1273	253	1555	264	1457	229	1934	252	1146	159
11	Shuck tight + apparently hollow	1132	253	2036	285	2223	234	2093	231	2379	191	1643	195
12	Mechanical damage and oil stain	806	279	1584	385	1847	343	1722	321	2169	251	1342	250
13	With shuck	789	149	1601	235	1884	222	1751	195	2208	176	1364	139
14	Shuck tight	958	218	1877	339	2156	319	1987	284	2446	270	1520	197
15	Shuck tight	936	220	1830	307	2104	264	1951	245	2403	184	1504	184
16	Insect hole	1095	290	2049	389	2285	341	2123	328	2510	286	1620	244
17	Insect hole	990	187	1929	280	2199	256	2033	230	2474	227	1557	165
18	Insect hole	1091	190	2067	271	2303	247	2136	227	2515	227	1634	163
19	Insect hole	932	202	1833	311	2102	302	1947	263	2376	299	1499	187
20	Good	527	122	1144	219	1417	230	1338	200	1791	219	1064	143
21	Insect hole	527	126	1135	226	1406	239	1331	210	1778	234	1061	149
22	Good	512	157	1109	282	1372	295	1304	259	1733	284	1045	185
23	Insect hole	520	112	1127	203	1398	214	1324	188	1770	208	1058	135
24	Insect hole	627	157	1322	264	1606	267	1507	235	1981	249	1188	169
25	Oil stain	662	110	1383	192	1674	197	1559	171	2054	185	1216	120
26	Insect hole	532	146	1148	271	1422	296	1342	256	1804	310	1064	177
27	Insect hole	757	166	1544	257	1826	242	1705	218	2161	217	1333	164
28	Good	603	111	1274	198	1557	207	1463	180	1935	199	1154	126
29	Oil stain	499	104	1084	190	1347	202	1277	177	1711	200	1024	127
30	Good	554	128	1192	229	1468	243	1387	215	1842	248	1103	155

**Table C.5 Weights: actual and X-ray estimated, for nutmeat in fabricated pecan.**

Sample No.	Actual wt., g	Estimated weight, g											
		25 kVp		30 kVp		35 kVp		40 kVp		45 kVp		50 kVp	
		Or. * 1	Or. 2	Or. 1	Or. 2	Or. 1	Or. 2	Or. 1	Or. 2	Or. 1	Or. 2	Or. 1	Or. 2
1	1.78	2.30	2.18	2.19	2.11	1.86	1.78	1.68	1.59	1.73	1.59	1.62	1.50
2	1.81	2.36	2.78	2.24	2.69	1.97	2.37	1.78	2.12	1.74	2.05	1.59	1.82
3	1.10	1.72	2.64	1.64	2.52	1.49	2.31	1.36	2.11	1.19	1.88	1.11	1.71
4	1.50	2.15	1.44	2.05	1.40	1.79	1.25	1.61	1.12	1.54	1.07	1.41	0.95
5	0.62	0.75	1.83	0.72	1.75	0.63	1.60	0.56	1.46	0.48	1.31	0.46	1.18
6	1.92	2.43	2.53	2.32	2.37	2.03	2.04	1.82	1.84	1.68	1.80	1.55	1.68
7	1.39	1.72	1.28	1.66	1.23	1.43	1.06	1.29	0.95	1.20	0.90	1.11	0.81
8	2.48	3.19	3.26	2.95	3.08	2.50	2.59	2.27	2.33	2.24	2.27	2.22	2.18
9	1.36	2.12	2.33	2.04	2.24	1.82	1.99	1.64	1.79	1.55	1.71	1.38	1.52
10	1.84	2.07	2.90	1.99	2.79	1.78	2.48	1.61	2.22	1.53	2.11	1.36	1.88
Correlation with actual weight		0.95	0.59	0.95	0.58	0.94	0.50	0.94	0.48	0.95	0.58	0.95	0.62
Mean estimation error, g		0.50	0.74	0.40	0.64	0.15	0.37	-0.02	0.17	-0.09	0.09	-0.20	-0.06
Estimation error, %		31.68	46.68	25.32	40.30	9.48	23.14	-1.13	10.95	-5.86	5.70	-12.57	-3.66

\*Or. - Orientation

**Table C.6 Weights: actual and X-ray estimated, for nutmeat in 'unknown' pecan samples.**

Sample No.	Actual wt., g	Estimated weight, g											
		25 kVp		30 kVp		35 kVp		40 kVp		45 kVp		50 kVp	
		Or.* 1	Or. 2	Or. 1	Or. 2	Or. 1	Or. 2	Or. 1	Or. 2	Or. 1	Or. 2	Or.1	Or.1
1	3.02	4.45	4.77	4.20	4.48	3.51	3.73	3.17	3.37	3.23	3.47	1.54	3.27
2	3.45	5.27	5.05	5.01	4.77	4.31	4.01	3.89	3.63	3.79	3.69	3.50	3.47
3	3.51	4.71	5.42	4.43	5.11	3.78	4.33	3.42	3.92	3.37	3.95	3.18	3.69
4	1.91	3.02	4.83	2.87	4.57	2.45	3.94	2.20	3.56	2.17	3.47	1.98	3.18
5	2.21	3.38	4.14	3.22	3.93	2.79	3.36	2.50	3.01	2.44	3.01	2.18	2.71
6	2.08	2.92	3.17	2.69	2.93	2.12	2.41	1.91	2.19	1.92	2.32	1.95	2.20
7	1.37	2.37	3.11	2.25	2.97	1.91	2.58	1.71	2.31	1.51	2.25	1.46	1.97
8	2.08	2.55	3.45	2.38	3.24	1.92	2.66	1.71	2.38	1.71	2.39	1.62	2.26
9	1.88	2.98	2.64	2.82	2.45	2.30	1.96	2.08	1.78	2.19	1.93	2.03	1.86
10	2.03	3.10	3.24	2.85	2.98	2.28	2.41	2.06	2.16	2.20	2.31	2.13	2.19
11	0.19	2.10	2.02	1.96	1.90	1.78	1.72	1.67	1.60	1.42	1.36	1.40	1.32
12	0.85	2.89	3.21	2.75	3.02	2.45	2.62	2.20	2.37	2.02	2.23	1.81	2.04
13	0.31	2.05	2.84	1.96	2.72	1.79	2.46	1.64	2.25	1.46	1.98	1.33	1.83
14	0.35	1.71	2.28	1.62	2.18	1.48	1.99	1.37	1.82	1.19	1.63	1.12	1.47
15	0.13	0.34	2.16	0.32	2.07	0.29	1.89	0.26	1.73	0.22	1.57	0.21	1.41
16	0.42	5.64	0.97	5.35	0.92	4.89	0.84	4.50	0.78	3.94	0.68	3.65	0.62
17	0.35	1.19	0.68	1.13	0.65	1.03	0.59	0.95	0.54	0.83	0.47	0.78	0.44
18	0.28	0.70	0.14	0.66	0.13	0.60	0.12	0.56	0.11	0.49	0.09	0.47	0.09
19	0.52	0.50	2.34	0.48	2.25	0.44	2.05	0.41	1.87	0.36	1.69	0.33	1.51
20	3.61	4.01	4.15	3.74	3.82	3.04	2.99	2.73	2.67	2.98	3.01	2.85	2.94
21	3.34	3.33	3.90	2.95	3.48	2.28	2.67	2.06	2.41	2.27	2.72	2.33	2.77
22	3.25	4.40	4.28	4.02	3.86	3.13	3.04	2.82	2.75	3.06	2.98	3.11	3.11
23	3.14	3.43	3.84	3.12	3.48	2.41	2.69	2.18	2.41	2.47	2.73	2.44	2.75
24	1.84	3.69	3.43	3.50	3.24	2.90	2.61	2.60	2.35	2.60	2.49	2.42	2.36
25	1.17	2.47	3.13	2.34	2.96	1.93	2.48	1.70	2.20	1.67	2.18	1.53	1.95
26	2.88	3.08	3.49	2.79	3.15	2.14	2.54	1.91	2.28	2.16	2.47	2.10	2.44
27	0.56	1.89	3.31	1.81	3.20	1.63	2.81	1.48	2.54	1.36	2.38	1.23	2.15

Sample No.	Actual wt., g	Estimated weight, g											
		25 kVp		30 kVp		35 kVp		40 kVp		45 kVp		50 kVp	
		Or.* 1	Or. 2	Or. 1	Or. 2	Or. 1	Or. 2	Or. 1	Or. 2	Or. 1	Or. 2	Or.1	Or.1
28	1.32	2.68	3.11	2.46	2.87	2.00	2.34	1.80	2.11	1.79	2.16	1.73	2.05
29	1.9	2.85	2.50	2.54	2.23	1.93	1.69	1.74	1.51	1.92	1.69	1.99	1.76
30	2.42	2.77	3.97	2.54	3.67	2.01	2.91	1.81	2.61	1.93	2.79	1.93	2.74
Correlation with actual value		0.70	0.79	0.67	0.76	0.58	0.68	0.56	0.67	0.70	0.79	0.70	0.84
Mean estimation error, g		-1.11	-1.41	-0.92	-1.20	-0.48	-0.71	-0.26	-0.47	-0.25	-0.50	-0.10	-0.38
Estimation error, %		-28.22	-49.02	-28.88	-44.61	-16.09	-31.51	-10.56	-22.96	-11.15	-24.51	-4.61	-20.20

\*Or. - Orientation



**Table C.7 Correlation between actual and estimated weights and estimation error values for 'unknown' pecans having good quality.**

	Estimated weight, g											
	25 kVp		30 kVp		35 kVp		40 kVp		45 kVp		50 kVp	
	Or.* 1	Or. 2	Or. 1	Or. 2	Or. 1	Or. 2	Or. 1	Or. 2	Or. 1	Or. 2	Or.1	Or.1
Correlation with actual value	0.79	0.80	0.75	0.75	0.69	0.67	0.70	0.67	0.79	0.79	0.75	0.87
Mean estimation error, g	-0.93	-1.24	-0.69	-0.97	-0.09	-0.32	0.17	-0.04	0.08	-0.18	0.25	-0.08
Estimation error, %	-32.84	-61.01	-30.89	-51.17	-4.40	-20.92	9.97	-2.95	5.61	-12.53	15.61	-6.26

\*Or. - Orientation

**Table C.8 Feature comparison for 'unknown' pecan samples.**

<b>Sample No.</b>	<b>External appearance</b>	<b>Internal conditions after opening</b>	<b>Decision based on % area occupancy</b>	<b>Decision based on mean pixel intensity</b>	<b>Decision based on mean local variation</b>	<b>Features visible in X-ray image</b>
1	Good	Good	Accept	Accept	Accept	One cotyledon slightly smaller than other, no damage to shell or nutmeat, no insect
2	Mechanical and apparent weevil damage	Mechanical and insect damage	Accept	Accept	Accept	Damage to shell visible, high pixel intensity on the inside of nutmeat
3	Good	Large air gap, one cotyledon smaller than the other	Accept	Accept	Accept	One cotyledon much smaller than the other, no damage to shell or nutmeat
4	Good	Large air gap, one cotyledon smaller than the other	Reject	Reject	Reject	Nut not fully filled, one cotyledon small, large air gap, no damage to shell
5	Mechanical damage	Mechanical damage	Reject	Reject	Reject	Nut not fully filled, mechanical damage
6	Good	Good	Accept	Accept	Accept	Good nut, however, central 'woody' portion not visible for segmentation
7	Good	Good	Accept	Accept	Reject	Good nut
8	Good	Good	Accept	Accept	Accept	Good nut
9	Shuck tight	One cotyledon smaller than the other	Reject	Accept	Accept	Good nut
10	Shuck tight	Good	Accept	Accept	Accept	Good nut, one cotyledon slightly smaller than other
11	Shuck tight + apparently hollow	Virtually no nutmeat	Reject	Reject	Reject	Empty nut, a shape similar to nutmeat can be observed with difficulty
12	Mechanical damage and oil stain	Mechanical damage	Accept	Reject	Reject	Mechanical damage to the shell and nutmeat can be seen very clearly in orientation-2

<b>Sample No.</b>	<b>External appearance</b>	<b>Internal conditions after opening</b>	<b>Decision based on % area occupancy</b>	<b>Decision based on mean pixel intensity</b>	<b>Decision based on mean local variation</b>	<b>Features visible in X-ray image</b>
13	With shuck	Shriveled	Reject	Reject	Reject	Image is distinctly different due to shuck, segmentation of nutmeat was difficult
14	Shuck tight	Shriveled	Reject	Reject	Reject	Little or no nutmeat, segmentation was difficult
15	Shuck tight	Immature	Reject	Reject	Reject	Little or no nutmeat, bright nutmeat area
16	Insect hole	Virtually no nutmeat	Reject	Reject	Reject	Little or no nutmeat, bright nutmeat area
17	Insect hole	Virtually no nutmeat	Reject	Reject	Reject	Little or no nutmeat, bright nutmeat area
18	Insect hole	Virtually no nutmeat	Reject	Reject	Reject	Little or no nutmeat, bright nutmeat area
19	Insect hole	Virtually no nutmeat	Reject	Reject	Reject	Little or no nutmeat, bright nutmeat area
20	Good	Good	Accept	Accept	Accept	Good nut
21	Insect hole	Insect damage to one cotyledon from inside	Accept	Accept	Accept	Insect hole on shell visible, slight insect damage caused brighter spots in nutmeat portion
22	Good	Good	Accept	Accept	Accept	Good nut
23	Insect hole	Insect damage and dead insect present	Reject	Reject	Accept	Visible insect damage and insect
24	Insect hole	Substantial insect damage	Reject	Accept	Accept	Visible bright spots but extent of insect damage is not much
25	Oil stain	Large air gap, nutmeat was all black though no insect or physiological damage	Reject	Accept	Accept	Good nut but air gap more than other good nuts
26	Insect hole	Insect damage	Reject	Accept	Accept	Insect hole visible

<b>Sample No.</b>	<b>External appearance</b>	<b>Internal conditions after opening</b>	<b>Decision based on % area occupancy</b>	<b>Decision based on mean pixel intensity</b>	<b>Decision based on mean local variation</b>	<b>Features visible in X-ray image</b>
27	Insect hole	Virtually no nutmeat	Reject	Reject	Reject	Little or no nutmeat, bright nutmeat area
28	Good	Has dead insect	Accept	Accept	Accept	Good nutmeat, no insect visible
29	Oil stain	Has dead insect	Accept	Accept	Accept	Insect and damage visible
30	Good	Has dead insect	Accept	Accept	Accept	Insect and damage visible

## APPENDIX – D – PHOTOGRAPHS OF EQUIPMENT



Figure D.1 The X-ray imaging system showing shielded box, X-ray tube controller, computer, and monitor.

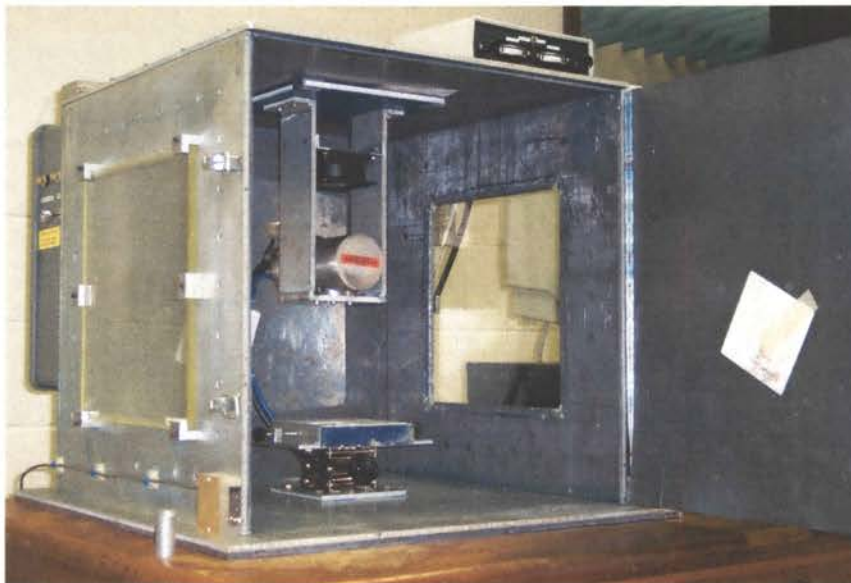


Figure D.2 View inside the shielded box showing X-ray tube above and camera mounted on adjustable platform.

## APPENDIX - E -- COMPUTER PROGRAMS

### Program - 1

*% Program for manual assignment of Region of Interest (ROI)*

*% Written by Nachiket Kotwaliwale*

clear all; clc; pack memory; close all; warning off; tic

*% Image inputs*

for samp=1:10; *% sample no. from 1 to 10*

kvp=20; *% kvp 25, 30, 35, 40, 45, 50*

position=1; *% Orientation, only two values 1 or 2*

ma=1;

h=strel('disk',5);

*% Read the product image at 20 kvp & 1 ma to get image map*

fileid=strcat('M:\Research\Processing\Pecan\_x-ray\fab\_samples\',num2str(samp),'\pos',num2str(position),'\_k20m100.raw');

fp=fopen(fileid,'rb','b');

if fp>0

img=fread(fp,[1024,1022],'uint16');

end

img=img';

img=img(12:1011,13:1012);

fclose('all');

*% Read a blank image*

fileid=strcat('M:\Research\Processing\Calibration\_raw\Blank\_460ms\k20m1000.raw');

fp=fopen(fileid,'rb','b');

if fp>0

blk=fread(fp,[1024,1022],'uint16');

end

blk=blk';

blk=blk(12:1011,13:1012);

fclose('all');

*% Identify background based on attenuation and store the image map*

tmp=img./blk;

tpm1=tmp<0.8;

tpm1=imopen(tpm1,h);

tpm1=imfill(tpm1,'holes');

*% Now read the required image*

fileid=strcat('M:\Research\Processing\Pecan\_x-ray\fab\_samples\',num2str(samp),'\pos',num2str(position),'\_k',num2str(kvp),'m',num2str(ma\*100),'.raw');

fp=fopen(fileid,'rb','b');

if fp>0

img=fread(fp,[1024,1022],'uint16');

end

img=img';

```

img=img(12:1011,13:1012);
fclose('all');
[x,y]=find(img>4095);
if length(x)>=1
    img(x,y)=(img(x-1,y)+img(x,y-1)+img(x-1,y-1)+img(x+1,y-
1)+img(x+1,y)+img(x+1,y+1)+img(x,y+1)+img(x-1,y+1))/8;
end
img2=uint16(img.*double(tpm1));

ind2=find(img2~=0);
img3=uint8(double(img2)/4);
img3(ind2)=imadjust(img3(ind2),stretchlim(img3(ind2)),[]);
figure;
myarea=roipoly(img3);
fin_ind=find(myarea); % Final indexes for the nutmeat portion
no_shell=fin_ind;
close all;

end %samples
toc

```

### Program - 2

*% This program is to find empty space inside the shell boundary, i.e. percent area occupancy*  
*% Program written by Nachiket Kotwaliwale*

```

count=1;
for samp=1:10 % No. of samples from 1 to 10 for fabricated samples
    for position=1:2 % Two orientations
        % Read indices for ROI-1
        roi_id_NS=strcat('M:\Research\Processing\Pecan_x-
ray\fab_samples\NS_',num2str(samp),'_',num2str(position),'.mat');
load(roi_id_NS);
        % Read indices for ROI-2
        roi_id_nut=strcat('M:\Research\Processing\Pecan_x-
ray\fab_samples\ROI_',num2str(samp),'_',num2str(position),'.mat');
load(roi_id_nut);

out(count,1)=samp;
out(count,2)=position;
% Find ratio of the area of two ROIs
out(count,3)=length(fin_ind)/length(no_shell)*100;
count=count+1;
end
end

```

### Program - 3

*% Program to calculate mean intensity in the ROI-2*  
*% Written by Nachiket Kotwaliwale*  
clear all; clc; pack memory; close all; warning off; tic

```

% Initiate a counter
count=1;
v=[20 25,30,35,40,45,50];
curr=[1,1,1,0.75,0.5,0.5,0.25];
% Read a blank image for flat field correction
fileid=strcat('M:\Research\Processing\Calibration_raw\Blank_460ms\k2om1000.raw');

```

```

fp=fopen(fileid,'rb','b');
if fp>0
    blk=fread(fp,[1024,1022],'uint16');
end
blk=blk';
blk=blk(12:1011,13:1012);
fclose('all');
blkmn=mean(blk);
blkcor=blkmn/mean2(blk);
blkcor1=repmat(blkcor,[1000,1]);

% Image inputs
for position=1:1
    for k=3:3
        for samp=1:10; % sample no. from 1 to 10
            kvp=v(k); % kvp 25, 30, 35, 40, 45, 50
            ; % only two values 1 or 2
            ma=curr(k);

%Read the required image

fileid=strcat('M:\Research\Processing\Pecan_x-
ray\fab_samples\',num2str(samp),'\pos',num2str(position),'_k',num2str(kvp),'m',num2str(ma*1
00),'.raw');

fp=fopen(fileid,'rb','b');
if fp>0
    img=fread(fp,[1024,1022],'uint16');
end
img=img';
img=img(12:1011,13:1012);
fclose('all');
[x,y]=find(img>4095);
if length(x)>=1
    img(x,y)=(img(x-1,y)+img(x,y-1)+img(x-1,y-1)+img(x+1,y-
1)+img(x+1,y)+img(x+1,y+1)+img(x,y+1)+img(x-1,y+1))/8;
end

% Read the ROI-2 indices
roi_id=strcat('M:\Research\Processing\Pecan_x-
ray\fab_samples\ROI_',num2str(samp),'_',num2str(position),'.mat');
load(roi_id);
if samp==5
    roi_id=strcat('M:\Research\Processing\Pecan_x-
ray\fab_samples\ROI_',num2str(samp),'_1_',num2str(position),'.mat');
    load(roi_id);
end

% Flat field correction
img=uint16(double(img)./double(blkcor1));

% Local variation in 5x5 window
window=5;
roi_corr=(window-1)/2;
H=fspecial('average',window);
h=strel('disk',roi_corr);
avg_im=imfilter(img,H);

```



```

var_im=abs(double(img)-double(avg_im));
new=zeros(1000,1000);
new(fin_ind)=1;

new=imerode(new,h);
fin_ind1=find(new);
new(fin_ind1)=var_im(fin_ind1);
new=double(new);

[n,bin]=imhist(img(fin_ind));
ind1=find(n~=0);
n=n(ind1);
bin=bin(ind1);

length(find(new(fin_ind1)>(mean(new(fin_ind1))+2*std(new(fin_ind1))))))

% Develop the output matrix
out(count,1)=kvp;
out(count,2)=samp;
out(count,3)=position;
% mean intensity in the ROI
out(count,5)=sum(img(fin_ind))/length(fin_ind);
% No. of pixels in the ROI
out(count,4)=length(fin_ind);
% St. Dev. of pixel intensity in ROI
out(count,6)=std(double(img(fin_ind)));
% Mean local variance in the ROI
out(count,7)=sum(new(fin_ind1))/length(fin_ind1);
% No. of pixels with local variance more than mean+/- 2*std
out(count,8)=length(find(new(fin_ind1)>(mean(new(fin_ind1))+2*std(new(fin_ind1)))&new(fin_ind1)<(mean(new(fin_ind1))-2*std(new(fin_ind1)))));
count=count+1;
end %samples
end %kvp
end % position
% write output to an MS Excel file with tab delimitation
dlmwrite('mean_gray.xls',out,'\t')
toc

```

#### Program 4

*% Program to estimate nutmeat weight from the X-ray images*  
*% Program written by Nachiket Kotwaliwale*

```

clear all; clc; pack memory; close all; warning off; tic
% The attenuation coefficient parameters
% The equation is  $\mu = OA + OB.t + OC.t^2 + OD.kvp + OE.kvp^2 + OF.t.kvp$ 

```

*% General Model*

```

OA=5.11604;
OB=-2.17637;
OC=0.43494;
OD=-0.15405;
OE=0.00155;
OF=0.02216;
%  $\mu_2$  and  $t_2$  are shell attenuation and thickness, respectively
mu_s=[4.690833333,3.627083333,3.175833333,2.696666667,2.489166667,2.270416667,2.21875];

```

```

t2=0.082;

% Initiate a counter
count=1;
col=2;

% Read attenuated image
v=[20 25,30,35,40,45,50];
curr=[1 1,1,0.75,0.5,0.5,0.25];
for kvp=20:5:50
ma=curr(find(kvp==v));
mu2=mu_s(find(kvp==v));
% Rearrange terms so that the attenuation equation becomes
%  $C.t^3+B.t^2+A.t+D=0$ 

A=OA+OD*kvp+OE*(kvp^2);
B=OB+OF*kvp;
C=OC;

% Develop Io image from the calibration model
% Read the calibration equation coefficients for all 1 million points

load M:\Research\Processing\Calibration_raw\Blank_460ms\coeff_raw

Io = ceil(fullcoeff(1,:)*ma+fullcoeff(2,:)*ma*kvp+fullcoeff(3,:));
Io=reshape(Io,[1000 1000]);

% Load the cone correction matrix
load(strcat('M:\Research\Processing\Pecan_x-ray\fab_samples\cone_corr.mat'));

for position=1:1; % only two values 1 or 2
for samp=10:10; % sample no. from 1 to 10

% Read the required image
fileid=strcat('M:\Research\Processing\Pecan_x-
ray\fab_samples\',num2str(samp),'\pos',num2str(position),'_k',num2str(kvp),'m',num2str(ma*1
00),'.raw');
fp=fopen(fileid,'rb','b');
if fp>0
img=fread(fp,[1024,1022],'uint16');
end
img=img';
img=img(12:1011,13:1012);
fclose('all');
[x,y]=find(img>4095);
if length(x)>=1
img(x,y)=(img(x-1,y)+img(x,y-1)+img(x-1,y-1)+img(x+1,y-
1)+img(x+1,y)+img(x+1,y+1)+img(x,y+1)+img(x-1,y+1))/8;
end

% Load region of interest map
roi_id=strcat('M:\Research\Processing\Pecan_x-
ray\fab_samples\ROI_',num2str(samp),'_',num2str(position),'.mat');
load(roi_id);

I=img(fin_ind);

```

*% Get values from blank image for the required indices*

`Io=Io(fin_ind);`

*% Calculate D for each point*

`D=(2*mu2*t2)+log(I./Io);`

*% Find thickness at each point*

*% cubicroots function was developed separately to find real root of a cubic equation*

`thick=cubicroots(C,B,A,D);`

`thick(thick<0)=0;`

`tria=zeros(1000,1000);`

`tria(fin_ind)=thick;`

*% Perform cone correction*

`tria_corr=tria.*(cone_corr_thick);`

`thick=tria_corr(fin_ind);`

`volume=((((48*10^-4)*153/163)^2*sum(thick)-(length(fin_ind))*((48*10^-4)*153/163)^2*0.1));`

`vol(count,1)=samp;`

*% Multiply volume with 0.95, the mean specific gravity of nutmeat*

`vol(count,col)=volume*0.95;`

`count=count+1;`

`if count>10`

`count=1;`

`col=col+1;`

`end`

`end %samples`

`end %position`

`end %kVp`

`kvp`

`vol`

`toc`

# VITA

Nachiket Kotwaliwale

Candidate for the Degree of

Doctor of Philosophy

Dissertation: FEASIBILITY OF PHYSICAL PROPERTIES AND SOFT X-RAY ATTENUATION PROPERTIES FOR NON-DESTRUCTIVE DETERMINATION OF QUALITY OF NUTMEAT IN IN-SHELL PECANS

Major Field: Biosystems Engineering

## Biographical:

Personal Data: Born in Raipur, India on November 12, 1966, the son of Pratibha and Prabhakar Kotwaliwale. Married to Shreya in Nagpur, India on March 3, 1995. Daughter, Gouri born in Ratnagiri, India on March 25, 1999.

Education: Higher Secondary School Certificate from St. Paul's Higher Secondary School, Raipur, India (1982), received Bachelor of Technology in Agricultural Engineering from J.N. Krishi Vishwa Vidyalaya, Jabalpur, India (1988) and Master of Engineering in Agriculture from Rajasthan Agricultural University, Bikaner, India (1990). Completed the requirements for the Doctor of Philosophy with major in Biosystems and Agricultural Engineering at Oklahoma State University in August, 2003.

Experience: Worked for M.P. Council of Science and Technology at Raipur, India as Research Assistant (1991-92). Worked for BEC Foods at Durg, India as Trainee Production Executive (1993). Employed by Indian Council of Agricultural Research as Scientist and posted at Central Institute of Agricultural Engineering, Bhopal, India (1993 - present).

Professional Association: American Society of Agricultural Engineers, Indian Society of Agricultural Engineers, Association of Food Scientists and Technologists (India), Institute of Engineers (India).